FUEL CELL SIMULATOR SYSTEM

CENTRE FOR NEWFOUNDLAND STUDIES

TOTAL OF 10 PAGES ONLY
MAY BE XEROXED

(Without Author's Permission)

MARTIN ORDONEZ

Fuel Cell Simulator System

By

Martin Ordonez, Ing.

A thesis submitted to the School of Graduate Studies in partial fulfillment of the requirements for the degree of Master of Engineering

Faculty of Engineering and Applied Science
Memorial University of Newfoundland

November 2005
St John's, Newfoundland, Canada

Library and Archives Canada

Published Heritage Branch

395 Wellington Street
Ottawa ON K1A 0N4
Canada

Bibliothèque et Archives Canada

Direction du Patrimoine de l'édition

395, rue Wellington
Ottawa ON K1A 0N4
Canada

Your file Votre référence
ISBN: 978-0-494-19386-0
Our file Notre référence
ISBN: 978-0-494-19386-0

NOTICE:
The author has granted a non-exclusive license allowing Library and Archives Canada to reproduce, publish, archive, preserve, conserve, communicate to the public by telecommunication or on the Internet, loan, distribute and sell theses worldwide, for commercial or non-commercial purposes, in microform, paper, electronic and/or any other formats.

The author retains copyright ownership and moral rights in this thesis. Neither the thesis nor substantial extracts from it may be printed or otherwise reproduced without the author's permission.

AVIS:
L'auteur a accordé une licence non exclusive permettant à la Bibliothèque et Archives Canada de reproduire, publier, archiver, sauvegarder, conserver, transmettre au public par télécommunication ou par l'Internet, prêter, distribuer et vendre des thèses partout dans le monde, à des fins commerciales ou autres, sur support microforme, papier, électronique et/ou autres formats.

L'auteur conserve la propriété du droit d'auteur et des droits moraux qui protège cette thèse. Ni la thèse ni des extraits substantiels de celle-ci ne doivent être imprimés ou autrement reproduits sans son autorisation.

In compliance with the Canadian Privacy Act some supporting forms may have been removed from this thesis.

While these forms may be included in the document page count, their removal does not represent any loss of content from the thesis.

Conformément à la loi canadienne sur la protection de la vie privée, quelques formulaires secondaires ont été enlevés de cette thèse.

Bien que ces formulaires aient inclus dans la pagination, il n'y aura aucun contenu manquant.

Canada

Abstract

Applied research and development of Fuel Cell (FC) power electronics is currently expensive and difficult to carry out due to high cost and lack of flexibility of FC stacks. Flexible affordable FC simulators are required to assist the development and testing of FC power electronics. Using FC simulators results in significant cost, space, and time reductions. It also provides a solution for safety standards problems and overcome the major issue of power sizing in FC stacks. A FC simulator can be constructed using a power converter that follows a reference signal generated by a FC model. The output voltage of the power converter is then controlled to behave according to the FC output characteristics.

This thesis describes in detail the development of two different FC simulator systems namely, a stand-alone FC simulator based on an empirical model and a low cost Digital Signal Processor (DSP), and real-time FC simulator based on a small single cell. A special fast dynamics power converter for FC simulators is designed, taking into consideration the dynamic requirements to successfully reproduce the behavior of a FC. A control scheme based on switching surface control is investigated to achieve near time optimal response in the converter. Laboratory prototypes of the two systems are implemented and investigated. It is shown that the first system provides the advantages of eliminating the dependence upon a computer, communication cards, and licensed software, thus resulting in a small low-cost system suitable for laboratory operation. The second system overcomes modeling drawbacks and expands the features of the existing designs by replacing the computer model of the FC with an actual small single FC. Experimental and simulation results are provided in the thesis to confirm the behavior of the simulators.

Acknowledgments

First and foremost I would like to express my sincere gratitude and appreciation to my supervisors Dr. Tariq Iqbal and Dr. John Quaicoe for their guidance, encouragement, advice, and support over the past two years.

Financial support for this project has been provided by National Science and Engineering Research Council of Canada (NSERC), Atlantic Innovation Fund (AIF) from Atlantic Canada Opportunities Agency (ACOA), and School of Graduate Studies, Memorial University of Newfoundland.

I would also like to thank Ms. Moya Crocker, Secretary to the Associate Dean of Graduate Studies and Research, and Dr. R. Venkatesan, Associate Dean of Graduate Studies and Research, for ensuring smooth operation of the administrative aspects of my graduate program.

Dr. P. Pickup and Dr. O. Yepez of the Department of Chemistry provided generous help and support with the fuel cell setup. Appreciation is extended to my friend Dr. Mariano Koen Alonso from Fisheries and Oceans Canada for useful discussions on various aspects of graduate studies. Finally, I would like to thank my former mentors Mr. Fernando Ghioldi from Deep-Ingenieria and Prof. Ramos Oros from National Tecnological University (UTN), Argentina for their encouragement to undertake a Master's degree.

Table of Contents

List of Figures

List of Tables

Nomenclature

Abbreviations

AC	:	Alternating Current
ADC	:	Analog to Digital Converter
AFC	:	Alkaline Fuel Cell
CAN	:	Control Area Network
CO	:	Carbon Monoxide
DC	:	Direct Current
DMFC	:	Direct Methanol Fuel Cell
DSP	:	Digital Signal Processor
EL	:	Electronic Load
EOC	:	End of Conversion
FC	:	Fuel cell
ISR	:	Interrupt Service Routine
MCFC	:	Molten Carbonate Fuel Cell
MEA	:	Membrane Electrode Assembly
OP	:	Operating Point
PAFC	:	Phosphoric Acid Fuel Cell
PEM	:	Polymer Electrolyte Membrane
PEMFC	:	Proton Exchange Membrane Fuel Cell
PFC	:	Power Factor Corrector
PI	:	Proportional Integral
R-K	:	Runge-Kutta Method
SCR	:	Silicon Controlled Rectifier
SMPS	:	Switching Mode Power Supply
SOFC	:	Solid Oxide Fuel Cell
SPI	:	Serial Peripheral Interface
SS	:	Switching Surface
ST	:	State Trajectory
U	:	Switch Utilization
UPS	:	Uninterruptible Power Supply

Symbols

a	: Parabola Semi-major Axis
b	: Parabola Semi-minor Axis
C	: Capacitor
d	: Duty Cycle
E	: Nerds Voltage
g	: Gaseous State
i_C	: Capacitor Current
i_{Cn}	: Normalized Capacitor Current
$i_{\max}$	: Maximum Admissible Current
i_o	: Output Current
I_{CELL}	: Fuel Cell Current
I_{OR}	: Rated Output Current of the Power Converter
I_T	: Switch Maximum Current
K	: Parabola Size Scaling Coefficient
l	: Liquid State
L	: Inductor
N	: Number of Single Cells in Series
P_O	: Rated Output Power of the Power Converter
P_T	: Product of Switch Maximum Voltage and Maximum Current
R	: Load Resistor
R_a	: Activation Overvoltage Equivalent Resistor
R_{cd}	: Critically Dumped Load Resistor
R_{ohmic}	: Electrodes and Electrolyte Equivalent Resistance
R_{SHUNT}	: Shunt Resistor
v_{cc}	: Input Voltage
v_{on}	: Normalized Output Voltage
v_o	: Output Voltage
v_r	: Power Converter Reference Voltage
V_{cell}	: Single Cell Voltage
V_O	: Fuel Cell Output Voltage
V_{OR}	: Rated Output Voltage of the Power Converter

V_r	:	Reference Voltage of the Electronic Load
V_s	:	Voltage Across Shunt Resistor
V_T	:	Switch Maximum Voltage
u	:	Switch State
α	:	Electrode Area Scaling Function
ΔV_{Act}	:	Activation Overvoltage
ΔV_{Trans}	:	Concentration Overvoltage
ΔV_{Ohmic}	:	Voltage Drop Due to Electrodes Resistance and Membrane Conduction
σ_2	:	Off State Switching Surface
σ_1	:	On State Switching Surface

To my loving wife and family

Chapter 1

Introduction

Fuel Cells (FC) are power sources that convert electrochemical energy into electrical and thermal energy in a clean and efficient manner. Fuel cells have the potential to meet a new generation of energy standards comprising low cost, high efficiency, low emissions, quiet operation, and ensures energy availability for the future. A basic FC arrangement is like a battery consisting of anode and cathode electrodes linked by electrolyte. However, unlike batteries, FCs can operate continuously while they are externally fed with reactant (fuel). As a result of a chemical reaction at the anode, electrons are generated. The electrons circulate externally through the desired electrical load towards the cathode producing work. The maximum theoretical potential generated by a single FC is 1.23V (Nerds voltage). However, due to several undesirable effects, the practical output voltage of a single FC lies below 1V. As most applications require a greater voltage, several single FCs are connected in series to form a FC stack.

Different types of FCs are currently under development and can be classified into three groups by their operating temperature. Solid Oxide Fuel Cell (SOFC) and Molten Carbonate Fuel Cell (MCFC) belong to the high temperature category (1000°C and 650°C respectively); Phosphoric Acid Fuel Cell (PAFC) operated in a range of medium temperatures (150-200°C); and Direct Methanol Fuel Cell (DMFC), Proton Exchange Membrane Fuel Cell (PEMFC), and recent developments in Alkaline Fuel Cell (AFC) belong to the low temperature group (80°C, 50-100°C, and 25-70°C respectively) [1], [2].

FCs can be used in a wide range of transportation, stationary power generation, and portable power applications [2], [3]. Application of FC in automotive power trains has been receiving more attention in the past years [4]. Even though commercial vehicles are not yet available, the major automotive companies in partnership with FCs producers are developing and testing FC cars. Moreover, some existing FC pilot projects in public transportation have proven the advantages of this concept [5]. Recent substantial improvements in PEMFC put this technology ahead of the other types of FCs for transportation applications. The main advantages of PEMFC are high power density, no moving parts, and water as a byproduct. PEMFCs are also being tested in golf carts, scooters, underwater vehicles, and light airplanes [6], [7], [8].

The stationary power generation segment includes utility power plants, building power generation (for hospitals, office buildings, schools, and airports), and low power residential applications [9], [10]. PAFC is a mature FC technology that is commercially available, which is particularly suitable for stationary power generation. The efficiency of electrical power generation of PAFC goes beyond 40%. In addition, a high percentage of the steam produced by this FC (~85%) can be used for cogeneration or heating purposes. Another important advantage of this FC technology is that it can be fuelled with hydrogen that contains carbon monoxide (CO), making the fuel choice more flexible. On the other hand, low power density (bulky system) and catalyst cost are some of the disadvantages of PAFC.

Portable power applications are a potential huge market for FCs systems [11]. The high energy density of fuel and high power density of FCs will allow placing them in portable devices and running many hours beyond the existing battery technologies [12]. Future FC applications include power supply for notebooks, palms/pocket PCs, cell phones, pagers, digital and video cameras, as well as other devices currently powered by batteries. Since DMFCs have the simplest arrangement and methanol can be easily stored, DMFCs are undoubtedly the best candidate for portable power applications.

The FC systems described above require several auxiliary equipment to operate in addition to the FC stack: fuel management, air management, thermal management, and water management [1], [2]. These subsystems are designed to meet specific requirements for each FC technology and application. Hydrogen FCs primarily fuelled with hydrocarbons also require a complex fuel processor/reformer conversion stage. The fuel management subsystem includes pipes, tank, and pressure regulators to control fuel at the anode inlet. The air subsystem provides air/oxygen supply management in the cathode. An air blower can be used for low pressure supply. However, since high pressure air supply improves the overall performance of FCs, an air compressor is required. A liquid coolant or water circuit that interconnects the FCs stack to the heat exchanger (or radiator) provides thermal management to control the temperature of the FC stack. Water management system involves water removal from exhaust gas, storage, and reutilization for humidification of the reactant. In addition, if a reformer is used, water is also supplied to this stage.

FC stacks provide unregulated DC output voltage at their output terminals that change with the loading conditions. In order to integrate a FC system and application, a power management system is required. A power electronics converter is used to adjust the unregulated output voltage of the FC to meet the requirements of the specific application [13]. Since interaction between the load, power converter, and FC system exist, it should be addressed during design stages. In fact, integrated control strategies for the FC system and power converter are required to ensure good performance in the FC system while complying with the load demands. The design and development of FC power electronics is truly a formidable challenge. Furthermore, integrating FC systems with power electronics for a specific application is a tradeoff between several factors that involve an iterative process.

Applied research and development in FC power electronics is currently expensive and difficult to carry out due to high cost and lack of flexibility of FC stacks and subsystems. In general, the size of the FC auxiliary equipment (management of fuel, air, thermal, and water) is related to the size of the FC stack and the associated cost and space can be excessive. As a matter of fact, an expensive FC setup might not provide the flexibility required in terms of start up time and handling. Furthermore, since the power rating of FC stacks cannot be modified, a new FC stack should be purchased to match the required power rating. This research and development approach is clearly not convenient.

For the reasons stated above, flexible affordable FC simulators are required to assist the development and testing of FC power electronics. Using FC simulators results in a significant cost, space, and time reductions. It also provides a solution for safety standards problems and overcomes the major issue of power sizing in FC stacks.

1.1 Literature Review of Fuel Cell Simulators

The development of FC simulators has only recently gained attention. A FC simulator can be constructed using a power converter that follows a reference signal generated by a FC model. The output voltage of the power converter is then controlled so that it behaves like the FC output characteristics. The number of FC simulator reported in literature to date is very limited. An approach to a FC simulator was published in 2003 and consists of a power rectifier controlled by a computer model of a PEMFC [14]. A Proportional Integrative (PI) controller is employed to control the power converter. A SOFC simulator was recently reported using a commercial power supply and a curve fitting of the polarization curve [15]. Finally, a FC simulator based on the linearization of a PEMFC polarization curve and a Power Factor Corrector (PFC) power converter was presented [16]. The control strategy for the PFC power converter is a PI controller.

It can be inferred from the simulators described in the literature that three main components can be identified in a FC simulator: FC model, power converter topology, and the control scheme of the power converter. The following subsections provide a detailed literature review for each component of FC simulators.

1.1.1 Fuel Cell Models

Several FC models can be found in the electrochemistry literature. They can be classified as mechanistic and empirical models. In order to simplify experimentation, most models have been developed using laboratory single FC instead of FC stacks. Mechanistic models are based on electrochemical, mass transfer, fluid dynamics, and thermodynamics principles. Partial differential equations are employed to include dimensions and parameter variations [17], [18], [19]. Successful mechanistic models help to predict electrochemical processes and transport phenomena, which are needed to achieve further improvements in FCs technologies. Only a few mechanistic models that include dynamics have been developed [20], [21], [22]. Finally, dynamic models that account for water management have also been developed [23], [24]. The mechanistic models listed above have a complex mathematical nature and are solved using time consuming computational methods. Unfortunately, none of the existing mechanistic models can be solved on real time basis due to technological limitations. Since FC simulators are real-time systems, the use of a model with simple mathematical structure that can be computed with small effort is needed.

Empirical models show the advantage of a simplified mathematical representation in comparison with mechanistic models. Most empirical models characterize the electrical behavior of FC during steady state operation. Kim *et al.* [25] present an approach to represent the steady state polarization curve of PEMFC. Lee, *et al.* [26] obtained an improved model by extending the work in [25] to address the diffusion limitations on the cathode. Squadrito, *et al.* [27] introduced mass transport limitations empirically, which is also based on [25]. A semi-empirical approach was presented by Pisani [28] and Kulikovsky [29] for PEMFCs. Kulikovsky [30] also presented a semi empirical model of a DMFC by fitting experimental data. A hybrid model that combines empirical and mechanistic modeling was proposed for a commercial PEMFC by Amphlett *et al.* [31], [32], [33]. A model that predicts the dynamic transient response for the same commercial PEMFC is also proposed by Amphlett *et al.* [34]. Based on these hybrid models, an attempt to generalize and provide some geometric parameters has been proposed [35].

From the numerous FC models found in the electrochemistry literature only the work by Mann *et al.* [35] was included as part of a FC simulator. Correa, *et al.* [14] incorporated this FC model in a PC to provide a reference voltage to a power converter.

1.1.2 Converter Topologies

Four basic classifications of electrical power conversion exist: AC to DC, DC to DC, DC to AC and AC to AC. Since FCs are power sources that generate DC output voltage, power converters that produce DC output voltage are considered. Hence, AC to DC and DC to DC converters are investigated.

AC to DC converters present the advantage of direct connection to the AC line. The simplest way to achieve non-regulated AC to DC conversion is by using a diode bridge connected to an output filter. A similar arrangement where the output voltage can be controlled is obtained by replacing the diodes with Silicon Controller Rectifiers (SCR) [36]. This converter can be used for single-phase (4 SCRs) and three-phase rectification (6 SCRs). An LC filter with low cut of frequency is generally used to filter the pulsating waveforms generated by the bridge. The FC simulator approach by Correa *et al.* [14] uses a three phase fully controlled bridge rectifier to convert AC to DC.

Switched mode power supplies (SMPS) offer small weight and size, high efficiency, and excellent regulation to obtain DC to DC conversion. Operating SMPS with high switching frequency allows small size and weight of passive components leading to design with high power density. Three basic topologies can be identified: Buck or step down converter that produces an output voltage lower than the input voltage; Buck-Boost converter which is capable of voltage reduction as well as voltage increase; Boost or step up converter that produces an output voltage higher that the input voltage [36], [37]. Other converter topologies derived from the three basic topologies can be found: flyback, which is an isolated converter derived from the basic buck-boost topology; forward isolated converter derived from the basic buck topology; push-pull, which includes two switches and a center taped transformer (derived from buck); half bridge that contains two switches (derived from buck); full bridge that contains four switches (also derived from buck). Finally, the basic topologies can be used for AC to DC conversion. For example, an active rectifier (AC to DC conversion) with power factor correction can be obtained by using buck, buck-boost or boost topologies [38], [39], [40], [41].

Acharya *et al.* [15] proposed a FC simulator that employs a commercial programmable power supply from Magna-Power Electronics [42]. Even though important information such as transient response time can be found in [42], the topology of this power converter is not specified. Finally, Lee *et al.* [16] presented a FC simulator that uses a PFC based on a basic buck topology.

1.1.3 Control Schemes

The output voltage of a fully controlled bridge rectifier can be controlled by means of adjusting the firing angle of the SCRs [36]. The power converter of the FC simulator by Correa *et al.* [14] has a voltage close loop with a classic PI controller [43], [44]. The control strategy used for FC simulator based on a PFC converter [16] is also a PI controller. A good approach for the design of controllers for SMPS based on classic compensators can be found in [37]. Since a model of the SMPS is required, a state space average model should first be obtained [45].

State space averaging method has been extensively used in the area of power electronics converter control. However, this linear control approach presents some disadvantages when compared to non-linear control. In general, non-linear control schemes provide improved dynamic response and robustness [46], [47]. In fact, power converters are in nature non-linear systems, which can be classified as variable structure systems [48]. Hence, power converters can be controlled by sliding mode regime, switching surface control, or hysteresis control [47]. Unlike other FC simulators, this thesis takes advantage of a non-linear control scheme to successfully reproduce the electrical dynamic behavior of FCs.

1.1.4 Limitations of Previous Fuel Cell Simulators

As described in the preceding subsections, the FC simulator proposed by Correa *et al.* [14] uses a fully controlled bridge rectifier with PI controller. From the point of view of the power converter topology, this system has sluggish dynamic response due mainly to the large LC filter required to reduce the low frequency voltage ripple produced by controlled rectifier. This filter, with low cut-off frequency, limits the dynamic response of the converter and makes the converter bulky. In addition, there is a lack of parameter availability for the PEMFC model employed in this simulator. Commercial confidentiality is perhaps one of the reasons why FC producers do not release the parameters.

The FC simulator of a SOFC [15] is based on a polynomial curve fitting of the polarization curve. Since the polarization curve only represents the steady state behavior for a given operating condition (fuel concentration and temperature), this implementation is not able to reproduce the dynamic behavior introduced by the double layer capacitance phenomenon [1]. This leads to inaccurate conclusions for current ripple operation or sudden load changes. In addition, the simulators in [14] and [15] depend upon a computer, communication cards, and licensed software, which add cost and increase the size of the system.

Finally, the FC simulator based on a PFC power converter [16] has a serious inherent problem with the selected topology. In order to achieve power factor correction with a PFC topology, sinusoidal current waveform is extracted from the AC line through a rectifier circuit. This current is supplied to the output filter capacitor of the converter producing low frequency voltage ripple [36]. Provided that the FC delivers DC output voltage with no ripple during steady state operation, using a PFC topology results in a poor reproduction of the FC output voltage behavior. In addition, the FC model employed in this simulator is based on linear regression fit of the polarization curve. This approach, not only departs from the highly non-linear characteristics of FCs polarization curve, but also neglects the dynamic effect introduced by the double layer capacitor.

In order to obtain a good reproduction of the electrical dynamic behavior of a FC two preliminary conditions should be fulfilled:

- The double layer capacitor should be included in the model to accurately model the dynamic behavior of the FC.
- The converter should have a fast dynamic response that minimizes error during transients or current ripple operation.

In a FC simulator with an ideal power converter, the accuracy of the emulation depends upon the FC model. On the other hand, the performance of the FC simulator using an ideal model is limited by the response of the power converter. Given that neither an ideal power converter nor a perfect FC model can be achieved, the overall performance of the system will be determined by a proper choice of power converter and FC model. For example, the FC simulator proposed in [14] is inherently limited by a sluggish power converter, whereas the FC simulator in [15] cannot be used to evaluate dynamic response due to the nature of the model. A review of the literature shows that the dynamic behavior of FCs is not well understood. For this reason it is first necessary to investigate the dynamic characteristic of the FC before attempting to design the FC simulator.

1.2 Thesis Objectives

Evaluation of the few available literature on recent development of FC simulators reveals limitations associated with modeling accuracy and power converter performance. The main objective of this thesis is to develop a FC simulator system that provides improved accuracy while enhancing the realism of the emulation. To this end, the following components that determine the effectiveness of a FC simulator will be addressed throughout the thesis: FC model that provides reference signal to the system, topology of the power converter, and selection of the control scheme for the power converter.

The electrical behavior of an actual FC will be first studied and analyzed with the objective of gaining insight into the steady state and dynamic operating characteristics of FCs. The experimental results obtained through this study will be used to provide understanding of the parameter of a FC generic model. The power converter topology selection and its control strategy will be addressed considering the experimental dynamic response of the FC under different types of load. Finally, two different approaches to a FC simulator will be presented.

1.3 Thesis Organization

The development of the FC simulator is organized into various units and presented in seven chapters for easy reading and quick access to specific information. The thesis begins with the problem definition, literature review, and thesis objectives in chapter 1.

Chapter 2 contains the study and analysis of the electrical behavior of a Direct Methanol FC (DMFC) by focusing on the electrical dynamic characterization of a single DMFC. The results from laboratory tests on a single DMFC are presented. These results provide insight into the dynamic behavior of the DMFC and an understanding of the parameters that are used to model the DMFC.

The development of a special Electronic Load (EL) for FC systems is presented in chapter 3. This low cost EL was used to perform custom automated tests on the FC and the power converter throughout the work. The EL plays an important role as part of the hardware in the loop concept described in chapter 6.

In chapter 4, the development of a fast dynamics power converter for FC simulators is described. The power converter was designed taking into consideration the dynamic requirements to successfully reproduce the behavior of a FC. A control scheme based on switching surface control is first investigated and then employed to achieve near time optimal response in the converter.

A stand-alone FC simulator based on an empirical model and a low cost Digital Signal Processor (DSP) is presented in chapter 5. The system provides the advantages of eliminating the dependence upon a computer, communication cards, and licensed software, resulting in a small low-cost system. Experimental results in a laboratory prototype presented in the chapter show that the simulator accurately emulated the steady state and dynamic behavior of an actual FC under constant current steps loading condition.

In chapter 6 a novel real-time FC simulator based on a small single cell is proposed. This system overcomes modeling drawbacks and expands the features of the existing designs by replacing the computer model of the FC with an actual small single FC.

Chapter 7 presents the conclusions of the thesis and recommendations for further work.

Chapter 2

Dynamic Behavior of a Direct Methanol Fuel Cell

Fuel cells (FC) are devices that convert electrochemical energy into electrical and thermal energy. Among several types of fuel cells, Direct Methanol Fuel Cells (DMFCs), also known as Alcohol-fed Fuel Cells, are considered more practical than hydrogen based cells for portable applications. The main reason is that the number of additional equipment required to run the cell is reduced to minimum and the possibilities of storing methanol is more convenient. A brief overview of the electrochemical process of the DMFC is presented in the chapter with a view to obtain a generic electrical model of the FC.

The aim of this chapter is to clarify the electrical behavior of DMFC by focusing on the electrical dynamic response of a single DMFC. Even though dynamic experimental results of FCs have been included in previous work [33] [34], this chapter presents extended experimental results from an electrical point of view to cover the most important expected dynamics. Since the selected DMFC setup is well known and has been extensively used in electrochemistry laboratories [80], it is not in the scope of this work to undertake performance comparison of this standard arrangement with other FC setups or membranes. Instead, the characterization of the dynamic behavior is addressed. Discussions regarding the operating points, power extraction, and FCs model are also included. The work described in this chapter was presented at Newfoundland Electrical and Computer Engineering Conference (NECEC) in 2004 [49].

A fast dynamic electronic load was a part of the requirement to perform the experiments. For this reason, a flexible FC electronic load was built and is described in detail in chapter 3. This chapter illustrates the DMFC dynamics behavior to clarify "what can be expected" from a fuel cell before starting any power electronics design.

2.1 Direct Methanol Fuel Cell Description

Figure 2.1 shows the cross-section of a DMFC, where three different types of layers can be identified as: Polymer Electrolyte Membrane (PEM) in the center, catalyst coated porous electrodes for methanol oxidation in the anode, and oxygen reduction in the cathode. These three components comprise the DMFC Membrane Electrode Assembly (MEA). The PEM is a perfluorosulfonic acid based polymer (Nafion), the anode catalyst is a Platinum-Ruthenium (Pt–Ru) alloy, and the cathode catalyst is Pt black. The Pt-Ru and Pt catalysts are spread onto a porous carbon fiber to form the conductive electrodes of the anode and cathode respectively.

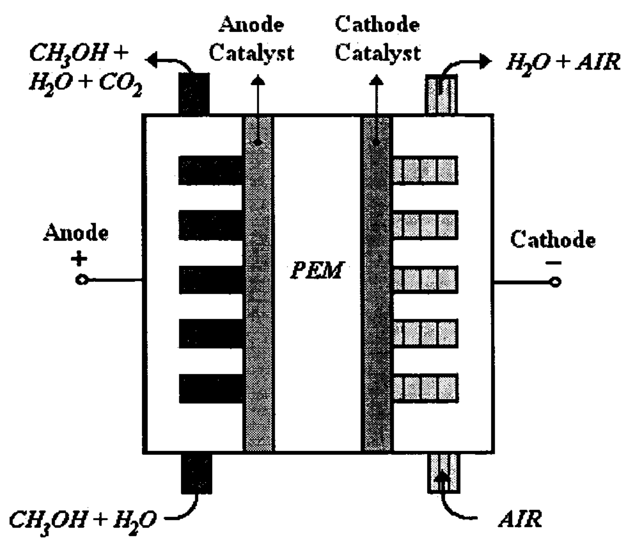

Fig. 2.1 Cross-section of the DMFC

Figure 2.2 shows a picture of a 5.3 cm^2 MEA including the PEM and the two electrodes. The MEA is placed between plates that contains channels for fuel or air distribution and provides electrical contact with the porous electrodes. Figure 2.3 shows a picture of internal view of the plates where the small channels can be identified.

Fig. 2.2 Electrode Membrane Assembly: PEM, anode and cathode porous electrodes

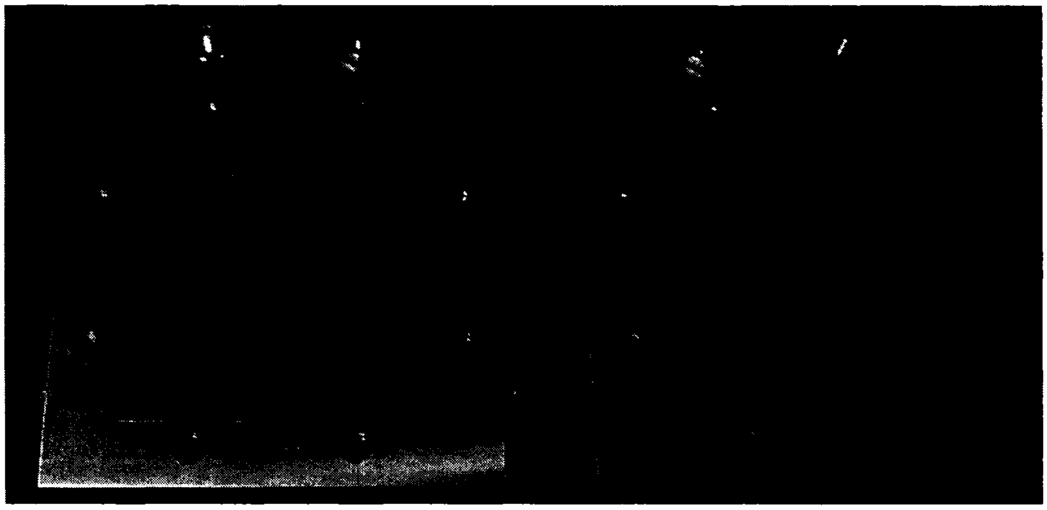

Fig. 2.3 FC plates: anode (left) and cathode (right)

As the name suggests, the DMFC is directly supplied with methanol and water through the reactant channel of the anode plate. The fuel reaches the catalyst layer where the chemical reaction occurs resulting in carbon dioxide, protons, and electrons. The protons are transported through the PEM towards the cathode. The electrons circulate externally through the desired electrical load towards the cathode producing work. Since the cathode is fed with air, the proton and electrons that reach the cathode reduce the oxygen in the air to form water. The electrochemical reaction in the anode of the DMFC can be described as

$$Anode: CH_3OH(l) + H_2O(l) \rightarrow CO_2(g) + 6H^+ + 6e^-, \qquad (2.1)$$

where (l) is liquid state and (g) is gaseous state. On the cathode side the reaction is

$$Cathode: \frac{3}{2}O_2(g) + 6H^+ + 6e^- \rightarrow 3H_2O(l) \qquad (2.2)$$

Finally, the overall reaction is given by

$$Overall: \quad CH_3OH(l) + \frac{3}{2}O_2(g) \rightarrow CO_2(g) + 2H_2O(l) \qquad (2.3)$$

2.1.1 Fuel Cell Model

A generic FC model involving the electrochemical phenomena is described below. As can be seen in Fig. 2.2, the generic FC model can be represented as an electrical circuit. The ideal voltage developed by E corresponds to Nerds equation that is a function of the fed methanol concentration. The theoretical predicted value lies around 1.23V for a single cell. However, a typical practical open circuit output voltage stays below 0.8V. Several effects cause a voltage drop or irreversibility, namely, activation losses (Taffel equation), fuel crossover and internal currents, ohmic losses, and mass transport. A simple general equation gives a conceptual description of all the effect combined [1], [35]:

$$V_o = E - \Delta V_{Ohmic} - \Delta V_{Act} - \Delta V_{Trans} \qquad (2.4)$$

The second term ΔV_{Ohmic} represents the voltage drop due to the electrodes resistance (electrons) and membrane conduction properties (protons). The third term of the equation ΔV_{Act} corresponds to the activation of the anode and cathode, which depends primarily on the cell temperature, the catalyst effectiveness, and the roughness of the electrodes. Finally, ΔV_{Trans} is due to a change of the concentration of the reactants in the region of the electrodes. In addition, there is an important element known as "charge double layer" closely related to the electrical dynamic behavior of the FC. An equivalent capacitor C was found suitable to represent this phenomenon [1]. The action of the equivalent capacitance in conjunction with ΔV_{Act} and ΔV_{Trans} is described as follows:

$$\frac{d(\Delta V_{Act} + \Delta V_{Trans})}{dt} = i_o \cdot \frac{1}{C} - \frac{\Delta V_{Act} + \Delta V_{Trans}}{R_a \cdot C} \qquad (2.5)$$

where i_o is the FC output current, and R_a is a non-linear resistor that produces both ΔV_{Act} and ΔV_{Trans} drops during steady state operation.

The resulting electrical equivalent model of the FC is shown in Fig. 2.4. For a given operating condition, i.e. specified temperature, fuel concentration, and air flow, the parameters in the model will remain constant, except for the non-linear resistor which is a function of the FC output current i_o. A change in the operating conditions produces a change in the values of the model parameters.

Figure 2.5 shows the output characteristics or polarization curve of the FC model under steady state operation. The curve shows the non-linear effect of the resistance R_a.

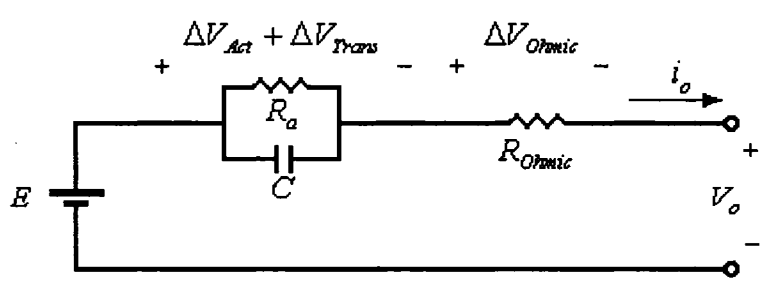

Fig. 2.4 Electrical equivalent model the FC

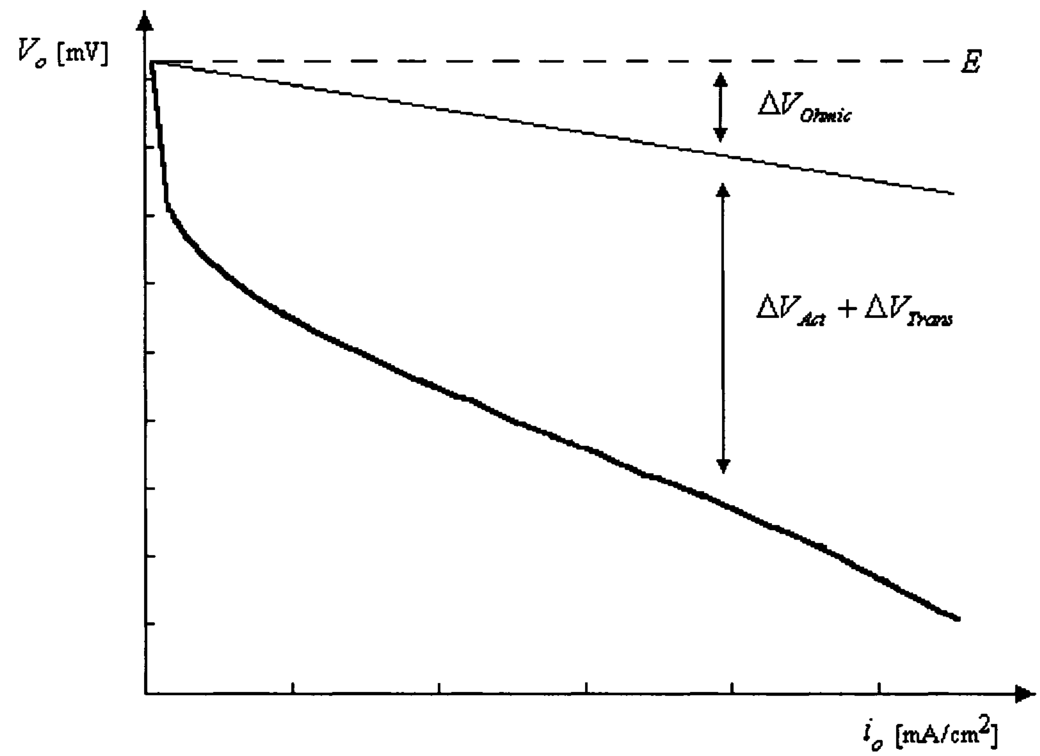

Fig. 2.5 FC polarization curve

2.1.2 Fuel Cell Setup Description

The single FC used in this research is of a DMFC type and is shown in Fig. 2.6. It was made available to us at the Chemistry Department, Faculty of Science. The Anode, consisting of 4 mg/cm^2 Pt/Ru blank and 15% Nafion and 14% PolyTetraFluoroEthylene (PTFE) on Toray carbon fiber paper, was donated by H Power Corp. The cathode, donated by Ballard Power Systems, consists of 4 mg/cm^2 Pt black on PTFE treated Toray carbon fiber paper. Before its operation Nafion115 membrane (Aldrich) was cleaned using 5% H_2O_2(aq), 1M H_2SO_4(aq) (1 h at 60-80°C in each solution) and water.

The membrane and electrodes ($5.3cm^2$) were placed into brass die and pressed for 3 min at 130°C with Carver Laboratory Press (model M) under 155 kg/cm^2 pressure.

The MEA was evaluated in a commercial 5.3 cm^2 active area cell fed with 1 Mol aqueous MeOH at 0.15 *mL/min* and dry air at fixed flow rate of 75 *mL/min* Experiments were conducted at a cell temperature of 60+/-1 °C. Several tests were performed to determine the dynamic behavior of the fuel cell.

Fig. 2.6 DMFC experimental setup

2.2 Dynamic Behavior of the Fuel Cell

For the FC setup described above the steady state polarization curve basically depends on the cell operating temperature, methanol concentration, and flow rates (operating conditions). A change in the operating conditions modifies the performance of the FC, and hence the polarization curve. It should be pointed out that the transition from a given polarization curve to another is sluggish. The main reason for this behavior is that a mechanical actuator with slow response is used to change the FC operating conditions. Hence, a fast dynamic response of this power source should not be expected by means of modifying the operating conditions. However, a dynamic behavior of the FC exists when the output current changes for fixed operating condition. A number of step tests described below were performed to determine the dynamic behavior of the fuel cell. In this section the dynamic behavior of the single DMFC is investigated for the following operating conditions:

- 1 M aqueous MeOH at 0.15 *mL/min*
- Dry air at fixed flow rate of 75 *mL/min*
- Cell temperature at 60+/-1 °C.

The goal of the investigation is to characterize the behavior and determine the operating limits of the FC for step changes in the output current, output power demands, sudden resistive load changes, and current ripple operation.

2.2.1 Current Steps

The experimental results described in this section were performed using the electronic load for FC systems described in chapter 3. The electronic load is programmed to force a constant current at the output of the FC. As a result of the current demand, the FC output voltage changes dynamically. Figures 2.7 and 2.8 show the experimental results obtained for a series of current step tests. The FC under test was able to cope with the sudden current demands, delivering the output current immediately. The bold line of the *v-i* graph of Fig.2.7 represents the steady state polarization curve. The Operating Point (OP) after a transient completion should therefore lie on this steady state curve. The dashed curve on the *v-i* graph corresponds to the OP trajectory or dynamic path for the series of current steps. The initial OP starts at $20mA$ and $650mV$. Once the first current step is applied, the OP "jumps" to the demanded $100mA$ while the voltage decreases to $625mV$. Thereafter, the OP remains at a constant current locus of $100mA$ and in steady state the voltage settles to $500mV$. For the remaining current steps the OP continues behaving in the same fashion. Two important points can be highlighted from this experiment: 1) The FC is able to adjust its output current instantaneously to match the current demand, and 2) the OP can depart significantly from the steady state polarization curve during transients. Since the area under the OP represents the instantaneous output power of the FC, its trajectory during current steps transients reveals output power beyond and below the steady state power availability. It can be noticed from Fig. 2.7 that positive current steps (i.e. from $100mA$ to $200mA$) lead to a transitorily OP over the polarization curve, thus providing extra power during transients. On the other hand, negative current steps (i.e. from $200mA$ to $100mA$) result in a transitorily OP below the polarization curve leading to a reduced power delivery during transients.

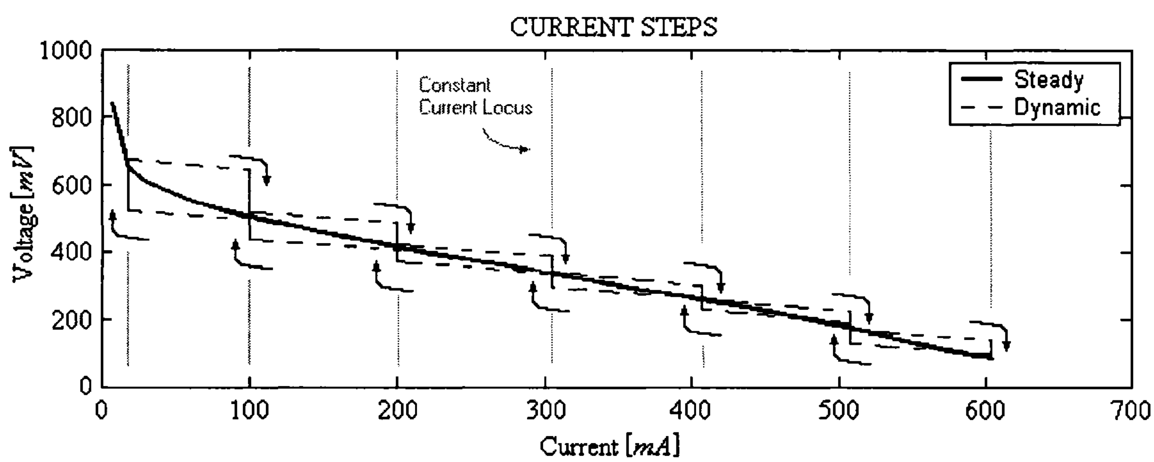

Fig. 2.7 The dynamic response of the DMFC to a series of current steps: *v-i* plot.

The *v-i* plot presented in Fig. 2.7 provides a simple approach to represent both the steady state polarization curve and the trajectory of the OP during transients without time as a variable. In order to clarify the time evolution of the FC dynamics, a time domain plot is included in Fig. 2.8. In the same way as Fig. 2.7, the initial current step of Fig. 2.8 starts with $20\,mA$ and increases to $100\,mA$ for $t = 0$. The FC output voltage starts at $650\,mV$ and decreases during the transient until it reaches $500\,mV$. A second current step from $100\,mA$ to $200\,mA$ is applied for $t = 6\,s$ and the output voltage decreases again as a result of more output current. For the remaining positive current steps, the voltage continues to reduce until it reaches the steady state value. When $t = 36\,s$ a successive negative current steps start resulting in an increase of the output voltage. The voltage transient for each current step (both positive and negative) seems to behave like a first order system with a time constant of $\sim 1.5\,s$ except for the very first and last current steps. This is due to the highly non-linear nature of the FC in the low current region. The instantaneous power evolution is also shown in Fig. 2.8 with a thin line, which shows instantaneous peak power beyond steady state power for positive current steps, and instantaneous power below steady state power for negative current steps.

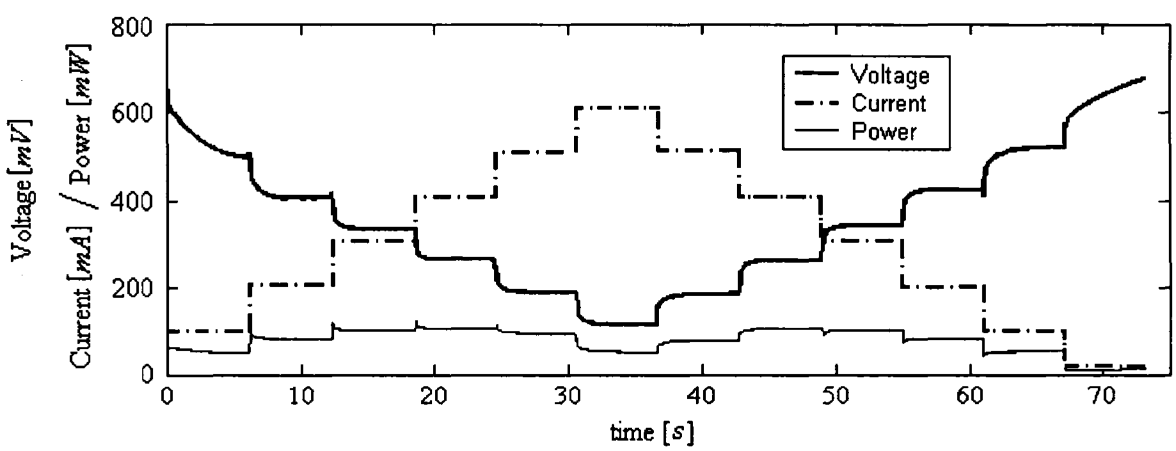

Fig. 2.8 The dynamic response of the DMFC to a series of current steps: Time domain plot.

2.2.2 Constant Power Steps

A test of constant power steps was performed with the objective of clarifying that the DMFC can cope with the sudden power demands within its power limits. Further comments about peak power availability beyond the maximum power point are included at the end of the chapter.

Figure 2.9 and 2.10 depict the *v-i* and time domain plots for this test. The dashed line on the *v-i* plot shows the trajectory of the OP for consecutive power steps demand ($52.4mW$, $86.0mW$, and $104.5mW$). The initial OP, located at the top of the steady state curve, denotes a no-load condition. When the first power step demand is applied the OP "jumps" to the corresponding constant power locus. After that the OP progressively moves towards the intersection between the power locus and the steady state polarization curve. The remaining power steps behave in the same way. The time domain plot shows how the current increases to compensate for the progressive voltage reduction until the final OP is reached after a transient of 17 seconds for the first step and about 3 seconds for the following steps.

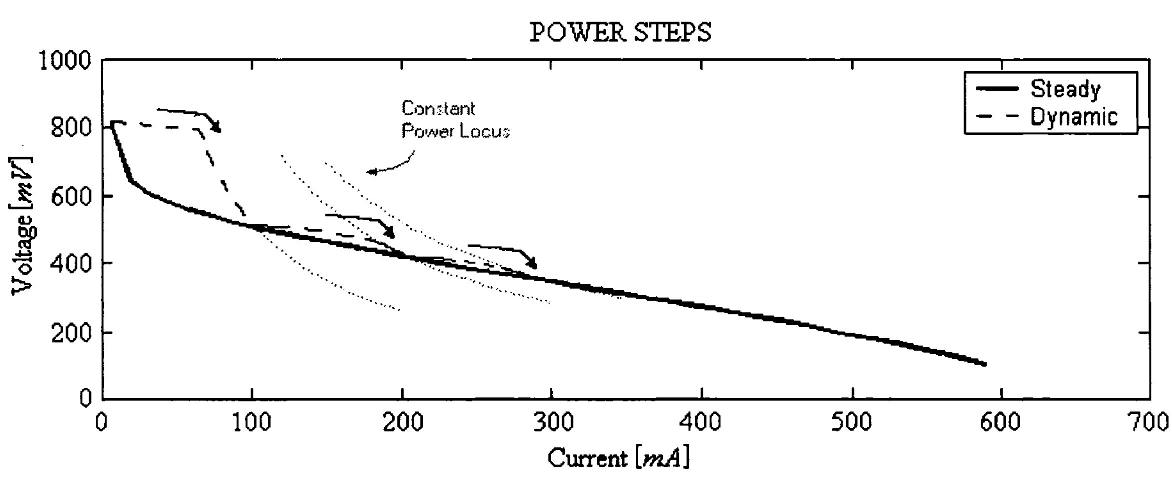

Fig. 2.9 The dynamic response of the DMFC to a series of power steps: *v-i* plot

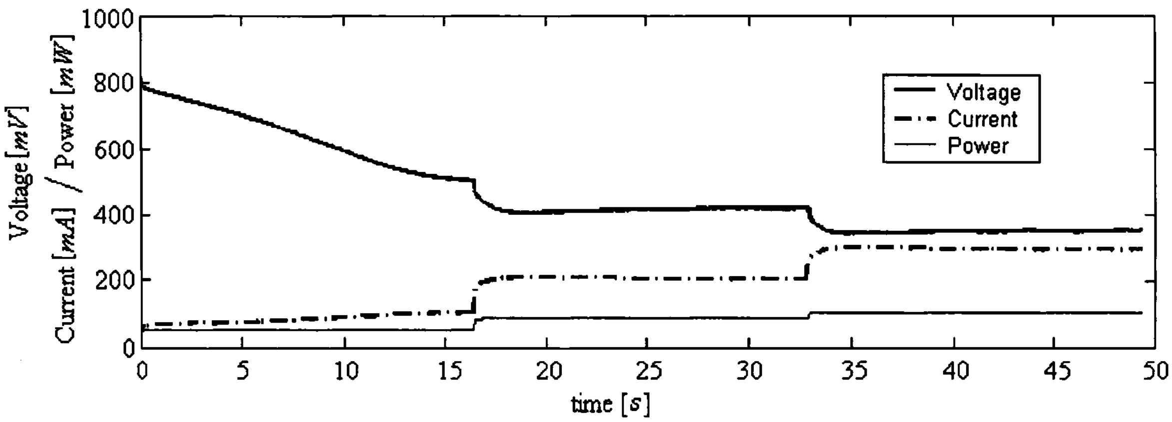

Fig. 2.10 The dynamic response of the DMFC to a series of power steps: Time domain plot

2.2.3 Resistive Steps Test

This test was conducted by performing sudden resistive changes and is intended to explain the behavior of the FC under a simple load resistance variation. The experiment was performed with 4.76Ω for the first step, followed by 2.11Ω, 1.11Ω, 0.64Ω, 0.41Ω, and 0.21Ω. The experimental results are depicted in Fig. 2.11 and 2.12 for *v-i* plot and time domain plot respectively. The application of a resistive load to the FC forces the OP on the *v-i* plot to stay at some point on the corresponding constant resistance locus (straight lines through the origin). At the beginning of the transient, the OP lies far from the steady state polarization curve. Thereafter, the OP is directed towards the polarization curve following the trajectory of the constant resistance locus. When the following step change in resistance is applied, the OP is forced to "jump" to a new constant resistance locus as can be appreciated on the *v-i* plot of Fig. 2.11. While the dashed line on the *v-i* plot represents the OP dynamic trajectory, the time domain plot of Fig. 2.12 gives more insight into the transient duration. The voltage transient for each resistive step shows a time constant of about $1.5s$ except for the very first step in the low current region. This is due to the highly non-linear nature of the FC for light loading conditions.

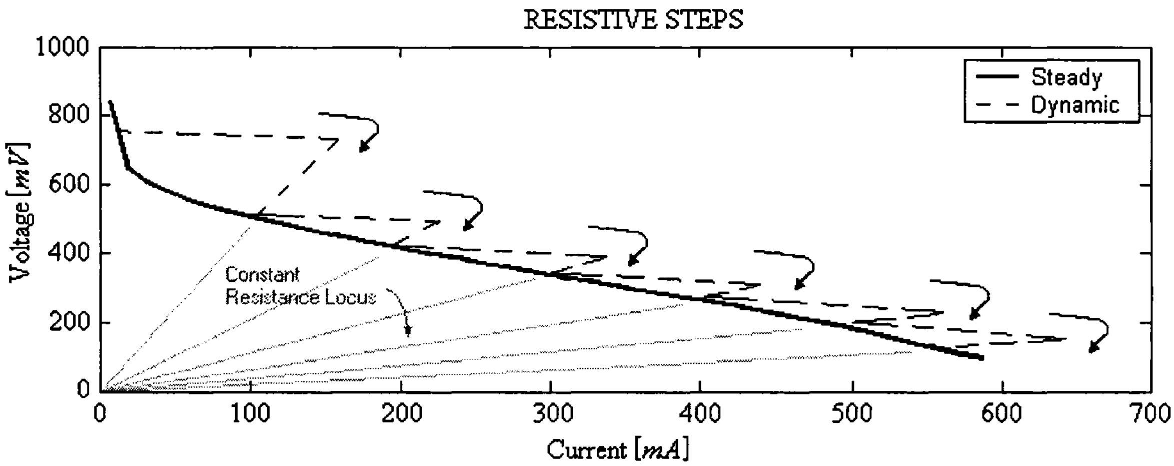

Fig. 2.11 The dynamic response of the DMFC to a series of resistive steps:

v-i plot.

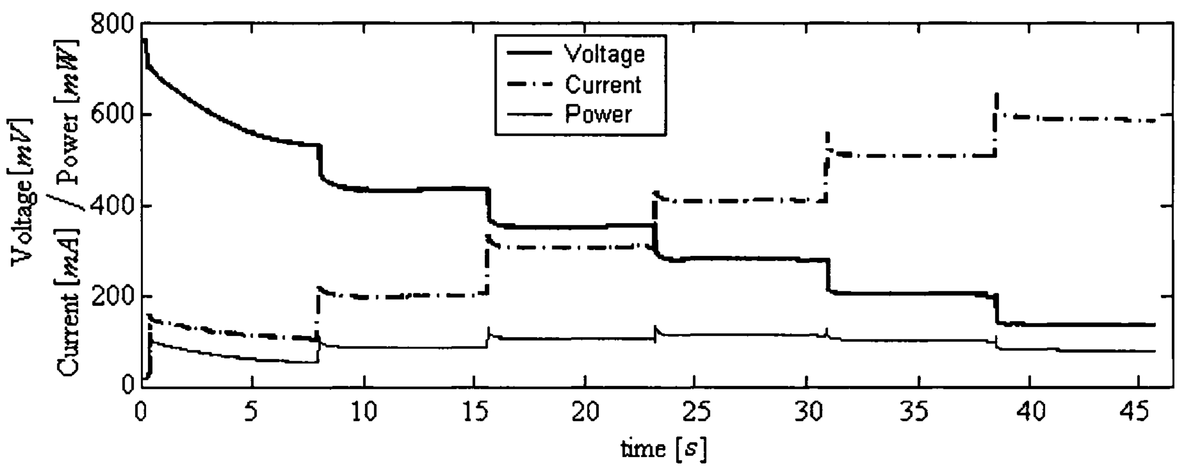

Fig. 2.12 The dynamic response of the DMFC to a series of resistive steps:

Time domain plot

2.2.4 Current Ripple Test

Fuel cell inverters are included among the promising applications for FC systems. Portable inverters, distributed power generation, Uninterruptible Power Supplies (UPS), avionics inverters, are some of the application areas of FCs [50], [51]. AC current ripple on the DC power source is inherent to single-phase and three-phase inverters. For single-phase inverters, the frequency of the ripple is double the frequency of the output voltage. Commercial FC behavior under 120Hz current ripple has been recently evaluated [52] and an analysis of its impact on the FC is still under study [53]. A conceptual understanding of the issue is essential for power electronics designers. Eliminating the ripple could imply a large FC output filter or an additional power electronics converter for the system.

Experimental results and discussion for a better understanding of the current ripple effect are presented in this section. Fig. 2.13 shows a *v-i* plot with a DC OP at $325\,mA$ with a superimposed 25Hz and 400Hz current ripple. Each frequency was tested individually but the plot includes an overlap for the two tests. Fig. 2.14 is a zoom-in of the previous *v-i* plot, which highlights the difference between the 25Hz and 400Hz tests. It can be noted that the current ripple for both frequencies has the same average value and both amplitudes are 50% of the declared central OP of $325\,mA$.

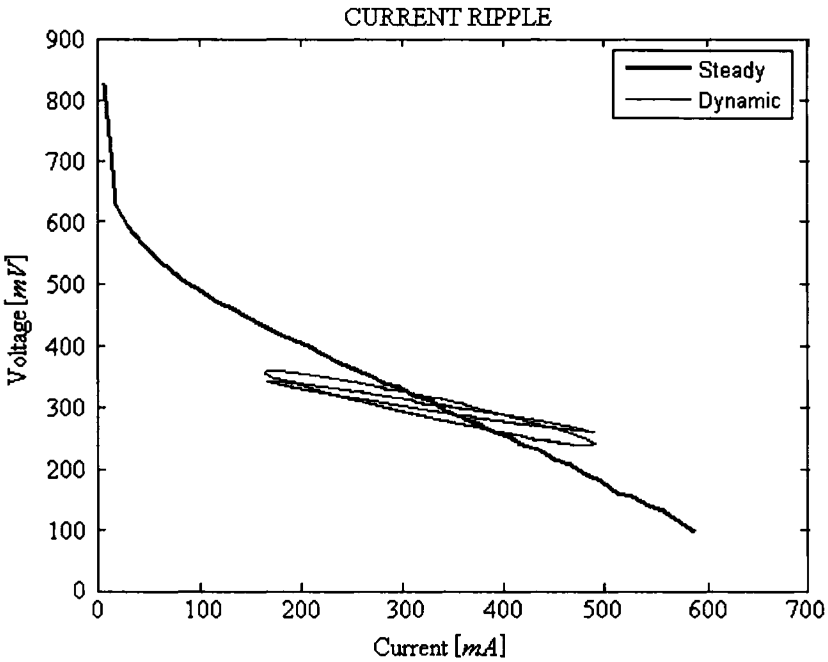

Fig. 2.13 DC+AC current test of the DMFC for 25Hz and 400Hz: *v-i* plot

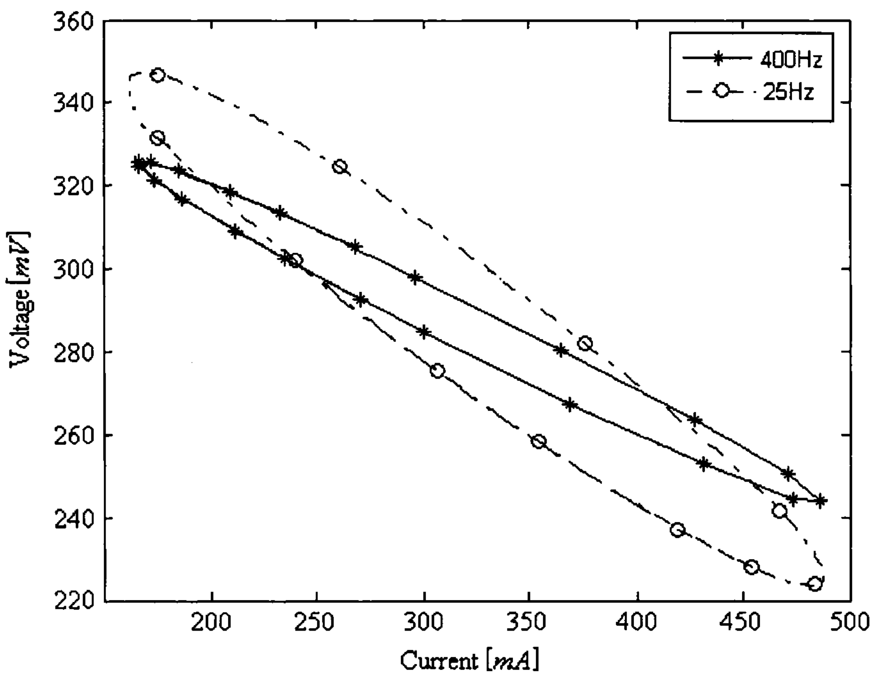

Fig. 2.14 DC+AC current test of the DMFC for 25Hz and 400Hz: Zoom of the *v-i* plot

As can be seen in the 400Hz test, the slope and the amplitude of the hysteresis trajectory are reduced. This leads to an increase in the output power availability in comparison with the 25Hz case. The hysteresis behavior, which denotes a phase difference between the output current and voltage, is associated with the double layer capacitor. If the frequency of the current ripple increases further, the hysteresis behavior disappears (the double layer capacitor impedance is significantly reduced) and the trajectory becomes a straight line with a slope (due to the R_{Ohmic} effect). This results in an increase of the output power. However, the average output power with current ripple always stays below the output power for the DC operating point. This is explained by the fact that the average current value for DC and DC+AC is the same and the only way to achieve the same output power is with a completely horizontal trajectory (constant voltage), which is not feasible due to the R_{Ohmic} effect. Fig 2.15 shows the time domain plot for the test already explained. The difference in voltage excursion is better appreciated in this graphic.

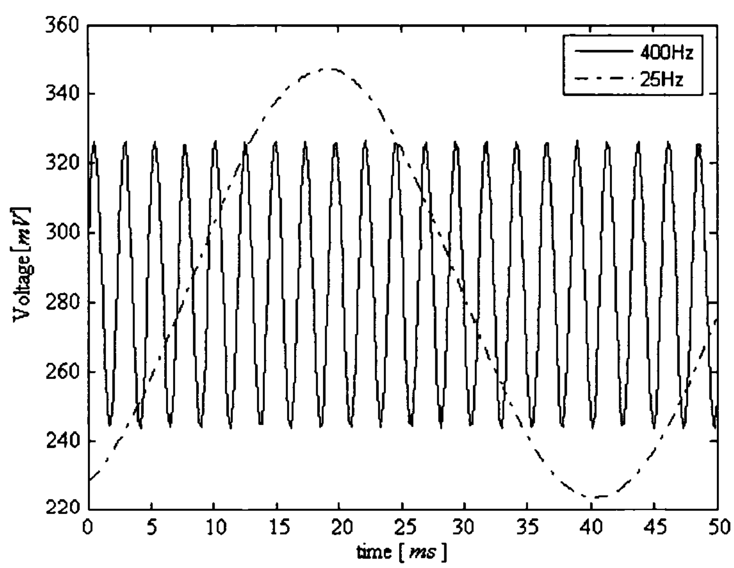

Fig. 2.15 DC+AC current test of the DMFC for 25Hz and 400Hz: Time domain plot

The power extraction for different current ripple amplitude and frequency as a percentage of the power without ripple is presented in Fig. 2.16. The test was performed for amplitudes of 10%, 30% and 50% of the DC OP ($325mA$). The curves show the decrease in power extraction when the amplitude of the ripple increases. An increase in the frequency of the current ripple helps to increase the power extraction. Hydrogen fuelled FCs, also known as Proton Exchange Membrane FC (PEMFC), reported similar effects. [52].

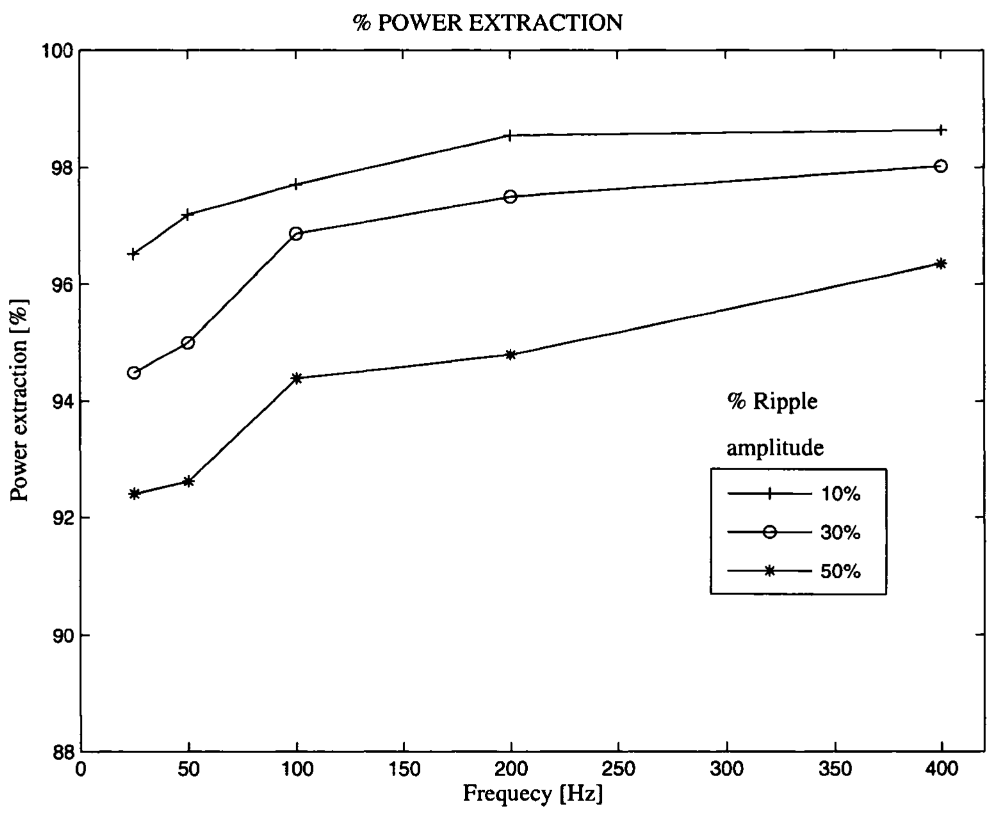

Fig. 2.16 FC power extraction with current ripple as a percentage of the power extraction without ripple.

2.3 Experimental Results and the Fuel Cell Model

The electrical model of the FC introduced in section 2.1 provides a reasonable model representation of the real FC considering its simplicity. However, obtaining those electrical parameters requires dealing with instrumental methods in electrochemistry [54]. In particular R_a is highly non-linear and depends upon the OP. In addition, for low current OPs the model deviates from the actual FC behavior. The following discussion is intended to provide a qualitative analysis of the experimental results from the viewpoint of the generic electrical model of the FC.

An inspection of the generic model presented in Fig. 2.4 reveals that any sudden current demand is transitorily driven by the double layer capacitance (C). This means that the resistor R_a is by-passed while C is being charged. Tests on the actual FC shows that a sudden change in the current demand produces an instantaneous voltage drop on the FC, which can be associated with the model drop due to R_{Ohmic}. Thereafter a first order voltage transient can be observed according to the capacitor charging process. During steady state operation, the capacitor is charged and its voltage is $\Delta V_{Act} + \Delta V_{Trans}$, which is the product $i_o \cdot R_a$. There is also evidence to support the idea of an almost constant R_{Ohmic} since every current jump is associated with a constant slope trajectory on the *v-i* characteristic. With respect to the hysteresis trajectories under current ripple operation, there is some coincidence between the model and the actual behavior. The hysteresis on the *v-i* plot is basically due to current and voltage phase shift. The current ripple is leading in relation to the voltage for frequencies where C has impedance in the order of R_a value. For a current ripple with a very low frequency (i.e. 0.1Hz) the C is neglected and the OP trajectory follows the steady state curve determined by R_a(non-linear) and R_{Ohmic}. On the other hand, a high frequency current ripple (i.e. 1kHz) defines a linear OP trajectory. The slope of the trajectory corresponds to the R_{Ohmic} effect but the pivot point is still the DC OP over the steady state polarization curve.

2.3.1 Peak Power Availability

Peak power availability beyond the maximum power point was detected during the experimental tests. Whenever the OP is below the maximum power point, a sudden current demand could force the OP to "jump" to a location where the instantaneous power is greater than the maximum power point. An explanation from the point of view of the model suggests that the transient lasts while C is charged to the R_a final potential. Fig. 2.17 shows a constant current step that is able to extract a peak power that is twice the maximum steady state power point. The final location of the OP over the steady state curve corresponds to the maximum power point. The area under the OP trajectory is the instantaneous power delivered by the FC. The thin dashed line on the *v-i* plot shows the output power vs. current for the steady state operation (not during transients). A time domain plot is included in Fig. 2.18 to clarify the transient evolution.

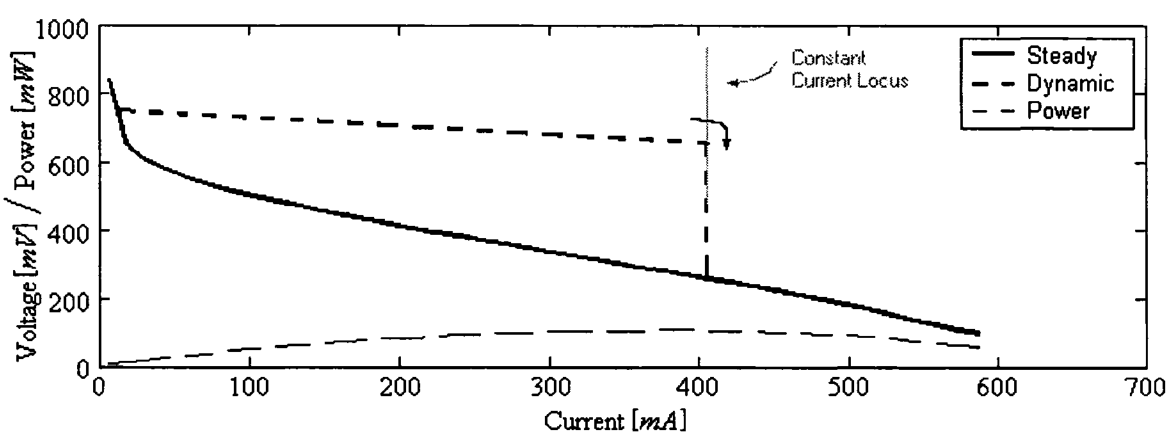

Fig. 2.17 FC peak power extraction from no-load to 400mA: *v-i* plot

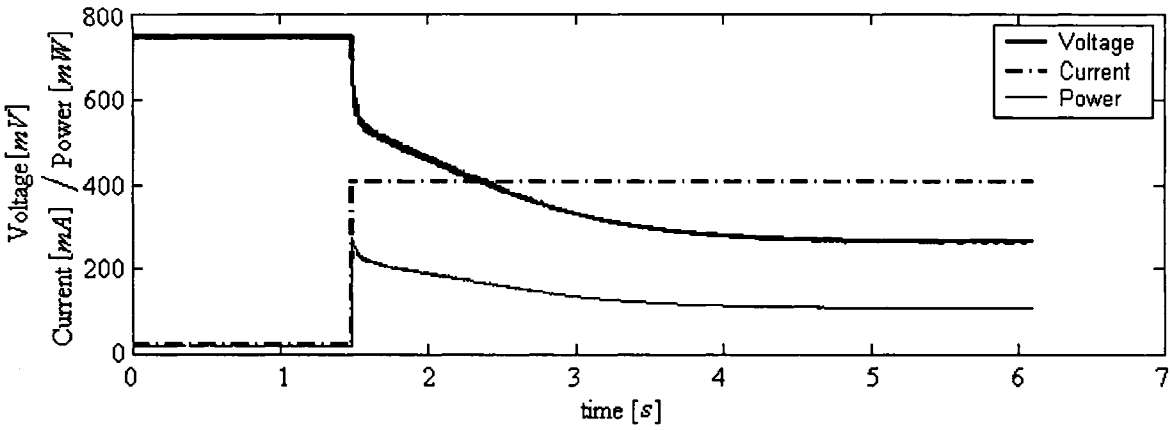

Fig. 2.18 FC peak power extraction from no-load to 400mA: Time domain plot

2.4 Summary

The dynamic behavior of a Direct Methanol Fuel Cell has been described, providing a clarification of the most expected dynamics with a simple approach. The electronic load used to perform the experimental dynamic test on the FC is described in Chapter 3. The experimental results were discussed and used to examine the accuracy of the generic dynamic model of the FCs. The experimental results are also used in chapter 4 to evaluate the dynamic requirements of the power converter to successfully reproduce the behavior of a FC.

Chapter 3

Electronic Load for Fuel Cell Systems

Measurement instruments for FC characterization, which are commercially available [55], mainly focus on electrochemistry techniques such as impedance spectroscopy and voltammetry. The main drawbacks of these instruments are lack of flexibility and high cost. Such instruments cannot be reprogrammed to perform custom automated tests. In this chapter, a special Electronic Load (EL) developed for FC characterization is presented.

The special features of the EL developed to perform the tests described in Chapter 2 are described. The EL design includes three basic components: power stage, instrumentation, and control software. In addition, two different versions of the EL employed during the course of this research are also covered in this chapter.

3.1 Hardware Description

The EL presented in this chapter is an embedded system that consists of a combination of hardware and software with the particular purpose of measuring FC's dynamic behavior. This section provides a description of the hardware that includes a power stage, instrumentation, and interface with a PC.

3.1.1 Power Stage and Instrumentation

Fig. 3.1 shows a conceptual schematic of the EL that includes the following components:

- Controlled current source
- Signal generator
- Signal conditioning stage

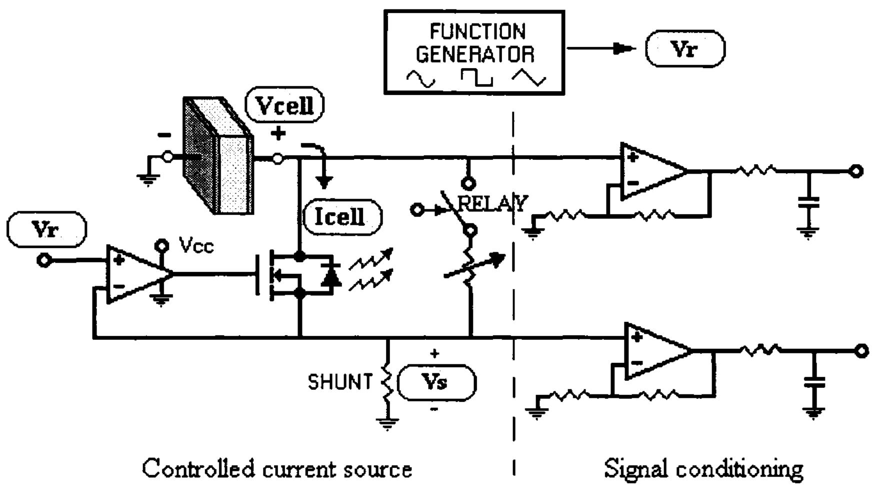

Fig. 3.1 Schematic of the electronic load power stage and instrumentation

The schematics of Fig. 3.1 can be divided into two parts: controlled current source on the left side of the dashed line, and signal conditioning stage on the right side of the dashed line. The current source operates according to its reference voltage V_r supplied by the function generator/PC. Provided that the operational amplifier inverting input follows the non-inverting input, it is expected that

$$V_s \approx V_r \tag{3.1}$$

The output voltage of the operational amplifier drives the MOSFET in such a way that the voltage developed across the shunt resistor (V_s) matches the reference voltage (V_r).

Thus, the MOSFET behaves like a variable resistor. This is achieved by controlling it over the linear region of its operating curve. When the reference voltage $V_r = 0$, the EL behaves like an open circuit. For $V_r > 0$ the EL varies its equivalent resistance, dissipating the power extracted from the FC into heat across the MOSFET and the shunt resistor. The fuel cell output current is given by

$$I_{CELL} = \frac{Vs}{R_{SHUNT}} = \frac{Vs}{R_{SHUNT}} \quad . \tag{3.2}$$

As can be seen in the experimental results in Chapter 2, the single FC provides an output voltage close to $100mV$ at maximum output current of $600\,mA$ in steady state operation. For this reason the MOSFET and the shunt resistor requires values in the order of $m\Omega$. Finally, a variable resistor is included in the design to allow the FC to be tested under resistance step changes. This is achieved by closing a relay as shown on Fig 3.1.

Current measurement is obtained by means of the voltage developed across the shunt resistor, while voltage measurement is taken directly from the FC terminals. The signal conditioning stage contains ultra-low offset operational amplifiers (AD8554) that adjust the current and voltage measurement to the required levels for Analog to Digital Converter (ADC) interfacing. Figure 3.2 shows a picture of the prototype described in this section.

3.1.2 Interfacing with a PC

The EL is connected to a PC through a RTI815 acquisition board. The RTI815 is equipped with 12 bits DAC and ADC, providing a good resolution for data acquisition and operation of the EL. The conceptual schematic of the complete system is shown in Fig. 3.3. The PC can control the function generator frequency and provide a reference voltage (Vr_1) to the EL power stage. A 'C' language software routine runs in the PC, controlling the EL in order to extract power out of the FC and perform the acquisition of the current and voltage measurements. This arrangement allows the fuel cell to operate within its limits during dynamic operation and also ensures a complete record of the current and voltage transitions.

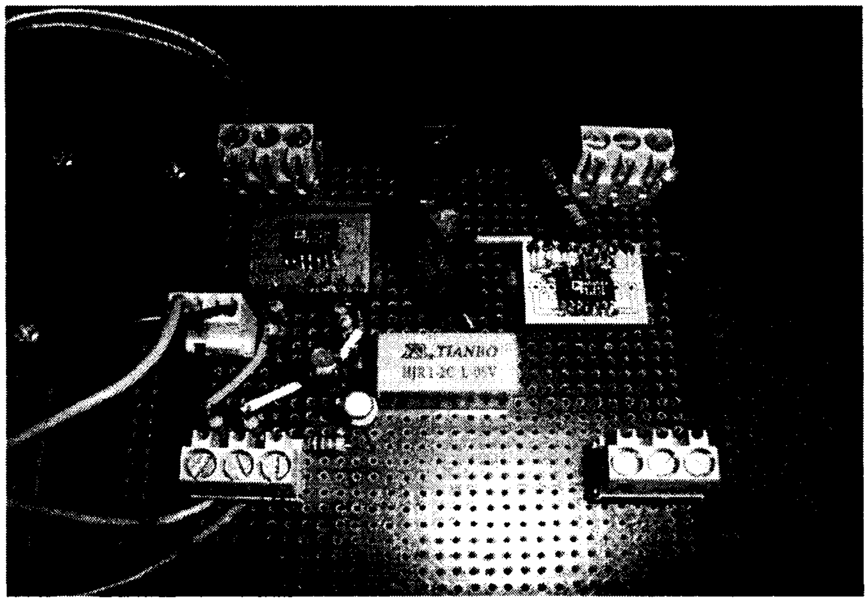

Fig. 3.2 Electronic load prototype

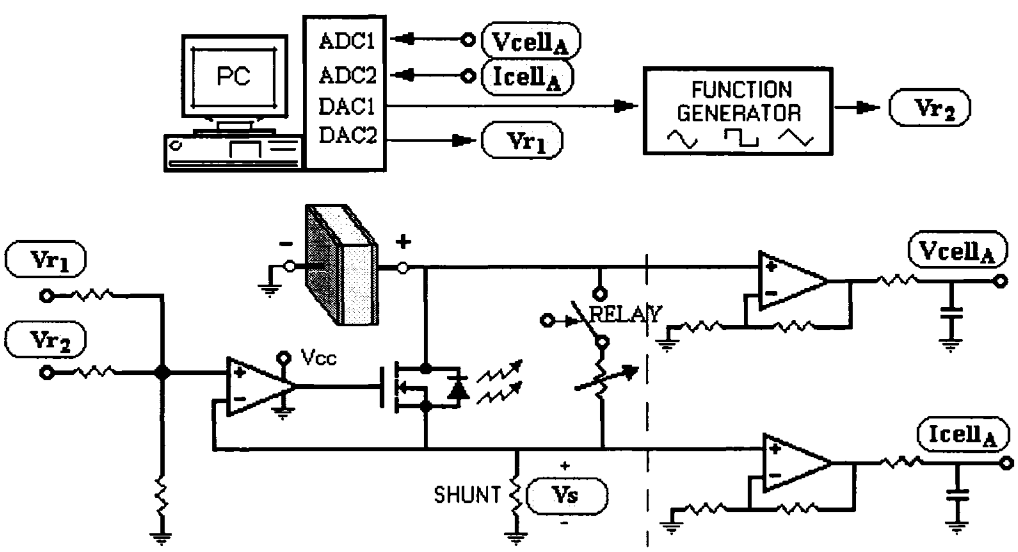

Fig. 3.3 Conceptual schematic of the electronic load

3.2 Description of the Software and Methodology

The EL system control and user interface was entirely programmed using 'C' language to provide a remarkable flexibility to the system. Among other features, the software is able to perform the following tasks:

- Determination of steady state polarization curve
- Current step tests
- Resistive load step tests
- Power step tests
- Current ripple tests (function generator is used in these tests)

The determination of the steady state polarization curve involves the acquisition of the steady state voltage and current values for a range of operating points (from the FC zero current to its maximum current). The time interval for each operating point measurement is typically 3 minutes to allow the OP to settle. The complete polarization curve routine could take several hours depending on the expected resolution (number of operating points). This routine starts measuring the open circuit output voltage of the FC. Thereafter, the EL is excited to extract a small current from the FC, waiting for a 3-minute time interval, and finally measuring the FC output voltage. A further increase in the current extraction is performed every 3 minutes and the voltage is measured until the maximum current of the FC is reached.

Current step tests are based on a pre-programmed routine that forces the cell to provide a desired current step change (i.e. $100mA$ to $400mA$ step). The procedure simply changes the EL reference signal while the FC current and voltage are being acquired.

Resistive load step test is a partially manual controlled test. First, the value of the passive load resistance is calibrated by hand. Once this is ready, the software routine enables the relay that connects the FC to the resistive load performing the acquisition of its voltage and current transient.

Power step tests require a more complex routine. The EL current reference signal (and thus the FC output current value) is set dynamically under a closed loop digital control strategy to meet a desired FC output power (i. e. 0mW to 200mW step).

Finally, the current ripple test allows the FC to be tested under DC+AC current ripple. The routine controls the function generator that provides the reference signal of the EL. This type of test is particularly useful to: a) evaluate the effect of current ripple operation (Chapter 2), and b) obtain the FC impedance characteristic (not covered in this work).

For all the described tests the voltage and current measurements are saved on a disk, and displayed on the screen.

3.3 An Advanced Electronic Load for Fuel Cell Systems

The operation and handling of FCs involves dealing with several additional equipment such as pumps, tanks, regulators, and piping interconnections. Since these laboratory FC systems are inherently bulky, it is desirable to have a small handy EL system that simplifies testing operations. Unfortunately, the EL approach presented in section 3.2.2 does not meet these requirements. The main disadvantage of this scheme is that the PC should be placed in proximity to the EL circuit board (and thus the FC) due to the analog interfacing. In addition, the PC should be completely dedicated to run real-time routines during tests, forcing the user to use an additional PC in a limited laboratory space.

An advanced EL is proposed to overcome these disadvantages. A Digital Signal Processor (DSP) controlled board was added to the existing EL board providing enhanced features. The DSP board was constructed with a low cost TMS320C DSP, which includes

Control Area Network (CAN) peripheral, Analog to Digital Converters (ADC), and Serial Peripheral Interface (SPI) that allow connectivity with TLV5636 fast serial Digital to Analog Converter (DAC) [56], [57], [58], [59]. Figure 3.4 shows a conceptual diagram of the proposed DSP based EL.

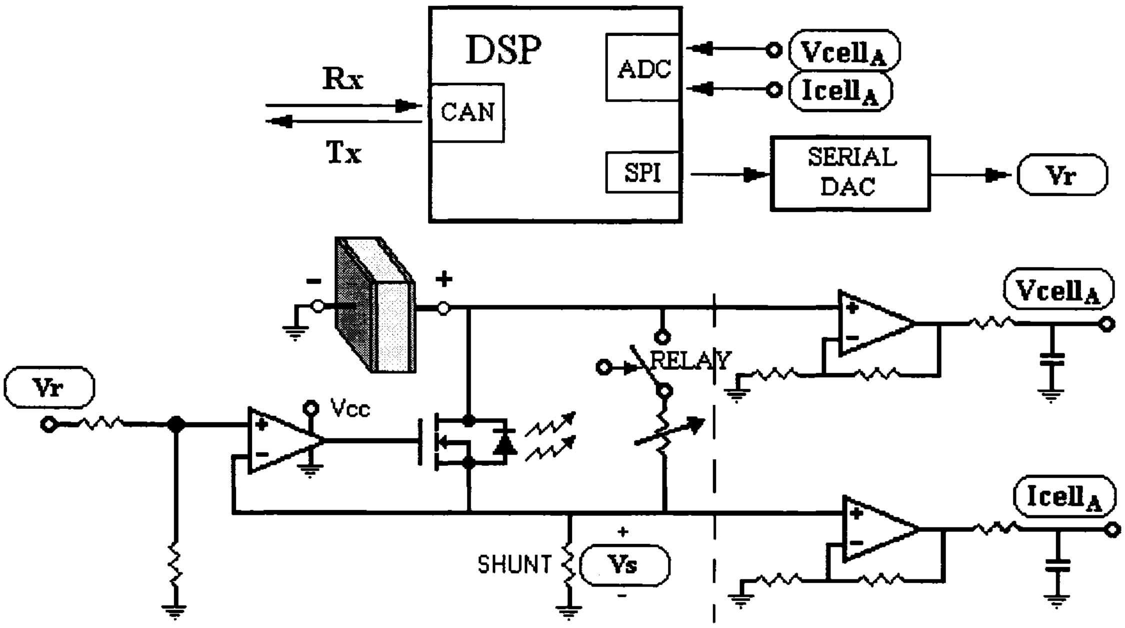

Fig. 3.4 Conceptual schematic of the DSP based electronic load

This special circuit provides effective parameter measurements and control of the EL power stage at a low cost with the additional advantage of the real-time processing capability of the DSP. The connection between the EL module and any other equipment is performed through glue-less 2 wires CAN bus [60], [61] that ensures robust high-speed data transmission under noisy electrical environments. Real-time tasks are performed by the DSP so that the PC, distantly located, can be used for any other purpose during tests. Figure 3.5 and 3.6 show pictures of the enlarged top and bottom view of the DSP board prototype. Finally the advanced EL for FC systems is shown connected to a DMFC in Fig. 3.7.

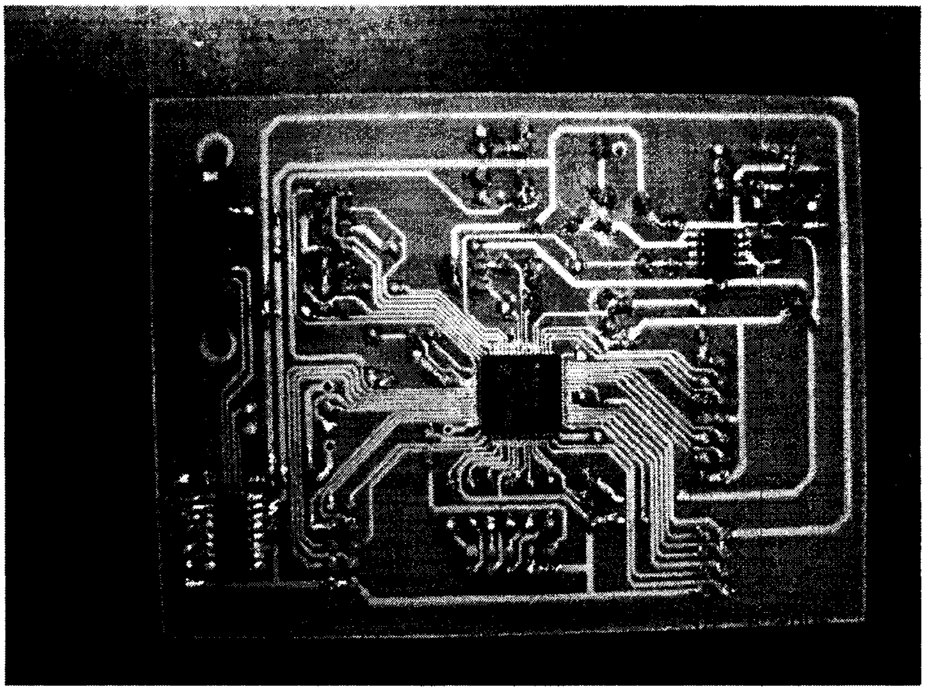

Fig. 3.5 DSP board top view

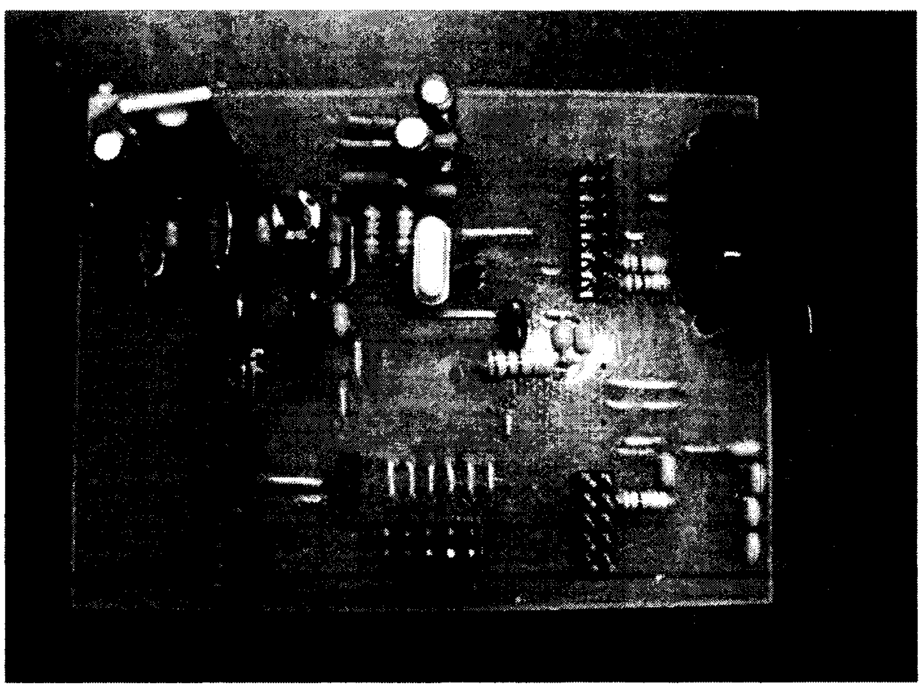

Fig. 3.6 DSP board bottom view

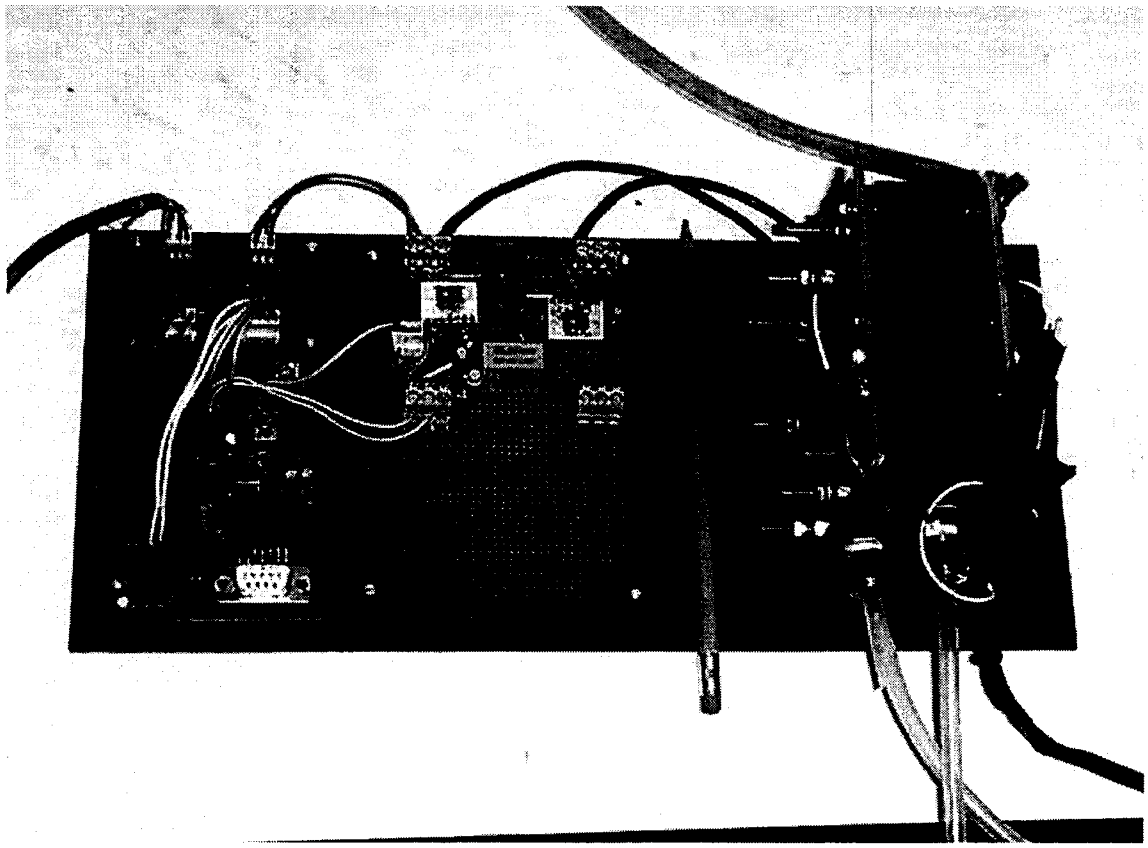

Fig. 3.7 The advanced electronic load

A more powerful EL was required to test the power converter described in chapter 4, which is a critical part of the FC simulator proposed in this thesis. Moreover, the final version of the FC simulator also required testing with an EL. In order to expand the power range of the advanced EL, a bigger power module was constructed. The expanded advanced EL with increased power capability is used to perform transient response tests presented in chapters 5 and 6. The principle of operation of the expanded advanced EL is similar to that of the basic EL described in section 3.1. Figure 3.8 shows a picture of the power stage of the expanded advanced EL.

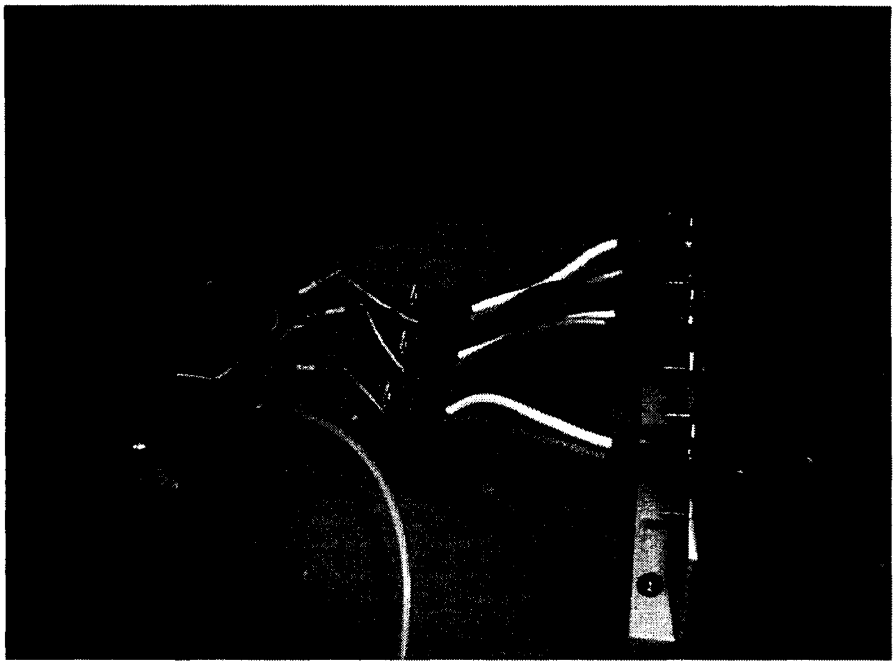

Fig. 3.8 Power stage of the expanded advanced electronic load

3.4 Summary

A low cost flexible Electronic Load (EL) for FC systems has been described in this chapter. This special EL design allows custom automated tests of the FC. The special features of the Electronic Load, such as power module expansion, and CAN bus communication with DSP-based control makes this system very attractive for FC as well as power supplies testing. Furthermore, the proposed EL is used to test the power converter described in chapter 4, and the entire FC simulator systems presented in chapter 5 and 6. Finally, the EL plays an important role as part of the hardware in the loop concept of chapter 6.

Chapter 4

Fast Dynamic Power Converter for Fuel Cell Simulators

Emulation of the electrical dynamic behavior of a FC can be achieved using a power converter with special characteristics. A suitable power converter design requires a complete evaluation of the dynamic response of the FC. As a general rule, the power converter should have at least a dynamic response comparable to the FC response. Failing to do so results in misleading reproduction of the FC behavior. This chapter takes into consideration the dynamic requirements of the power converter to successfully reproduce the behavior of a FC.

The analysis of the dynamic requirements of the power converter is based on the results obtained from the experimental testing of single FC under different loading condition as presented in chapter 2. The topology of the power converter is selected based on reversible power flow capabilities, switch utilization, and possibility of using a non-linear control strategy. The switching surface control strategy which belongs to the class of non-linear control based on variable structure theory has been shown to produce a better transient response than traditional small-signal based controller [62]. Details of a general procedure for the selection of a curved Switching Surface (SS) to control the Buck type converter are presented in this chapter. The analysis associated with the control strategy is based on the normalized representation of ideal SSs for different loading conditions. As a result of the investigation, a switching surface, referred to in this work as the elliptic natural unloaded SS is selected. This SS is shown to provide excellent transient behavior and no overshot during start up. Experimental results of the converter, including start up and resistive sudden load change, confirm the virtues of this control scheme. Finally, the implementation of the control strategy using a fixed point Digital Signal Processor (DSP) is described.

4.1 Analysis of the Power Converter Dynamic Requirements

Of the various transient responses presented in chapter 2, the FC operation under current ripple is the one that produces the fastest change in the FC output voltage. For convenience the characteristic of the FC under current ripple, discussed in chapter 2 is reproduced in Figs. 4.1 and 4.2. This behavior is particularly important since FC inverters (which produce current ripple) are essential components for the application of FC systems (portable power source, distributed power generation, UPS, avionics supply). The time domain plot of Fig. 4.2 shows how the single FC output voltage swings when DC current with ripple is extracted from the cell. The power converter output voltage that emulates the FC stack should tightly follow the voltage swing with a minimum phase shift. Failing to do so will result in misleading reproduction of the FC equivalent double layer capacitance. This may lead to wrong conclusions about the current ripple effect, which is related to a reduction in the FC output power [52].

In accordance with the experimental results of Fig. 4.1 and 4.2, the power converter must have a frequency response for large signal with unity gain and negligible phase margin beyond the expected current ripple frequency (i.e. 120Hz).

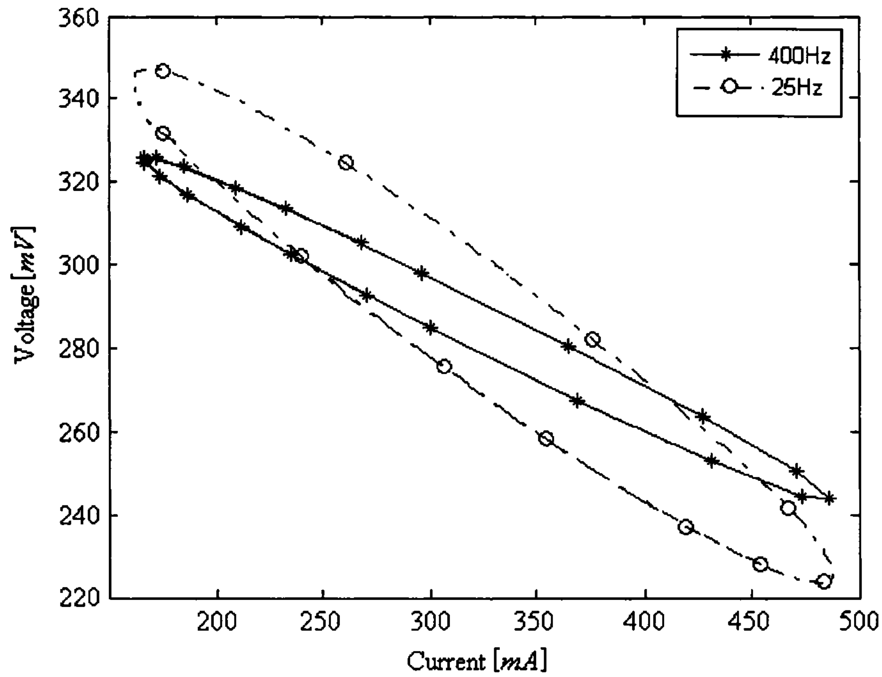

Fig. 4.1 DC+AC current test of the DMFC for 25Hz and 400Hz: Zoom of the v-i plot

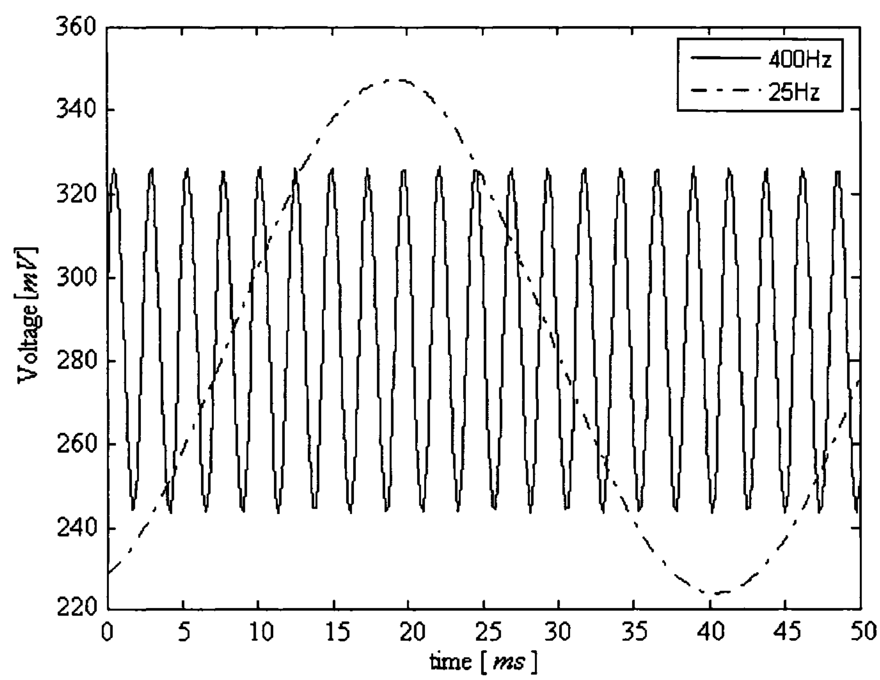

Fig. 4.2 DC+AC current test of the DMFC for 25Hz and 400Hz: Time domain plot

4.2 Power converter Topology selection

The power converter that emulates the behavior of the FC should have a fast dynamic response as explained in section 4.1. Two different converter categories are investigated in this section: the isolated converter and the non-isolated converter. It is demonstrated that the basic isolated converter experiences problems in reproducing the behavior of a FC. On the other hand, it is shown that a non-isolated converter with reversible power flow capabilities complies with the topological requirements to emulate the behavior of a FC.

4.2.1 Isolated DC/DC converter

Isolated DC/DC converters can be categorized as unidirectional and bidirectional core excitation. The unidirectional converters are flyback (derived from the basic buck-boost basic topology) and forward (derived from the basic buck topology). On the other hand, push-pull, half bridge, and full bridge topologies belong to the bidirectional category (all derived from the basic buck topology) [36]. Converters with bidirectional core excitation make better use of the transformer magnetic properties at the expense of additional switches. Fig. 4.3 shows the transformer and filter arrangements for the above mentioned power converters. It can be noticed from Fig. 4.3 that the diodes only permit forward current flow through the filter inductor L of the output power stages. This prevents the converter from extracting current from the filter capacitor when it is needed. During steady state with light loading conditions, this behavior is known as discontinuous conduction mode. A problem appears during transients, such as load removal or decrease in the voltage reference, which leads to a poor dynamic response. In order to illustrate

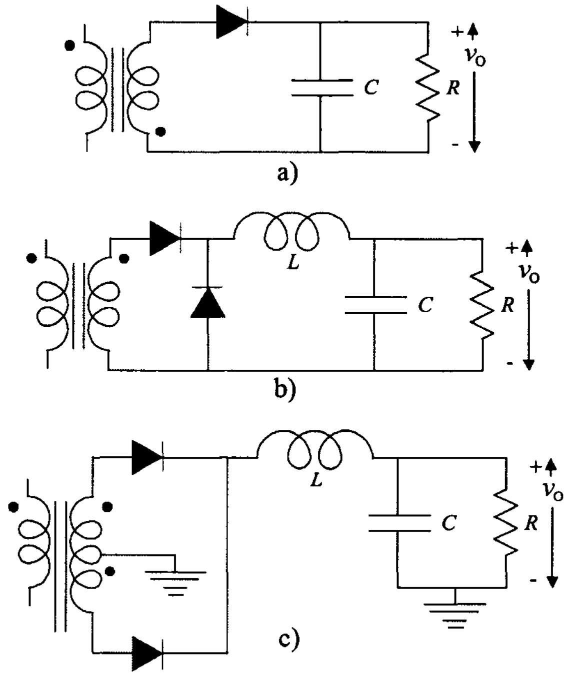

Fig. 4.3 Output stage of isolated power converters: a) flyback, b) forward and c) push pull, half bridge, and full bridge

this behavior, Fig. 4.4 and Fig. 4.5 show simulation results of the transient response of an isolated converter derived from the basic buck topology (Fig. 4.3b and Fig. 4.3c). The experiment emulates a possible behavior of a FC stack when DC plus 120Hz current ripple is extracted from its output. Following the experimental results of Fig. 4.1 and Fig. 4.2, the output voltage of the FC is reduced when the output current increases, while a reduction in the output current results in an increase of the FC output voltage. In order to emulate the FC behavior, the converter output voltage v_o is supposed to follow the voltage reference signal v_r, which is i_o dependant. It can be observed in Fig. 4.4 that the output voltage of the converter cannot follow the reference signal during the falling portion of the signal. Figure 4.5 reveals that the inductor current cannot be reversed (due to the diodes), thus the capacitor charges could not be removed to achieve the required voltage reduction. Instead, the load current naturally discharges the capacitor resulting in

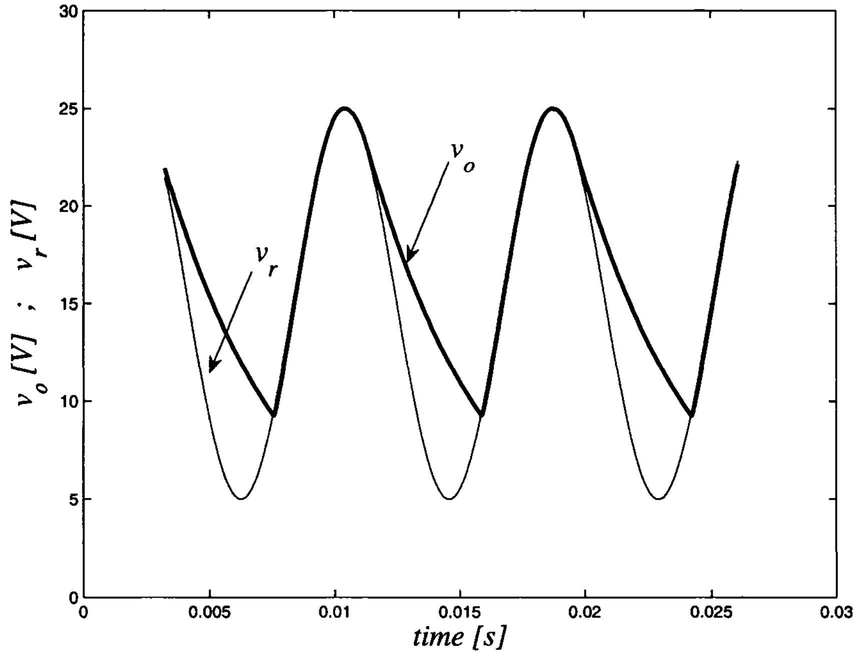

Fig. 4.4 Isolated converter reference and output voltage

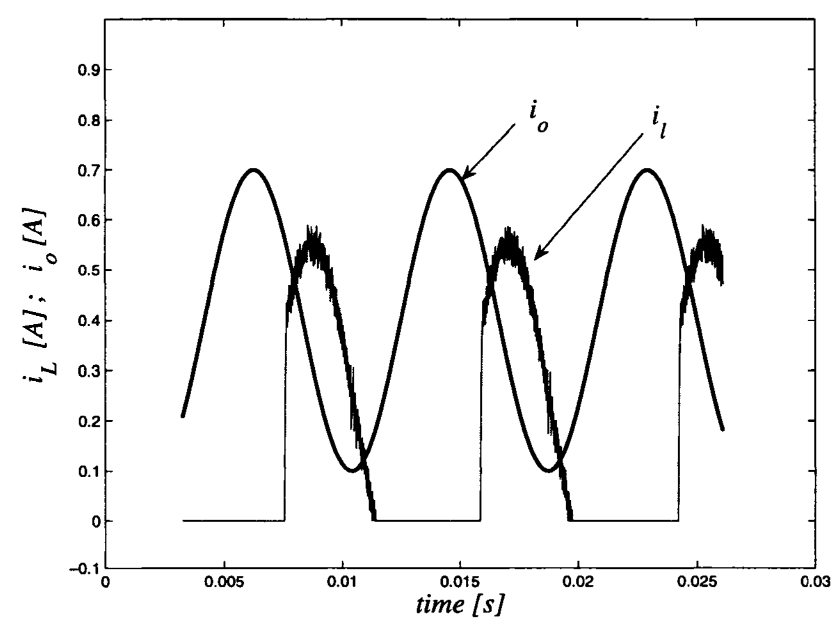

Fig. 4.5 Isolated converter inductor and output current

a poor transient response. This behavior is undesirable, making the isolated DC/DC converter unsuitable for a FC simulator. An isolated converter with reversible power flow would be able to remove charges from the filter capacitor[63], [64]. However, these reversible converters have the disadvantage of increased topological and control complexity. A solution to overcome these drawbacks is found in the non-isolated converter described in the following section.

4.2.2 Non-isolated DC/DC converter

Standard isolated converters do not possess reversible power flow capabilities. Under certain operating condition, the FC simulator power converter is required to remove charge from the filter capacitor. A reversible topology is selected to emulate the electrical dynamic behavior of FCs as explained in this section. A simple reversible topology is obtained by replacing the free wheeling diode with a switch in the buck converter as shown in Fig. 4.6 [36]. This topology behaves as a buck converter that does not operate in discontinuous conduction mode. Switch S2 can force a reverse current in the inductor, thus providing a faster discharge of the filter capacitor. Fig. 4.7 and Fig. 4.8 show simulation results of the transient response of the buck converter of Fig. 4.6. The experiment emulates a possible behavior of a FC stack when DC plus 120Hz current ripple is extracted from its output.

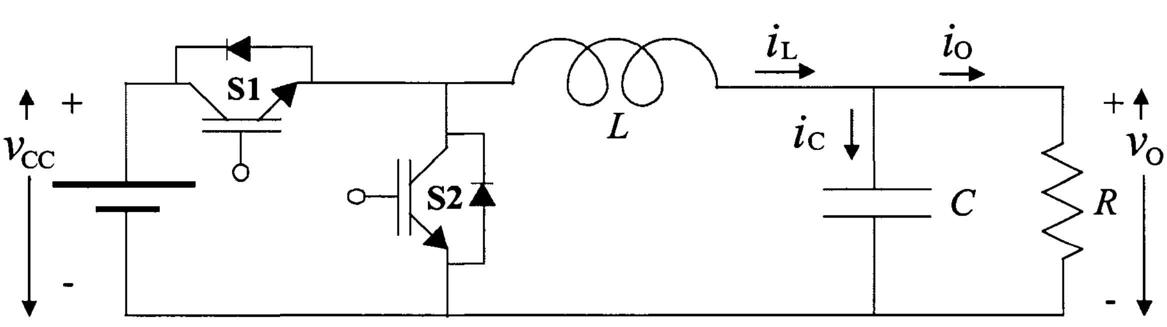

Fig. 4.6 Reversible buck converter

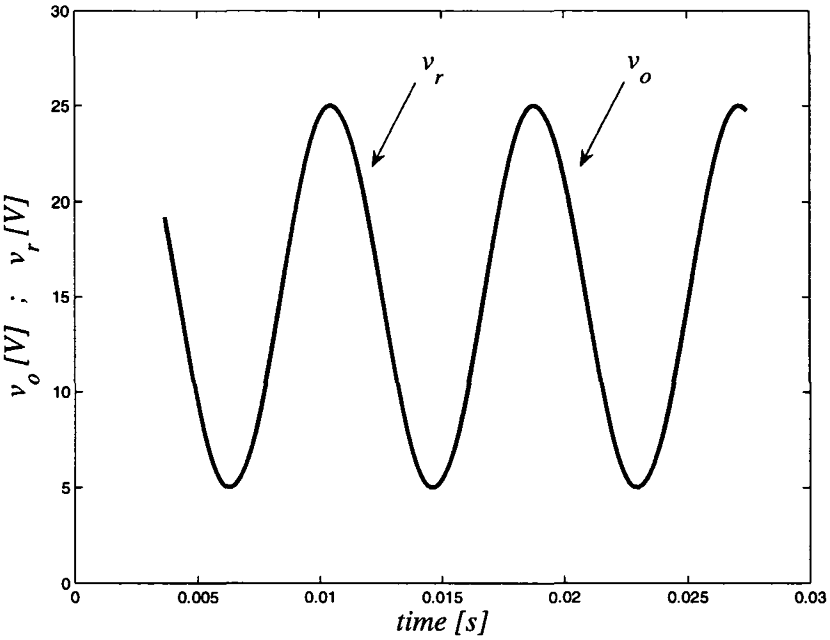

Fig. 4.7 Reversible converter reference and output voltage

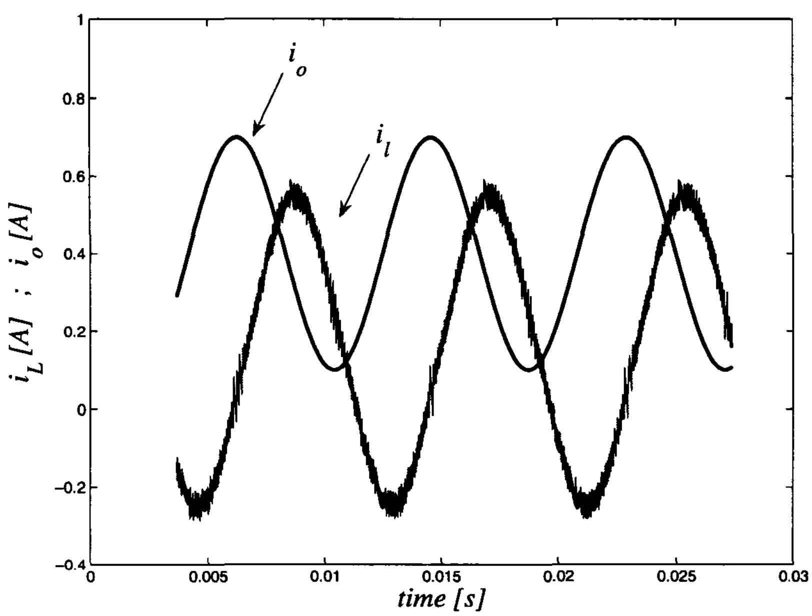

Fig. 4.8 Reversible converter inductor and output current

The simulation results show that the buck topology with an additional switch allows v_o to successfully follow v_r. In addition, this topology has the advantage of a better switch utilization (U) in comparison with other non-isolated topologies [36] [37]. Fig. 4.9 shows the switch utilization characteristics for various converters [36]. In Fig. 4.8 $P_T = V_T I_T$, where V_T and I_T are the switch maximum voltage and current respectively, and $P_O = V_{OR} I_{OR}$, where V_{OR} and I_{OR} are the rated output voltage and current respectively, and d is the duty ratio of the converter.

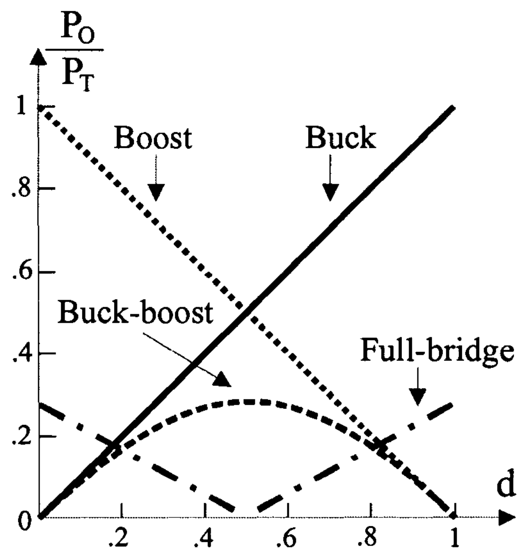

Fig. 4.9 Switch utilization

There is another important feature related to control strategy that makes the buck converter an attractive option. Buck converters are particularly suitable for switching surface control such as sliding mode and boundary control [46], [47], which are based on variable structure theory [65]. It has been demonstrated that non-linear control strategies based on variable structure theory show better transient response than traditional small signal based controllers and enhanced robustness for parameters variation [47]. Since fast dynamic response of the converter is a key requirement in FC emulators, it is desirable to employ a non-linear control scheme. Moreover, unlike other converters, the controllable states of the buck converter are continuous and accessible for measurement, which makes this variable structure system very attractive for non-linear control [46]. Finally, this work develops a systematic approach for the selection and clarification of the characteristics features of curved switching surfaces. Curved switching surfaces have gained attention in the power electronics research community [47] [66].

For the reasons stated above, the buck converter with reversible capabilities shown in Fig. 4.6 is selected for this work. A curved switching surface to control the converter with near time optimal response is selected as explained in the next section.

4.3 Selection of a Curved Switching Surface for Buck Converters

Control of step-down or buck converters have been extensively addressed for the past three decades with an uncountable number of approaches [45], [67], [68], [69], [70], [71]. This switching mode power converter can be classified as a simple case of variable structure system, which can be controlled by a sliding mode regime. Under this control strategy, the state variables of the converter move naturally without any restriction until they reach a sliding surface. Thereafter, the surface defines a path for the state variables towards the desired operating point [72]. The order of the system is thus reduced, causing a slower transition along the switching surface. In comparison with linear control schemes, improved dynamic response and robustness are the main advantages of the sliding mode control scheme. First order sliding surface and hysteresis control are well-established techniques that have been investigated [46], [47]. An improved transient response can be achieved by selecting a curved Switching Surface (SS), which avoids sliding regime or part of it, directing the state variables close to the desired operating point in just one switching action. A particular case of second order SS with enhanced dynamics was recently proposed [66]. However, a significant overshoot during start up with no load is produced. In addition, the characteristic features and behavior of this particular second order SS have not been adequately covered in the literature.

The goal of the work presented in this section is to develop a systematic approach for the selection and clarification of the characteristics features of SSs. The approach is based on a normalized representation of the ideal SSs for different loading conditions. A set of graphics in three dimensions is introduced to give a volumetric sense of the behavior of the converter and its control requirements during transients. As a result of the investigation, a SS referred to in this work as the elliptic natural unloaded SS is selected. This novel SS provides excellent transient behavior and no overshoot during start up. The general concept of using second order SS is also geometrically analyzed in this section to clarify its scope of behavior, features and limitations. Experimental results, including start up, current step, and sudden resistive load changes confirm the virtues of the control scheme.

4.3.1 Normalized Ideal Switching Surfaces

The basic buck converter is shown in Fig. 4.10. For simplicity the parasitic elements (eg. switch resistance, ESR, etc.) are neglected. The second order differential equation describing the converter is given by

$$LC\frac{d^2 v_o}{dt^2}+\frac{L}{R}\frac{dv_o}{dt}+v_o=v_{cc}\cdot u \tag{4.1}$$

In (4.1) u is the switch position in which $u=1$ represents an ON state, and $u=0$ represents an OFF state. The well-known solution for a second order system is given by

$$v_o=\exp(\alpha t)[A\cos(\beta t)+B\sin(\beta t)]+v_{cc}\cdot u \tag{4.2}$$

where,

$$\alpha = -\frac{1}{2RC} \;;\; \beta = \frac{\sqrt{4LC - \left(\frac{L}{R}\right)^2}}{2LC} \;;\; A = v_{o(0)} - v_{cc} \cdot u \;;\; B = \frac{\frac{d\,v_{o(0)}}{dt} - \alpha A}{\beta} \quad (4.3)$$

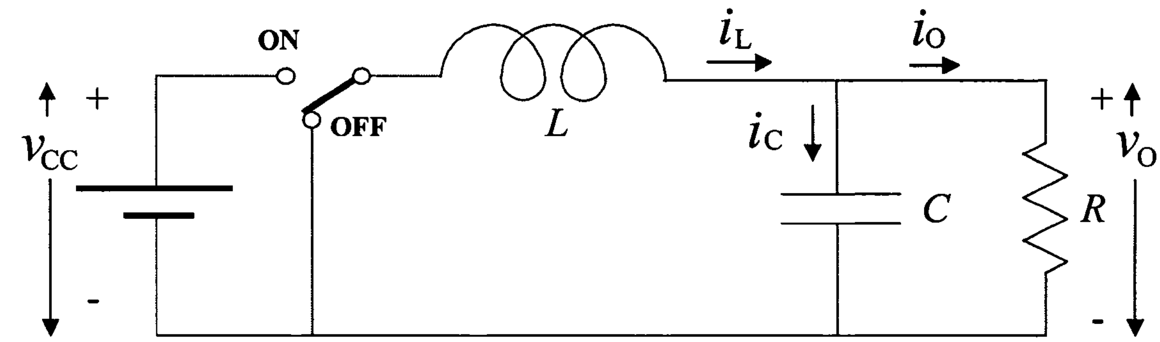

Fig. 4.10 Buck converter circuit

The analytical solution in (4.2) is evaluated under different loading conditions to establish the natural trajectories toward the desired operating point: $v_o = v_r$ (output voltage equals to reference voltage) and $i_C = C\frac{d\,v_o}{dt} = 0$ (capacitor current equals to zero). Each resistive loading condition results in a different natural trajectory that denotes an ideal SS. A set of ideal SSs for different loading conditions is depicted in a normalized plot in Fig. 4.11. In order to provide generality to the analysis, the variables used in Fig. 4.11 are normalized as follows:

$$v_{on} = \frac{v_o}{v_r} \;;\; i_{Cn} = \frac{i_C}{i_{\max}} \;\; for \;\; i_{\max} = \frac{v_r}{R_{cd}} \quad (4.4)$$

The normalization process leads to a unique representation of the SS for any possible buck converter. This is achieved by considering the load resistance R as a function of the output filter values L and C, where the basic resistance value is given by

$$R_{cd} = \frac{1}{2}\sqrt{\frac{L}{C}} \ . \tag{4.5}$$

Whenever $R = R_{cd}$ the filter-load combination behaves as a critical damped system. That is, if the switch in turned ON, v_o would converge to v_{cc} with no overshoot. A load resistance $R = R_{cd}$ can be considered as maximum permissible load that exceeds most design specification as explained in the next section.

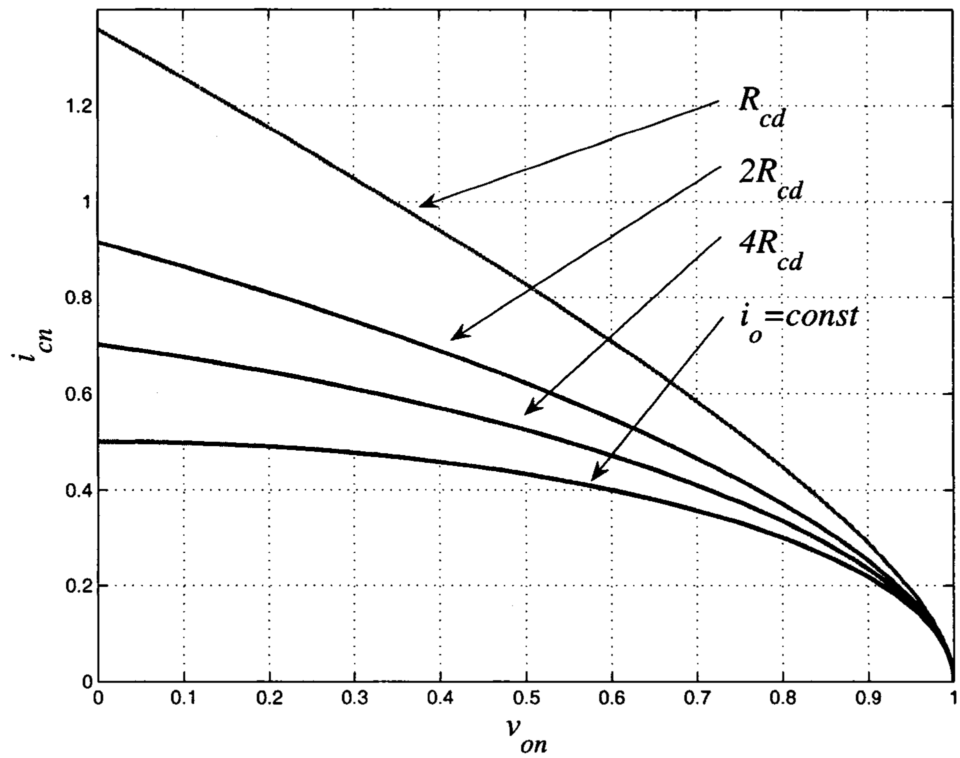

Fig. 4.11 Normalized ideal switching surfaces for R_{cd}, $2R_{cd}$, $4R_{cd}$, and i_o = constant

Since the evaluated cases range between two absolute possible limits, no load and extremely heavy loaded conditions, the corresponding boundaries between SSs (shaded region of Fig. 4.11) surround a possible optimal SS. In other words, the selection of a SS with fast dynamics should not lie outside this region. However, it should be noticed that no unique SS could solve the problem of different loading conditions (ie. R_{cd} or no load). To further investigate the selection of a SS, the transient response of the converter under sudden load changes should be examined.

4.3.2 Ideal Transient Response During Sudden Load Change

In order to provide more insight into the transient behavior of the buck converter, a set of 3D graphics is presented in Fig. 4.12 to 4.15 with the optimal response of the converter under sudden load changes. Since the ON state trajectories strongly depend on v_{cc}, the effect of the inverse normalized input voltage v_r/v_{cc} is included on one of the axes. Thus, a normalized 3D plot encloses the operating universe of any buck converter providing the required generality to evaluate transient responses.

Before the transient starts, the converter is operating at the desired operating point with no load, $v_o = v_r$, and $i_C = 0$. In Fig. 4.12 the maximum resistive load (R_{cd}) is applied to the output of the converter. The capacitor current instantly supplies $i_C = -i_{\max}$ current to the load, which locates the operating point far from the desired operating point. In order to obtain a time optimal response, the switch is turned ON until the state trajectory reaches the corresponding SS for R_{cd} loading. Thereafter, the switch is turned OFF and the state trajectory moves naturally towards the desired point, accounting for only one switching action during the transient. An important comment could be inferred from this graphic: The output voltage experiences a tremendous drop considering that an ideal control action has been performed (time optimal). This effect is even worse when the v_r/v_{cc} ratio approaches unity. The excessive voltage drop is unavoidable. It is concluded that R_{cd} must be considered as a severe sudden loading condition not applicable for most practical converters. In order to reduce the drop, the filter should be redesigned to establish a better filter-to-load relation.

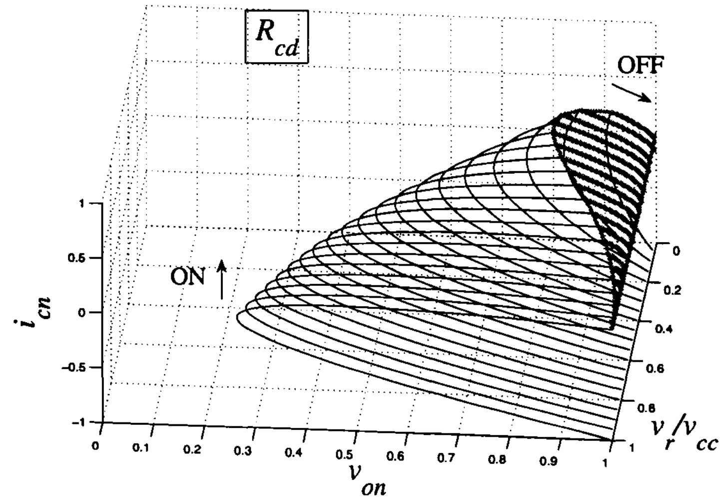

Fig. 4.12 Normalized optimal transient response of the buck converter under sudden load change: $R = R_{cd}$

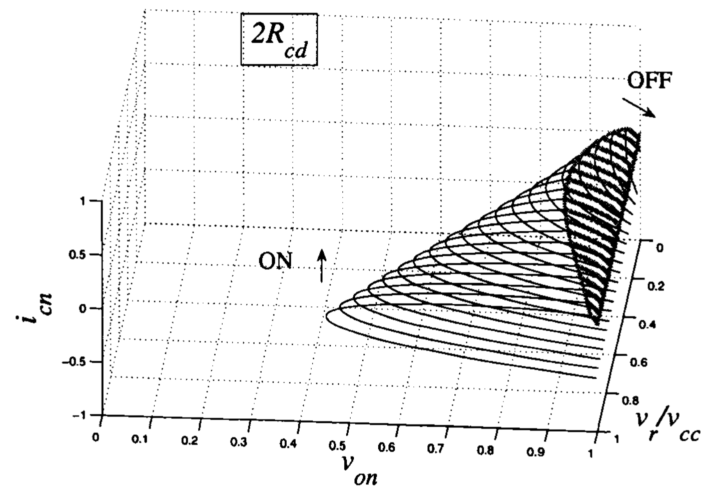

Fig. 4.13 Normalized optimal transient response of the buck converter under sudden load change: $R = 2R_{cd}$

The same procedure is performed with resistive loads of $2R_{cd}$ and $4R_{cd}$ to obtain Fig. 4.13 and Fig. 4.14 respectively. For the case of $2R_{cd}$ the voltage drop with ideal control action is still considerable. On the other hand, $4R_{cd}$ seems to be a more reasonable filter-to-load relation in terms of voltage drop during transients. Finally, Fig.

4.15 shows a time optimal transient response for a large sudden current step of $i_O = i_{\max}/4$. It should be noted that the SS for constant i_o provides an ideal time optimal response for any current step transient as well as start up with no load.

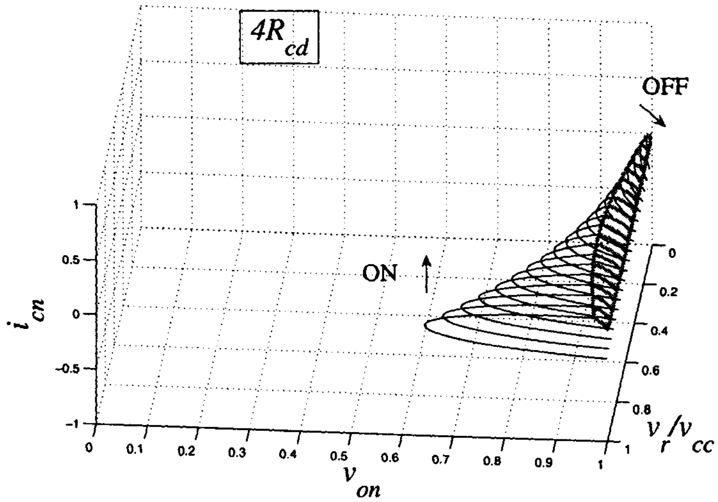

Fig. 4.14 Normalized optimal transient response of the buck converter under sudden load change: $R = 4R_{cd}$

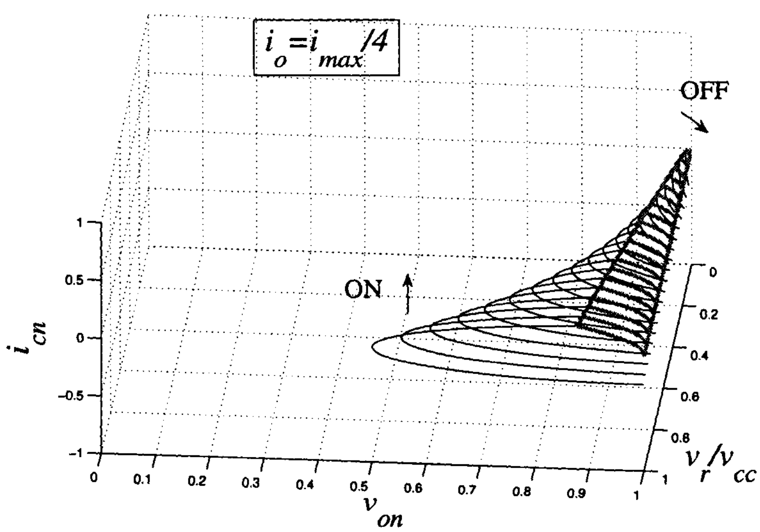

Fig. 4.15 Normalized optimal transient response of the buck converter under step load change with constant i_o

A simple approach that predicts the transient performance for any SS can be inferred from the normalized ideal SSs of Fig. 4.11. For any type of transient (i.e. start up or load change) a SS that lies above the corresponding ideal SS results in overshoot (the corresponding ideal SS only depends on the load resistance value R). On the other hand, a SS that lies below the corresponding ideal SS results in a poor transient response. The transient response improves as a given SS approaches the ideal SS.

An inspection of the ideal time optimal responses under different load transients (Fig. 4.12 to Fig. 4.15) reveals that the ON state trajectories reach the corresponding SS within a region where all the SSs are close. For convenience Fig. 4.16 recalls the graphic of Fig. 4.11, highlighting with a circle the region of convergence. Since the SS of $R = R_{cd}$ is eliminated due to excessive voltage drop, the boundaries of a possible SS for sudden load changes have been significantly reduced as indicated by the shaded region in Fig. 4.16. It is worth noting that any SS within the narrow shaded area would provide similar results during a sudden load change. This is due to the proximity of the SSs in this area.

The small shaded region of Fig. 4.16 makes the selection of a SS simpler. The natural unloaded SS (also defined as $i_o = \text{constant}$) located at the bottom of the SSs is selected as the control law for the following reasons:

- The natural unloaded SS ensures perfect time optimal response for a current step change, voltage reference change with constant current loading, and excellent response (within output voltage ripple) for sudden resistive load changes.
- Unlike any other SS, the natural unloaded SS guarantees no overshoot during start up under any loading condition (It is desirable to have a fast transient but not at the expense of overshoot).

- The mathematical formulation of the control law is simple and can be implemented on analog, digital or mixed signal circuits.

The natural unloaded SS was presented as a control law with simulation results of an example case [73]. Further work introduced in the following section allows the characterization of curved SSs to be investigated, evaluated and compared, leading to a simplification in the selection process.

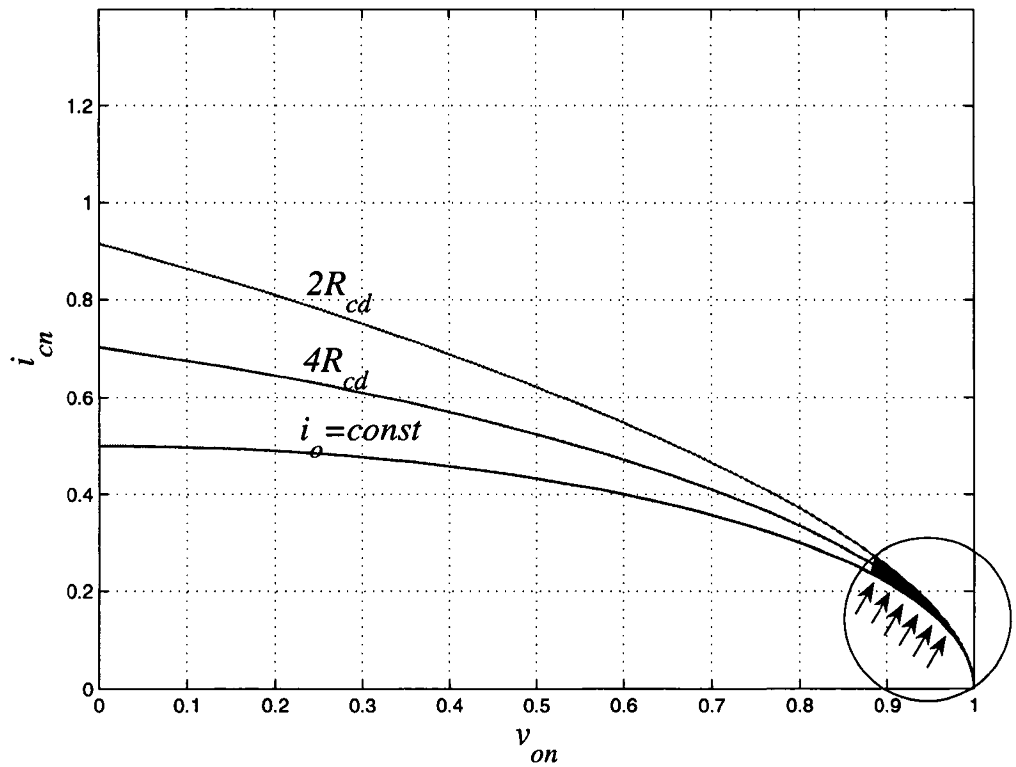

Fig. 4.16 Normalized ideal switching surfaces for $2R_{cd}$, $4R_{cd}$, and i_o = constant

4.3.3 Derivation of the Natural Unloaded Switching Surface

The goal of the following analysis is to develop a systematic procedure for selecting SSs. The control law is derived first and then the transient performance is evaluated using normalized 3D plots. The control law is obtained by evaluating (4.2) for

$\boldsymbol{R} = \infty$, $v_o(0) = v_r$, and $\frac{d\,v_o(0)}{dt} = \frac{i_c}{C} = 0$, which is the desired operating point with no resistive load (or constant current load). Solving (4.2) for v_o and its derivative results in the following periodic functions:

$$v_o = (v_r - v_{cc} \cdot u)\sin\left(\frac{t}{\sqrt{LC}} + \frac{\pi}{2}\right) + v_{cc} \cdot u \tag{4.6}$$

$$\frac{d\,v_o}{dt} = \frac{i_c}{C} = \frac{(v_r - v_{cc} \cdot u)}{\sqrt{LC}}\cos\left(\frac{t}{\sqrt{LC}} + \frac{\pi}{2}\right) . \tag{4.7}$$

Eliminating t from (4.6) and (4.7) results in,

$$\frac{i_c}{C} = \frac{(v_r - v_{cc} \cdot u)}{\sqrt{LC}}\cos\left[\sin^{-1}\left(\frac{v_o - v_{cc} \cdot u}{v_r - v_{cc} \cdot u}\right)\right] . \tag{4.8}$$

Since $\cos(\sin^{-1} x) = \sqrt{1 - x^2}$, the elliptic trajectories that include the desired operating point are given by

$$\frac{L}{C} i_c^{\,2} = v_r^{\,2} - v_o^{\,2} \text{ for } u = 0 \quad , \tag{4.9}$$

$$\frac{L}{C} i_c^{\,2} = (v_r - v_{cc})^2 - (v_o - v_{cc})^2 \text{ for } u = 1 \quad . \tag{4.10}$$

Finally, the control laws that define the switching surfaces are given by the following:

Case I: $i_c > 0$

$$\sigma_1 = \frac{L}{C} i_c^{\,2} + v_o^{\,2} - v_r^{\,2} = 0 \tag{4.11}$$

If $\sigma_1 < 0$ then $u = 1$, else $u = 0$

Case II: $i_c < 0$

$$\sigma_2 = \frac{L}{C} i_c^{\,2} + (v_o - v_{cc})^2 - (v_r - v_{cc})^2 = 0 \tag{4.12}$$

$$\text{If } \sigma_2 > 0 \text{ then } u = 1, \text{ else } u = 0$$

Normalized 3D graphics are presented in Fig. 4.17 and 4.18 to illustrate a generalized large-signal transient response with the proposed control strategy. The control action turns the switch ON when the transient is produced. Thereafter, when the state trajectories reach the natural unloaded SS, the switch is turned OFF allowing the state trajectories to move naturally in the direction of the desired operating point. For a sudden load change of $R = 4R_{cd}$, the SS contributes, in one switching action, more than 99% of the desired output voltage (Fig. 4.17). In the case of a more critical sudden load change of $R = 2R_{cd}$, one switching action contributes at least 97% for the worst-case as shown in Fig. 4.18. It should be pointed out that a sudden loading condition of $R = 2R_{cd}$ is unlikely to be found in practical designs since the voltage drop inherent in the filter to load relation is large.

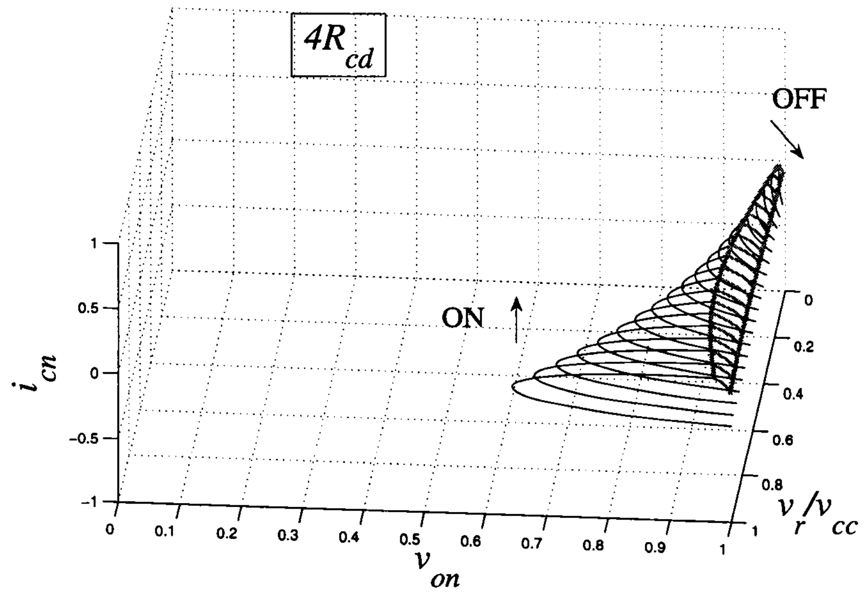

Fig. 4.17 Normalized transient response of the natural unloaded SS: $R = 4R_{cd}$

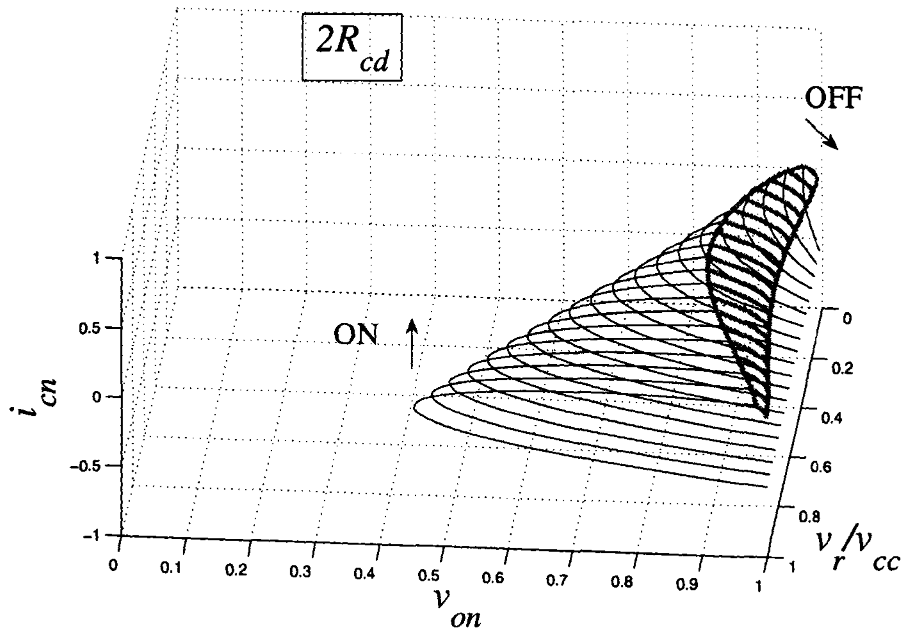

Fig. 4.18 Normalized transient response of the natural unloaded SS: $R = 2R_{cd}$

4.3.4 Discussion on the Use of Second Order Switching Surfaces

Both the natural unloaded SS and the second order SS can be geometrically classified as conic sections. The natural unloaded SS of (4.11) can be rearranged as

$$\frac{(v_o)^2}{{v_r}^2} + \frac{L}{C}\frac{(i_c)^2}{{v_r}^2} = 1, \tag{4.13}$$

which represents an ellipse with the form

$$\frac{(x)^2}{a^2} + \frac{(y)^2}{b^2} = 1. \tag{4.14}$$

On the other hand, a second order SS is a parabola of the form

$$(y-y_0)^2 = k(x-x_0) \tag{4.15}$$

It is of interest to investigate if a second order SS (parabola) can fit the natural unloaded SS (ellipse). The expression for a parabola with vertex $(a,0)$ that intersects an ellipse at $(0,b)$, as shown in Fig. 4.19, is given by

$$y^2 = \frac{b^2}{a}(a-x) \ . \tag{4.16}$$

Using (4.13), (4.14), and (4.16), a second order SS is obtained as

$$i_C^{\ 2} = v_r \frac{C}{L}(v_r - v_o) \ . \tag{4.17}$$

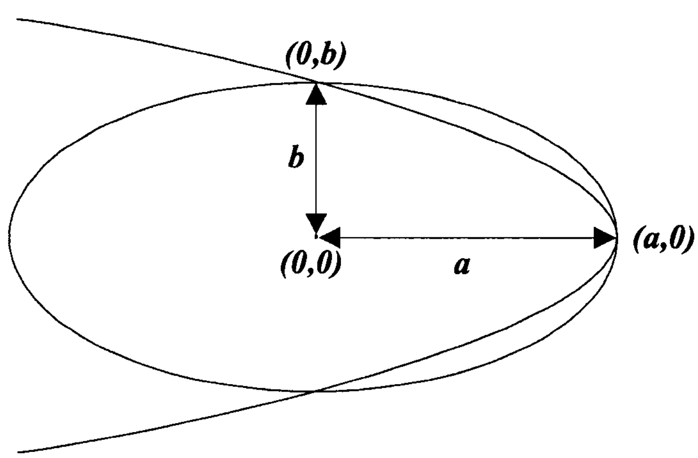

Fig. 4.19 Fitting the natural unloaded SS with a second order SS: Parabola approximating an ellipse

As can be noticed in Fig. 4.19, the parabola in (4.16) does not adjust to the ellipse in (4.14). Since parabolas differ in size, not in shape, the only option to improve the fit is to increase its size. Including a factor K in the right side of (4.17) results in the following equation,

$$i_C^2 = K v_r \frac{C}{L}(v_r - v_o) \ . \qquad (4.18)$$

A family of second order SS results from evaluating $1 \le K \le 3$. For the purpose of comparison, Fig. 4.19 shows a family of normalized second order SSs and the natural unloaded SS. In the normalized plot of Fig. 4.19 only a portion of the conical sections are presented in which $a = 1$ and $b = 0.5$. It can be noticed that none of the parabolas can properly fit the natural unloaded SS. Particularly, $K = 2$ provides a good fit around the area of convergence for sudden load changes. Outside the area of convergence, the parabola departs from the natural unloaded SS.

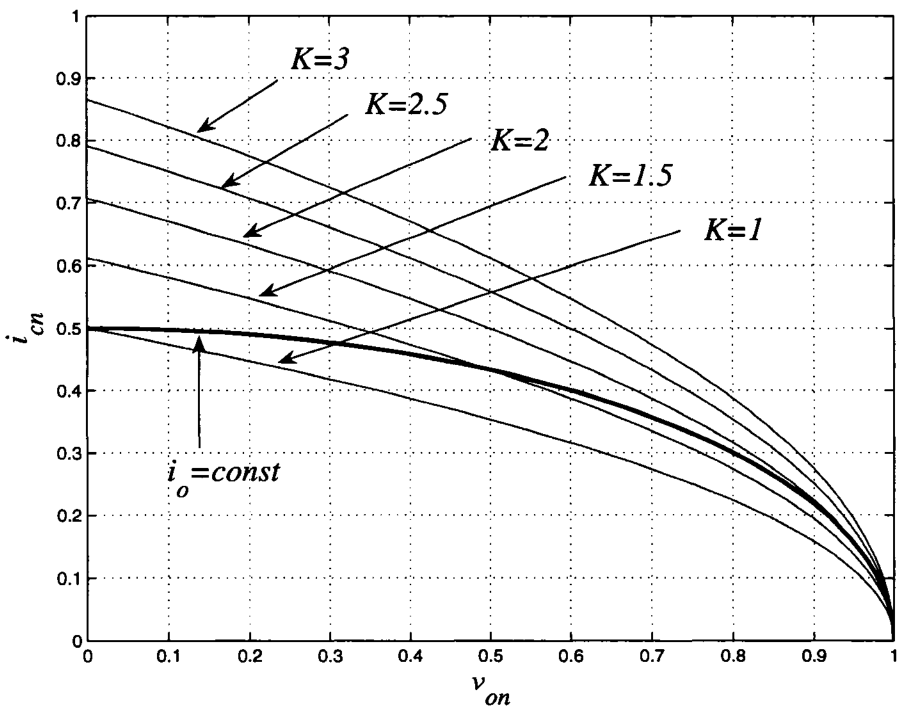

Fig. 4.20 Fitting the natural unloaded SS with a second order SS: Family of parabolas approximating an ellipse

A recent publication arrived at a second order SS with $K = 2$ using a different approach [66]. Since no geometrical analysis was included, the location of this particular case of second order SS within the normalized ideal SSs (Fig. 4.11) was unknown. The normalized graphics introduced in this work provide an aid to the analysis and study of curved SS. For sudden load changes, the transient response for the SS selected in this work is comparable to the response reported in [66], which is explained due to their proximity in the region of convergence. However, unlike the second order SS, the natural unloaded SS presents the advantage of eliminating the overshoot during start up with no load. In general, the natural unloaded SS provides time optimal response for voltage reference change with no-load or constant current load (start up with no-load is a particular case of voltage reference change), and time optimal response during a current step change.

4.4 Implementation of the Control Strategy With a Fixed Point DSP

Figure 4.21 shows a schematic that combines the converter and the natural unloaded SS representation. The state trajectories (ST), which are defined by the output voltage v_o and the capacitor current i_c, are compared against the natural unloaded SS. Depending on the ST location, the control law determines the switch state (ON/OFF). In Fig. 4.21 the ST is above the SS so the switch state remains OFF. As soon as the ST reaches the SS, the switch state changes to ON directing ST towards the desired operating point.

Readily available DSPs make possible the control and monitoring of complete power electronics systems. DSP architecture typically performs one instruction per clock cycle, which allows real time routines at a high frequency. Fixed point DSP is an ideal option for cost sensitive and space constrained power electronics designs [74]. Even though the programmer has to track for the number representation (i.e. Q-notation) and overflow/underflow, fixed point is still economically convenient in comparison with floating point DSPs.

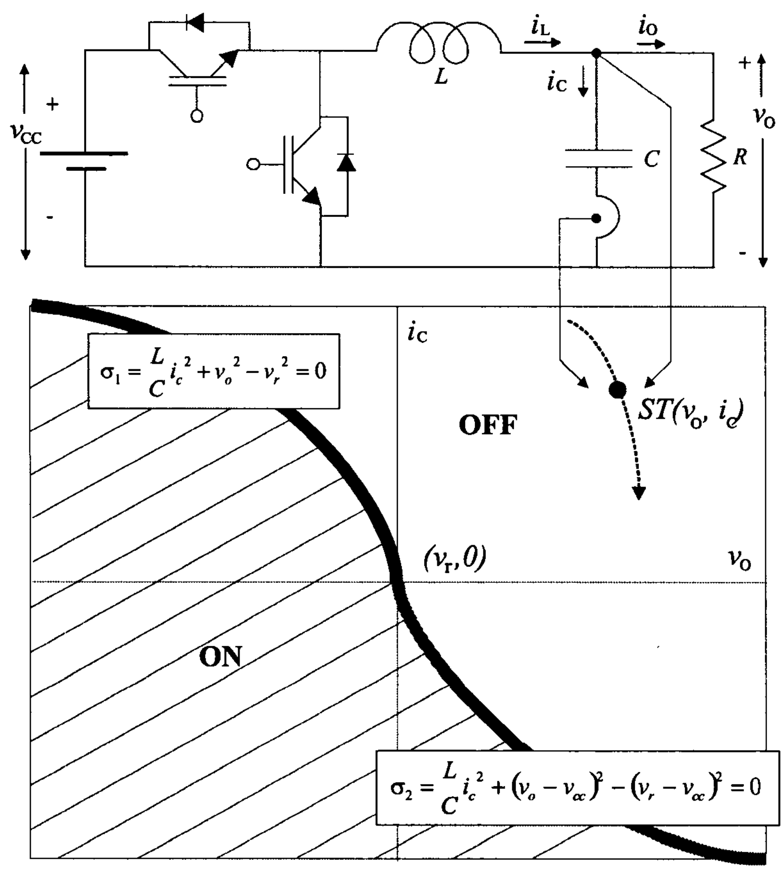

Fig. 4.21 Representation of the converter and the SS

The control scheme described above can be implemented in a fixed point DSP. An Interrupt Service Routine (ISR) of the ADC End of Conversion (EOC) starts the control algorithm. First, both output voltage v_o and capacitor current i_o are measured by the DSP using the ADC (signal conditioning is required). The sign of i_o determines whether

$$\sigma_1 = \frac{L}{C} i_c^{\,2} + v_o^{\,2} - v_r^{\,2} = 0 \tag{4.19}$$

or

$$\sigma_2 = \frac{L}{C} i_c^{\,2} + (v_o - v_{cc})^2 - (v_r - v_{cc})^2 = 0 \tag{4.20}$$

is used. Thereafter, the computation that compares the SS with the ST is performed to decide the switch state. Figure 4.22 shows a flow diagram of this routine.

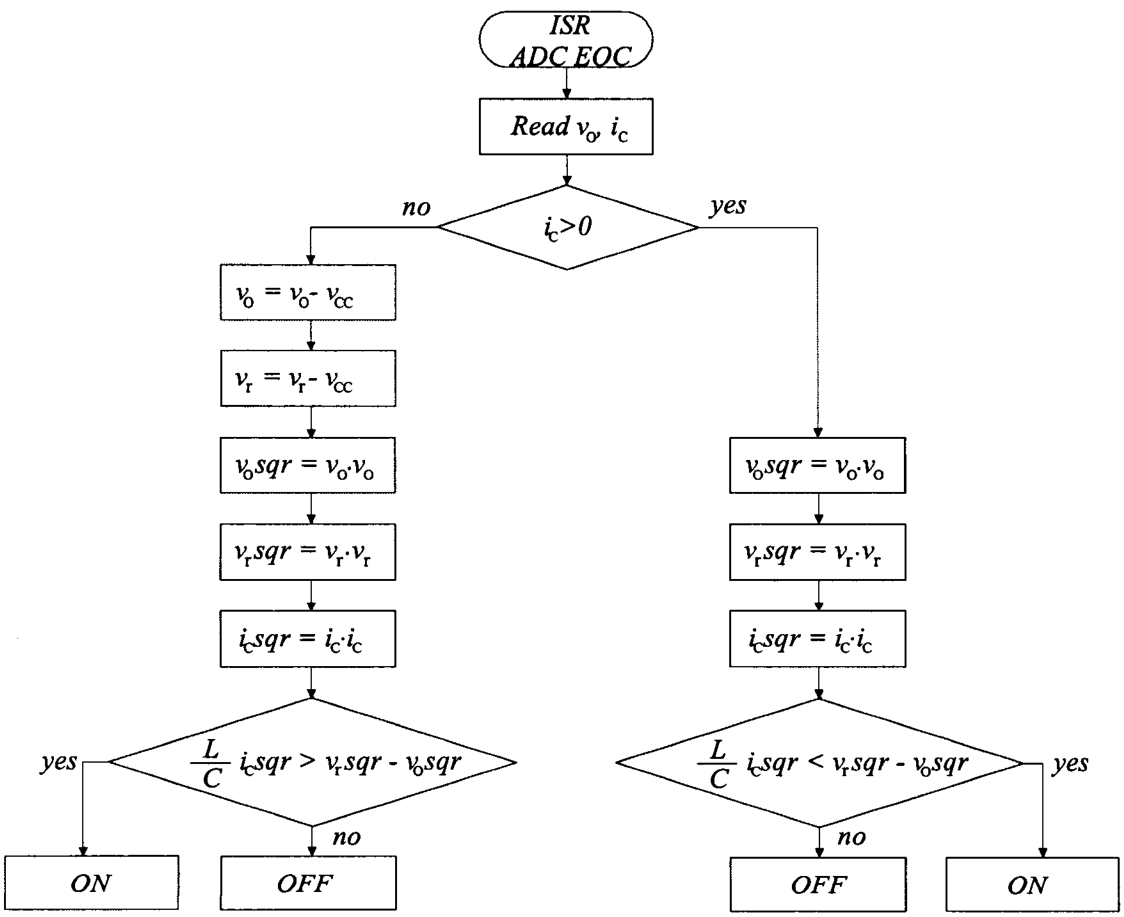

Fig. 4.22 Flow diagram of the DSP control routine

The number of operations to perform is deduced from the flow diagram and listed in Table 4.1. Since the number of operations required to perform the control law is low, the interrupt service routine can be run at a high frequency. Like in other digital controllers, sampling frequency is an issue in the stability of the close loop system.

Table 4.1: DSP number of operations

Task	Number of operations	
	$i_c > 0$	$i_c < 0$
Read ADC input	2	2
Compare	2	2
Multiplication	4	4
Difference	1	3
Set port (switch state)	1	1
Total	10	12

The DSP selected to implement the SS control scheme is a TMS320LF2407A 16-bit fixed-point from Texas Instrument. An evaluation board eZdsp LF2407A was employed for this purpose, which was programmed in 'C' language using Code Composer Studio. Isolated drivers were used to interface the DSP with the power stage. The parameters for the design example are presented in Table 4.2. The complete converter prototype is shown in Fig. 4.23 where the most important stages are identified.

Table 4.2: Buck converter parameters

$v_r = 30V$
$v_{cc} = 64V$
$L = 5mH$
$C = 50\mu F$
$R_{cd} = 5\Omega$

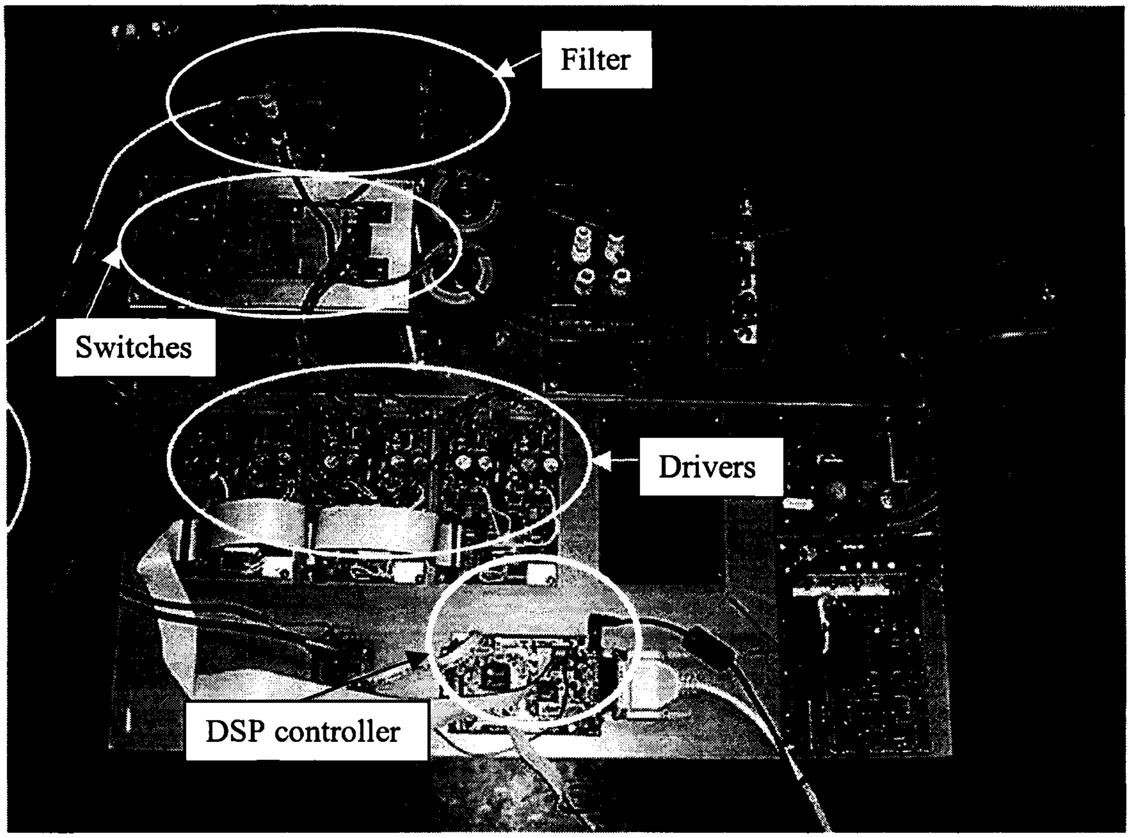

Fig. 4.23 power converter for the FC simulator: 1 kW prototype

4.5 Experimental and Simulation Results

Figure 4.24 shows a Matlab Simulink block diagram of the model used to perform the simulations. The subsystems (converter, load and the controller) are shown by the dashed lines. The converter model is a large signal model that contains all the elements of the actual circuit of Fig. 4.6. Two types of load transients, resistive and constant current steps, can be applied using this simulation scheme. The controller includes the natural unloaded SS explained in section 4.4.

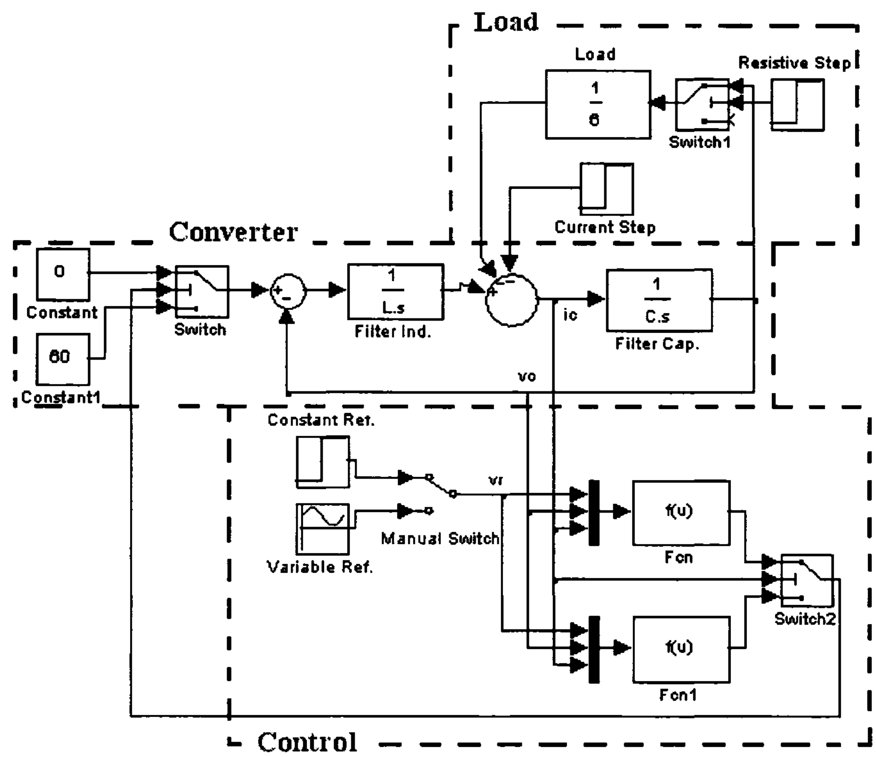

Fig. 4.24 Matlab Simulink block diagram of the power converter and control

Figure 4.25 shows the simulation results of the natural unloaded SS, depicting the output voltage, capacitor current, switch state, and output current for start up and sudden load change. The figure shows how the controller rejects the large signal perturbations with a near-time optimal response. Equivalent experimental results of the power converter response are presented in Fig. 4.26 for start up and sudden load change. During steady state, the converter switching frequency is inherently limited by a combination of the sampling frequency of the control stage and the SS. Experimental results of the transient response for resistive sudden load changes using the natural unloaded SS is shown in Fig. 4.27. As predicted by the analysis, the desired output voltage is achieved in one switching action during start up. The transient response during sudden load changes is also close to time optimal as described in section 4.3.3.

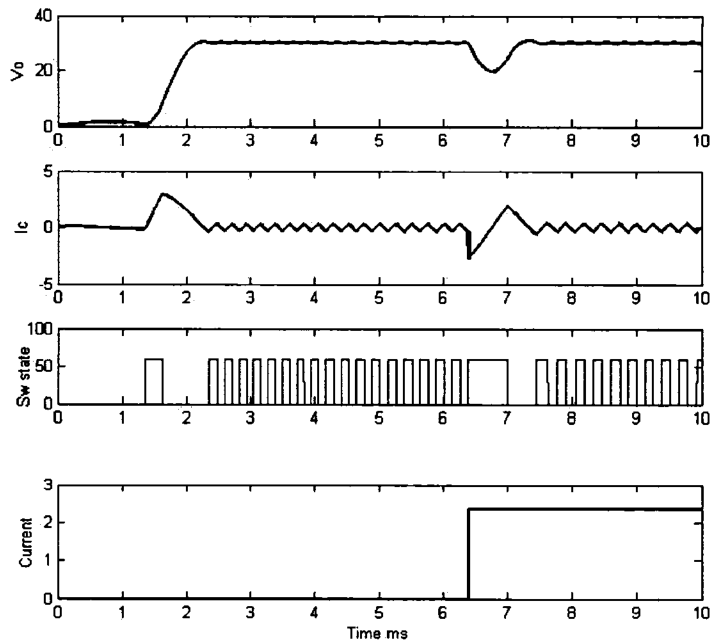

Fig. 4.25 Simulation results: Output voltage (V), capacitor current (A), switch state (V), and output current (A) during start-up and change in load current

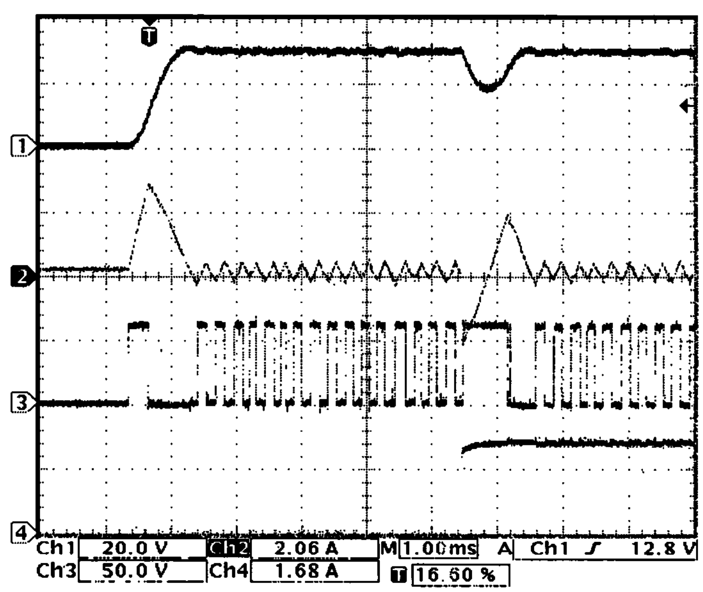

Fig. 4.26 Experimental results: Output voltage (Ch1), capacitor current (Ch2), switch state (Ch3), and output current (Ch4) during start-up and change in load

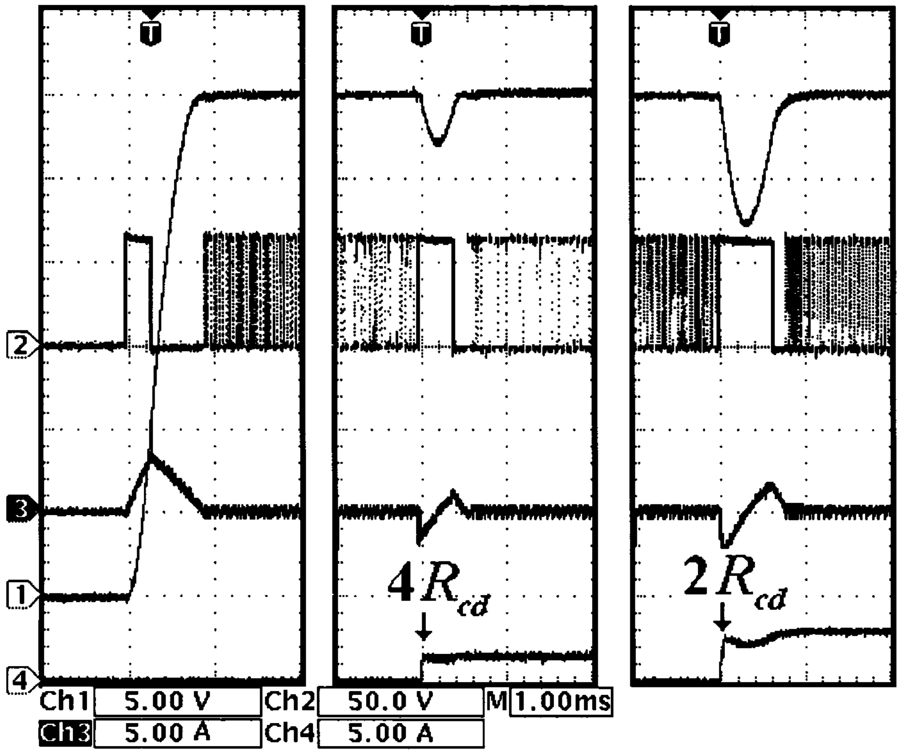

Fig. 4.27 Transient response using the natural unloaded SS: Output voltage (Ch1), switch state (Ch2), capacitor current (Ch3), and output current (Ch4) during start-up and sudden load change

Finally, the large signal frequency response of the power converter is shown in Fig. 4.28. The response complies with the dynamic requirement of power converters for FC simulators, i.e. large signal frequency response with unity gain and negligible phase margin beyond the expected current ripple frequency. Figure 4.29 shows the converter operating under a large signal sinusoidal reference.

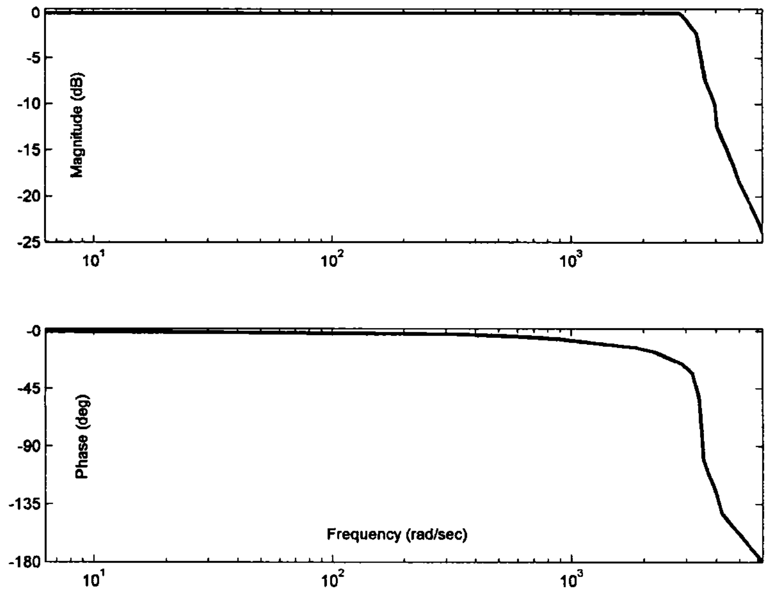

Fig. 4.28 Large signal frequency response of the power converter

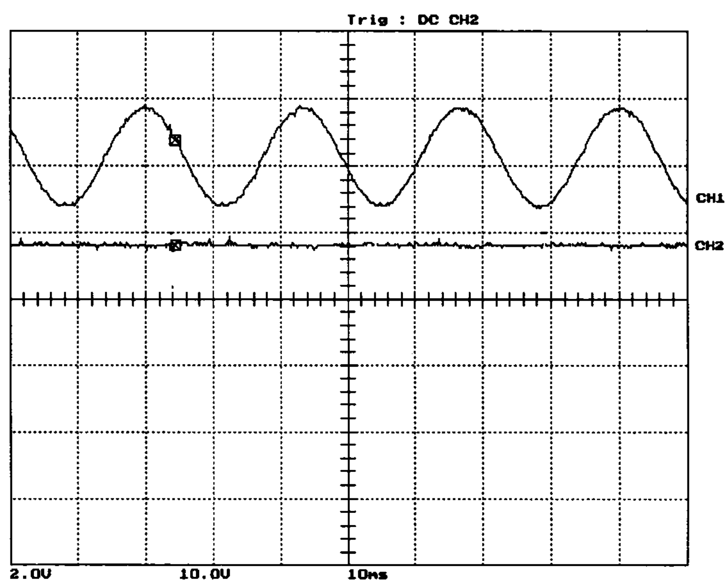

Fig. 4.29 Operation under variable voltage reference using the natural unloaded SS: Output voltage (Ch1), output current(Ch2)

4.6 Summary

A power converter for FC simulator systems with fast dynamic response has been presented in this chapter. A systematic procedure for the selection of a curved switching surface to control the converter based on normalized plots was proposed. The normalized 3D plots introduced in this chapter provide the required generality to evaluate transient performance for any given SS. As a result of the investigation, the elliptic natural unloaded SS, showing excellent transient behavior and no overshoot was selected. Finally, the strategy used to implement the control scheme in a DSP was also presented revealing a low computational requirement with a maximum of 12 operations. This special power converter is used in chapters 5 and 6 as part of a FC simulator system.

Chapter 5

Stand-Alone Fuel Cell Simulator

This chapter presents the development of a stand-alone FC simulator based on a low cost Digital Signal Processor (DSP). An empirical model of a Direct Methanol Fuel Cell (DMFC) is used to replace the complex electrochemistry equations used to model the FC. This results in a reduction of computational requirements and makes possible the implementation of the model in a fixed-point DSP. The procedure to build an empirical model based on dynamic tests performed on the FC is presented and can be extended to other FCs. The power converter described in chapter 4 is used to emulate the behavior of a FC stack, providing the required dynamic response and robustness during the transients. A description of the strategy used in the DSP to process the FC model is described. Experimental results comparing the behavior of the proposed simulator and the actual FC are also presented and discussed. The work described in this chapter was presented at the IEEE Canadian Conference on Electrical and Computer Engineering (CCECE) in 2005 [75].

Figure 5.1 shows a block diagram of the proposed stand-alone FC simulator. Both the power converter controller and the FC model are programmed in a fixed-point DSP, leading to a reduction of the parts and cost of the system.

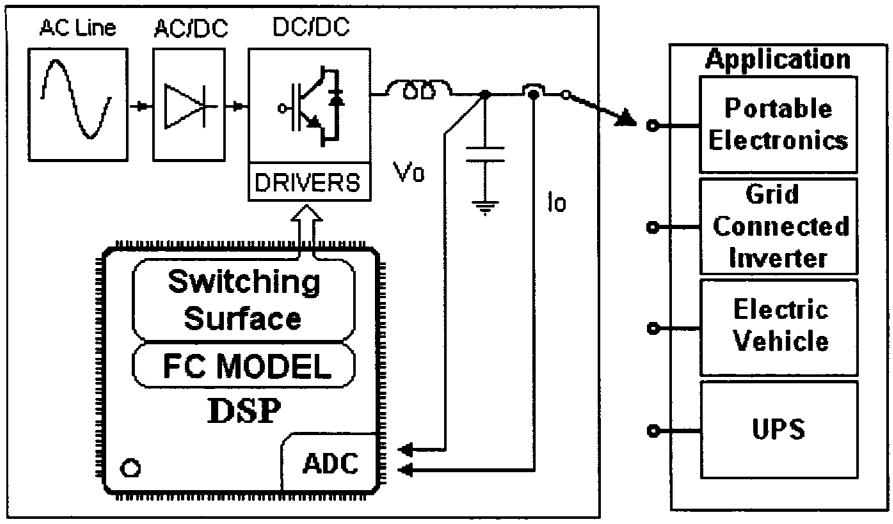

Fig. 5.1 Block diagram of the proposed stand-alone FC simulator

5.1 Obtaining the Parameters for the Model

The electrical FC model introduced in chapter 2 provides a reasonable approach to the real FC, considering its simplicity. For convenience, the model of Fig. 2.4, the polarization curve of Fig. 2.5, and the model mathematical representation (Eq. 2.4 and 2.5) are repeated in this chapter as Fig. 5.2, Fig 5.3, and Eq. 5.1 and 5.2 respectively.

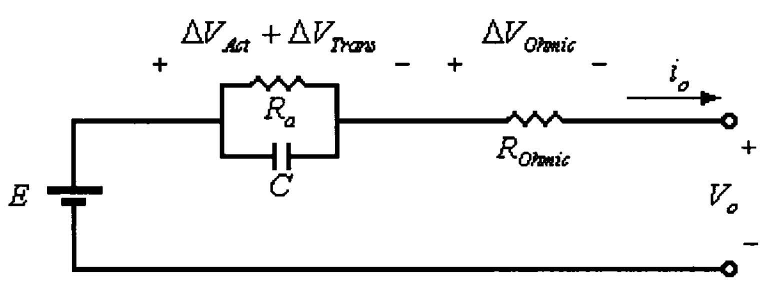

Fig. 5.2 Electrical equivalent model the FC

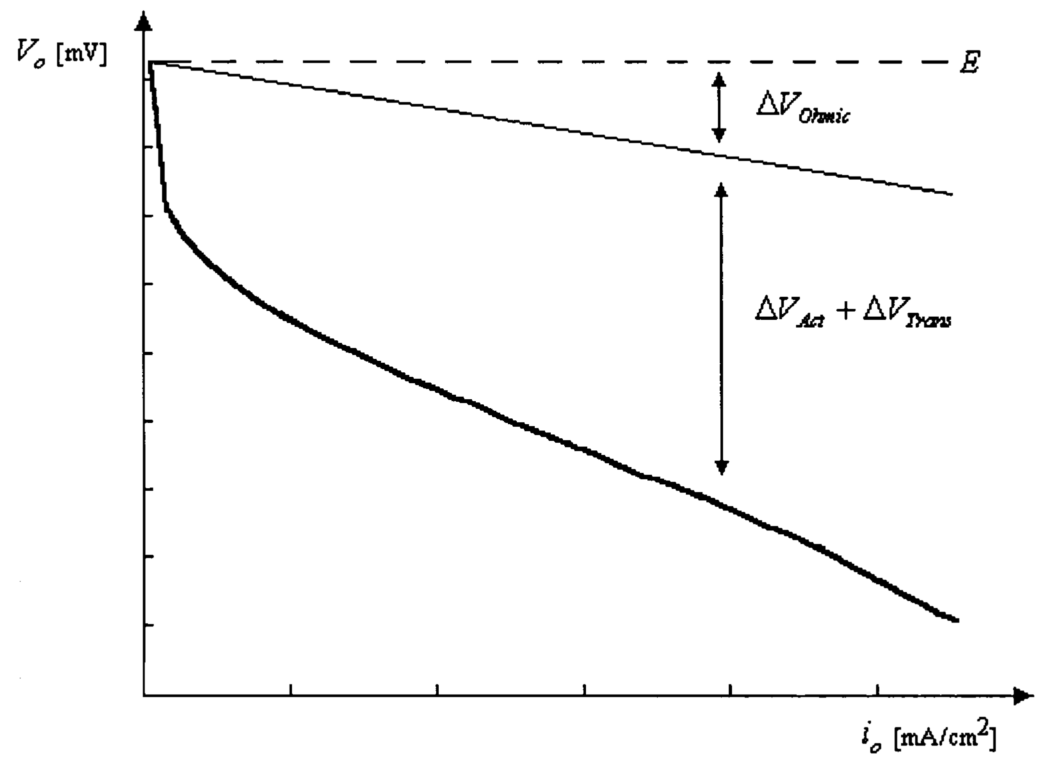

Fig. 5.3 FC polarization curve

$$Vo = E - i_o R_{ohm} - \Delta V_{Act} - \Delta V_{Trans} \tag{5.1}$$

$$\frac{d(\Delta V_{Act} + \Delta V_{Trans})}{dt} = i_o \cdot \frac{1}{C} - \frac{\Delta V_{Act} + \Delta V_{Trans}}{R_a \cdot C} \tag{5.2}$$

This model contains four parameters: open circuit output voltage E, voltage drops introduced by R_{ohm} and R_a, and the double layer capacitor C that produces a first order effect in the FC dynamic behavior.

In order to obtain the parameters for the FC setup described in section 2.2.2, the following simple procedure was followed:

1) E is obtained by measuring the open circuit output voltage of the FC. The measured open circuit voltage was E =824 mV.

2) R_{ohm} is indirectly measured by performing a current step test on the FC and computing the ratio of the output voltage drop and the current change at the instant where the step is produced. Alternatively, it can be obtained using impedance analysis [54], [55]. The obtained value for the resistance was $R_{ohm} = 0.254\,\Omega$.

3) R_a is a nonlinear function of the FC output current. The following equation is used to calculate the R_a vector for the entire operating range of the FC. The polarization curve is required for this computation and was obtained prior to this calculation.

$$R_a(i_o) = \frac{\left(E - V_O(i_o) - R_{ohm} \cdot i_o\right)}{i_o}, \tag{5.3}$$

where i_o is the FC output current and $V_O(i_o)$ is the steady state output voltage that is a function of the output current i_o. Figure 5.4 show plots of R_a, Y_a, and V_O as a function of i_o, where $Y_a = 1/R_a$.

4) C is obtained by fitting the time domain expression of the model to an actual step response on the FC. The value of C that gives the minimum Sum of Squares (S) for the following expression during a current step test is selected [76].

$$S = \sum_{u=1}^{n} \left[y_u - E + i_o \cdot R_{ohm} + i_o \cdot R_a \left(1 - e^{-\frac{1}{Ra \cdot C} t} \right) \right]^2 \tag{5.4}$$

where y_U is the measured response. The value obtained for the double layer capacitor was $C = 200\,mF$.

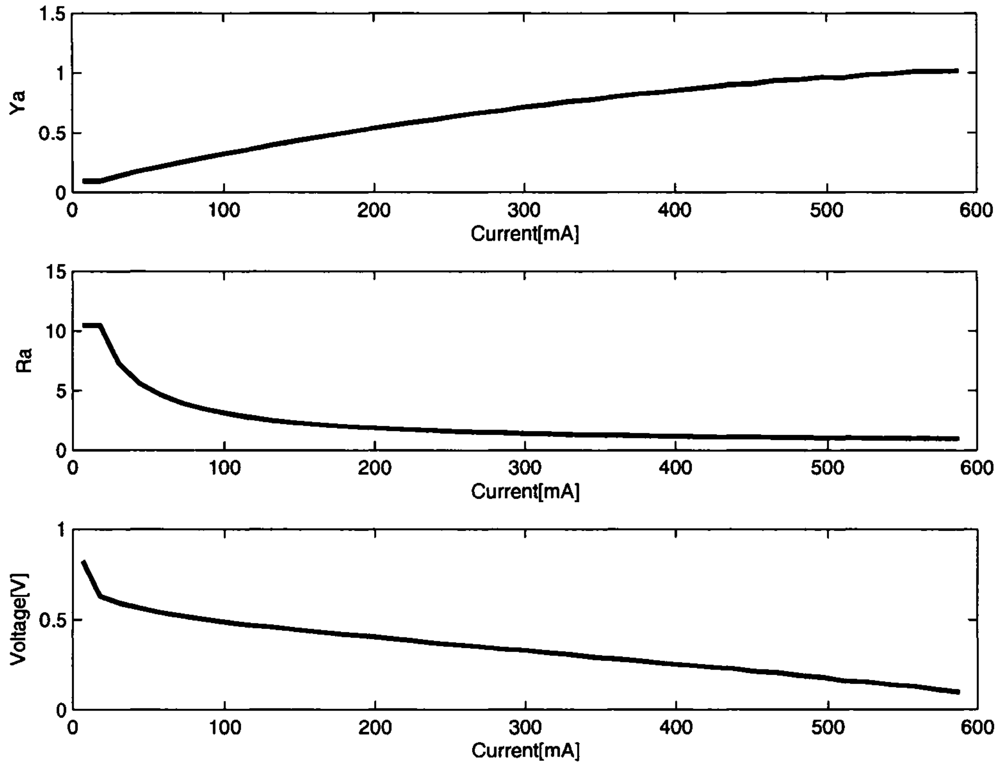

Fig. 5.4 Y_a (S), R_a (Ω), and V_O as a function of i_o

5.2 Simulation Results

The procedure of section 5.1 was followed to obtain the parameters of the FC empirical model. In order to validate this model, simulation results are compared with experimental results. For simplicity, a first simulation of the FC using the empirical model was performed using Matlab/Simulink as shown in Fig. 5.5. It can be noticed that the block diagram includes the four parameters E, R_{ohm}, R_a, and C. The activation resistance R_a is loaded as a lookup table.

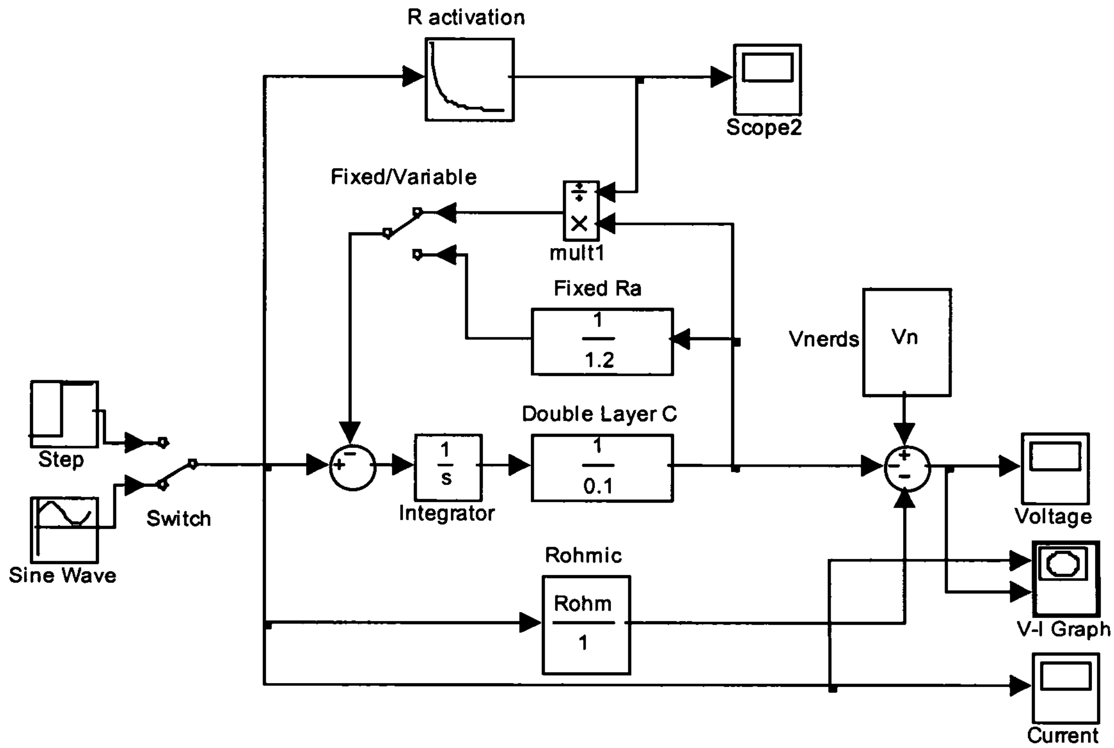

Fig. 5.5 FC empirical model: Matlab Simulink block diagram

Since the FC model (first order differential equation) is implemented in a DSP, a numerical method is required for its computation. Runge-Kutta method is one that numerically implements ordinary differential equations by using a trial step at the midpoint of an interval to cancel out lower-order error terms [77], [78]. This classical numerical method was programmed in 'C' code to compute the dynamic behavior of the FC. Experimental results for current step changes were compared to results obtained with Matlab Simulink and results computed by the 'C' code routine. Figures 5.6 to 5.9 show the response of the FC under current steps changes and the simulation results for the parameters given in section 5.1. Since the numerical response using Runge-Kutta method is exactly the same as the results in Matlab Simulink the traces are overlapped (referred as Model in the plot). The results show good match during current step transients.

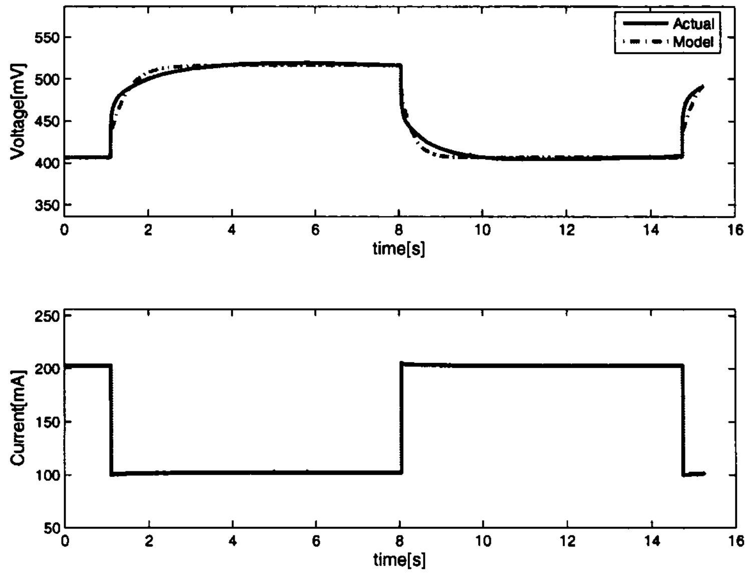

Fig. 5.6 Current step response from ~100mA to ~200mA: Actual FC vs. empirical model of the FC (Runge-Kutta/Simulink).

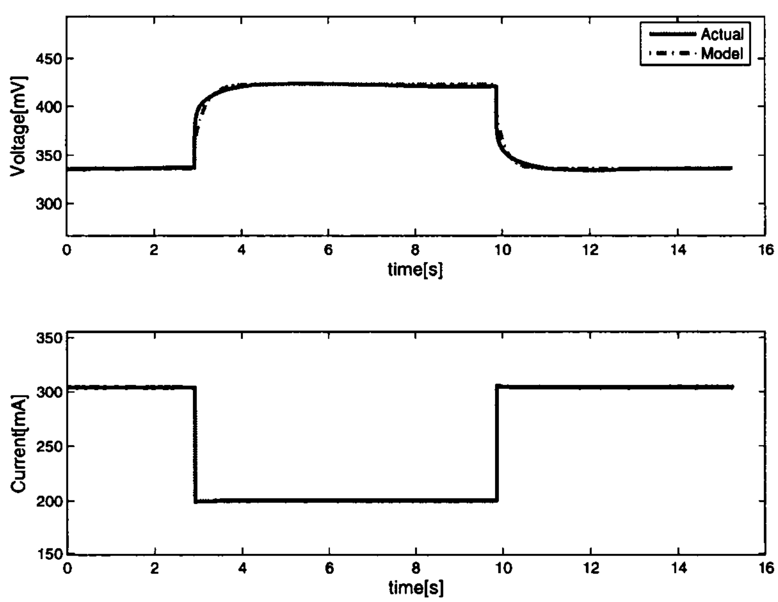

Fig. 5.7 Current step response from ~200mA to ~300mA: Actual FC vs. empirical model of the FC (Runge-Kutta/Simulink).

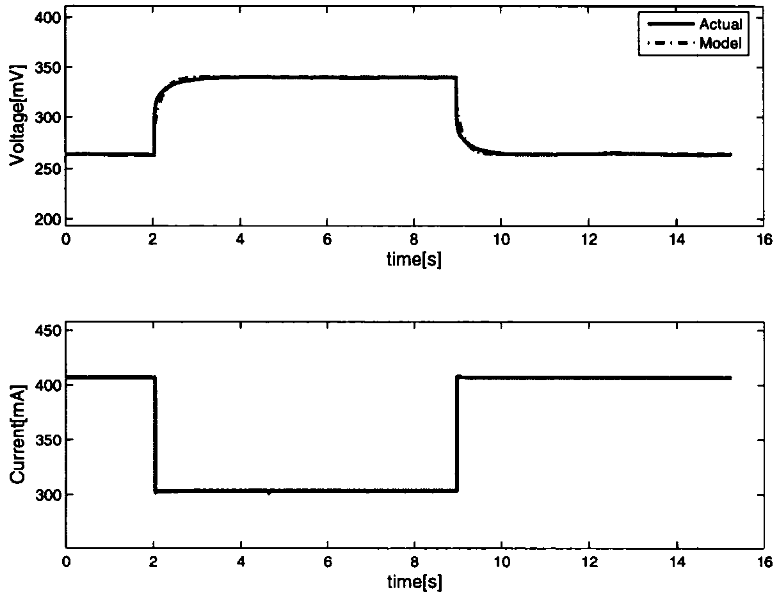

Fig. 5.8 Current step response from ~300mA to ~400mA: Actual FC vs. empirical model of the FC (Runge-Kutta/Simulink).

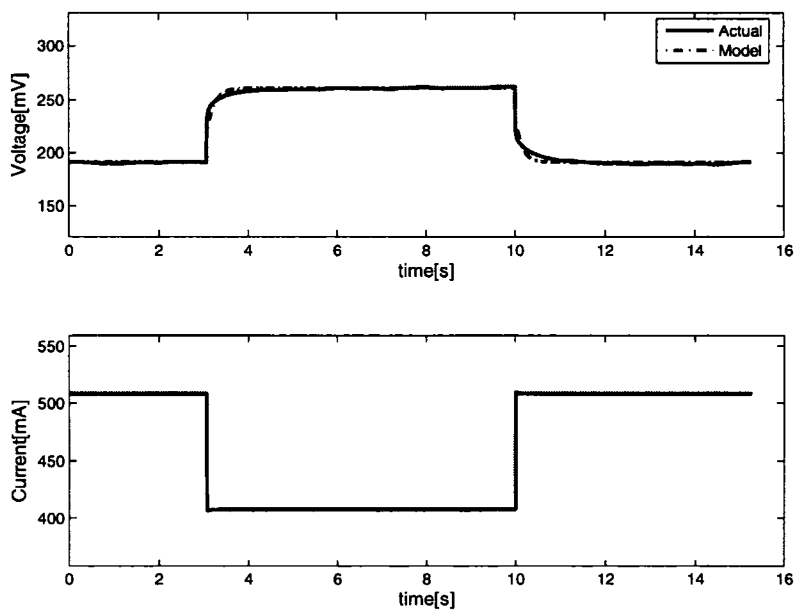

Fig. 5.9 Current step response from ~400mA to ~500mA: Actual FC vs. empirical model of the FC (Runge-Kutta/Simulink).

5.3 DSP-Based Implementation

The FC empirical model was implemented in a fixed-point DSP (TMS320LF2407A). This results in a low cost FC simulator with compact handy characteristics.

The flow diagram of the software is shown in Fig. 5.10. Two essential interrupt service routines (ISRs) called timer and ADC EOC (Analog to Digital Converter End of Conversion) are employed for the FC model and the control strategy respectively. The timer ISR acquires the converter output current i_o, which is the output current of the emulated FC, and computes the ordinary differential Eqs.5.1 and 5.2 of the FC model using Runge-Kutta (R-K) method. The output of the numerical method provides the new reference voltage v_r. The power converter output voltage v_o is controlled by the ISR of ADC EOC to follow the reference voltage v_r generated by the Runge-Kutta (R-K) calculations to emulate the dynamic behavior of the FC.

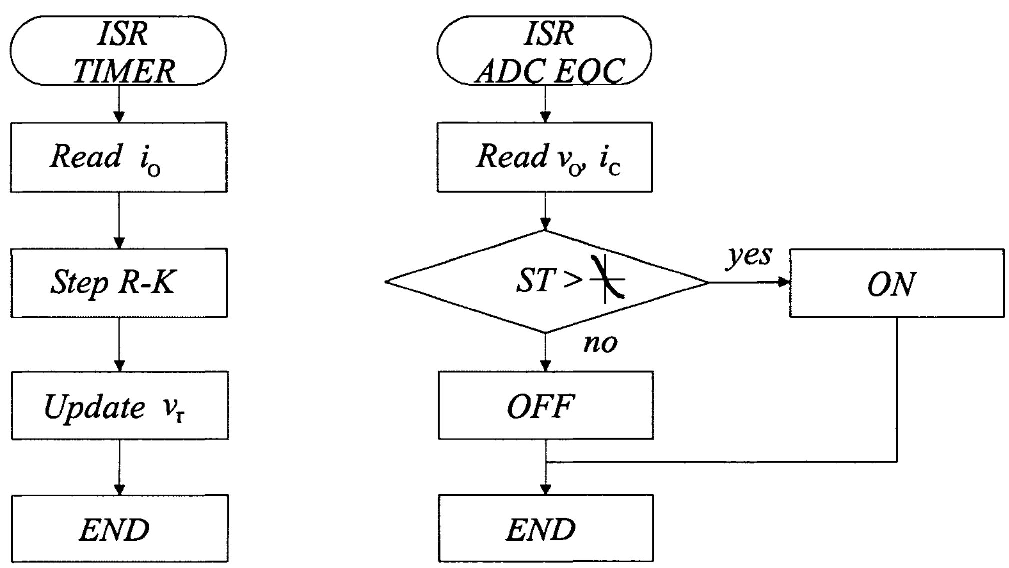

Fig. 5.10 Flow diagram for the FC model and converter controller

The ISR of the ADC EOC operates at a fixed frequency. This routine acquires the capacitor current i_C and the output voltage V_O that define the State Trajectories (ST) position at a given time. A comparison between a curved switching surface and the ST is performed to decide the control action. A complete explanation of this routine was presented in chapter 4.

5.4 Experimental Results and Comparisons

The FC setup described in section 2.1.2 is used in this chapter to obtain results for comparison. A series of 55 single cells was considered to obtain an equivalent FC stack. The empirical model was obtained following the procedure of section 5.1 and loaded on to the DSP according to the flow diagrams of section 5.3. The complete stand-alone FC simulator setup is shown in Fig. 5.11.

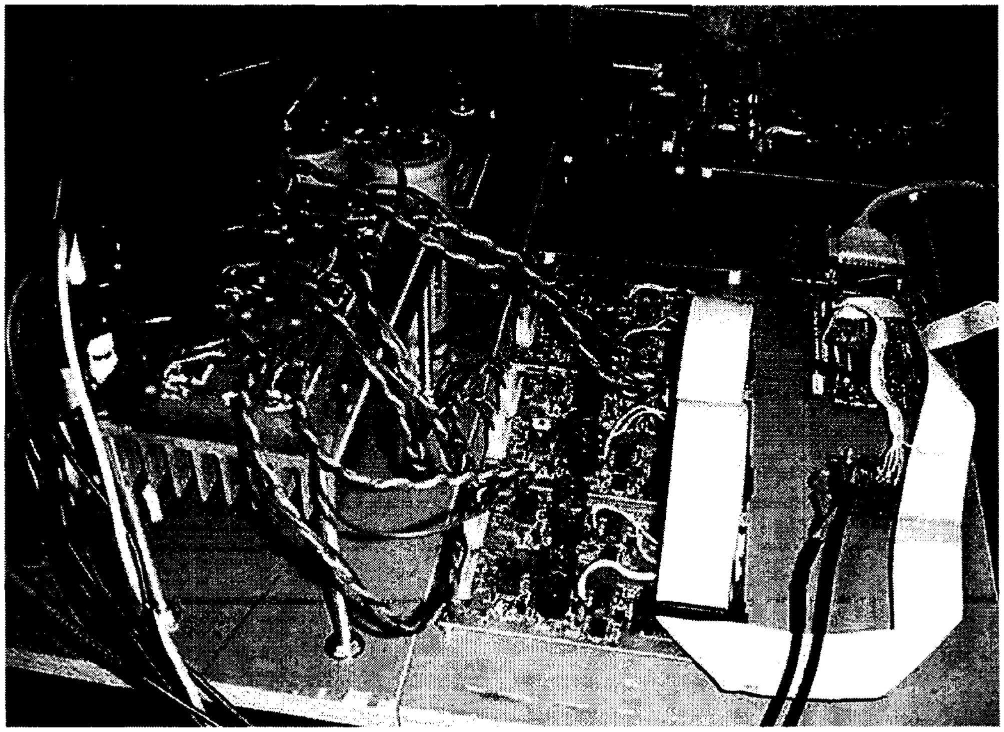

Fig. 5.11 Prototype of the FC simulator

A series of current step tests performed on the FC simulator and the actual FC are presented in Fig. 5.12 (voltage versus current characteristic) and Fig. 5.13 (time domain graphic). The polarization curve presented in Fig. 5.12 has an exact match between the FC simulator and the actual FC. The current step responses shown in Fig. 5.13 also shows a good match except for a deviation in the low current region. This is due to the highly nonlinear nature of the FC behavior in that particular region, which is not completely covered by the model. It is noticed in Fig. 5.12 that the trajectory of the operating point (dashed lines) experience a large deviation from the polarization curve (bold line) during the transient interval, revealing the effect of the double layer capacitor C. The simulator was able to reproduce this effect successfully. The operating point finally lies on the polarization curve after the transient interval.

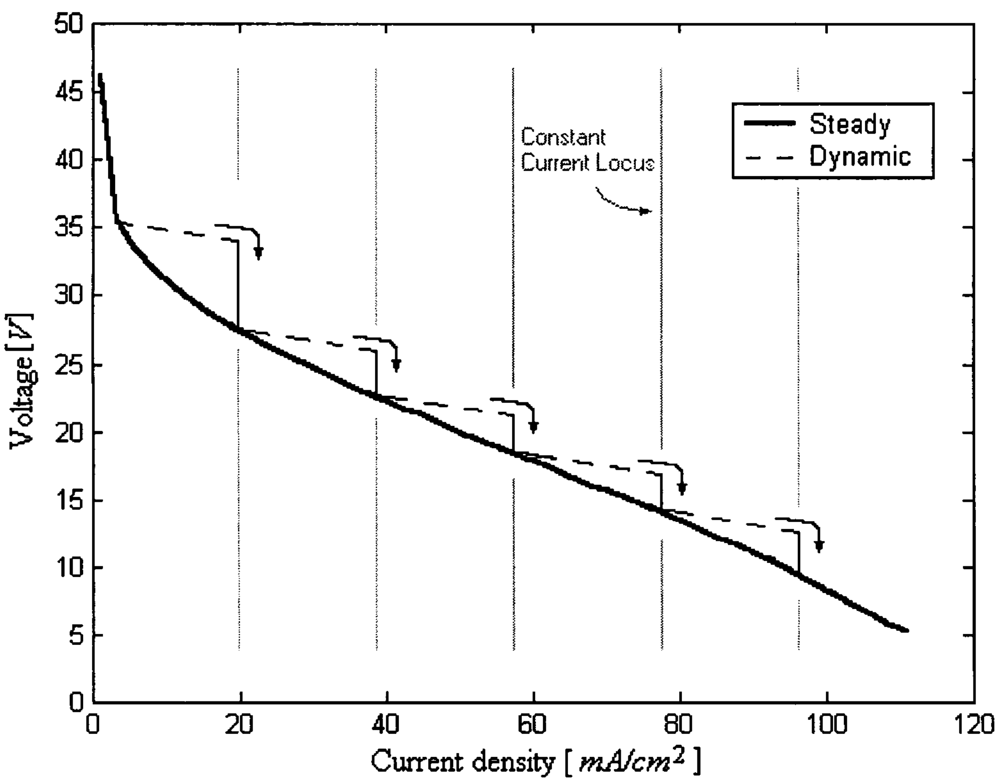

Fig. 5.12 Voltage-current characteristic

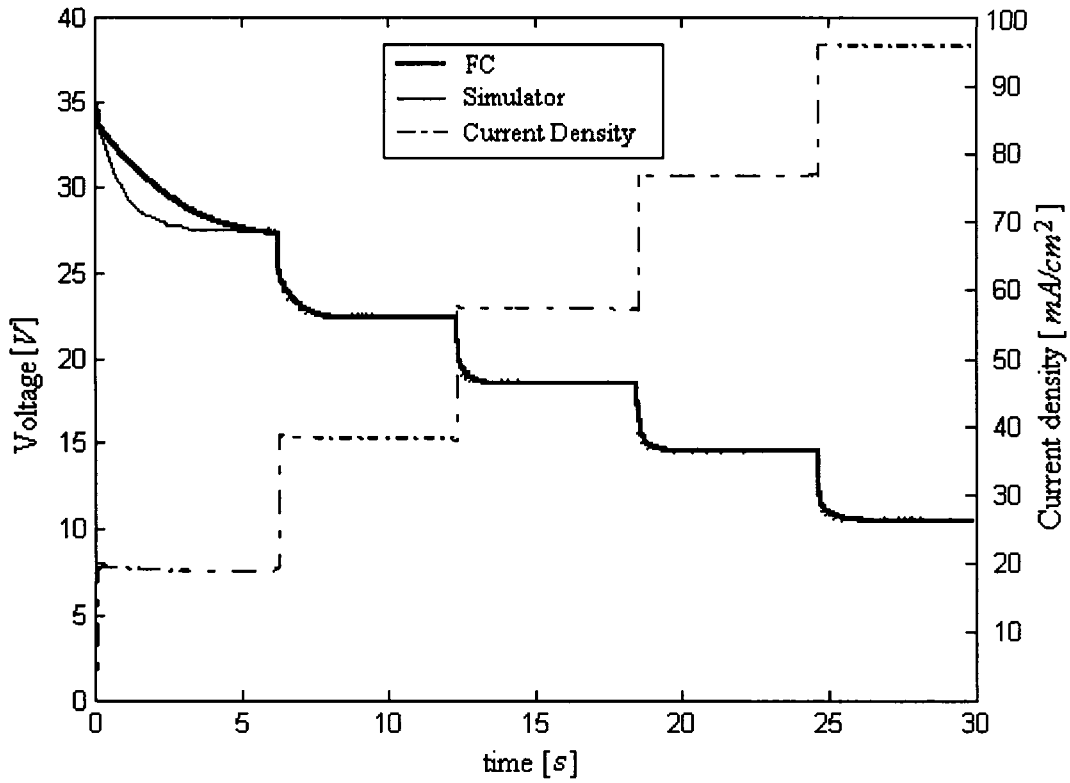

Fig. 5.13 Current steps responses

5.5 Summary

The development of a stand-alone FC simulator based on a low cost Digital Signal Processor (DSP) was presented in this chapter. Portability is the most important feature of this compact and handy FC simulator, which aids to simplify research tasks in laboratories. An empirical model of a FC that reduces the computational requirements was presented and implemented in a DSP. The power converter described in chapter 4 was used in this system to emulate the behavior of a FC stack. Experimental results comparing the behaviors of the proposed simulator and the actual FC showed a good match for steady state and dynamic operation of the FC under current steps changes in the load.

Chapter 6

A Novel Real-Time Fuel Cell Simulator Based on a Small Single Fuel Cell

A stand-alone FC simulator suitable for laboratory operation was presented in chapter 5. It provides the advantages of eliminating the dependence upon a computer, communication cards, and licensed software, resulting in a small low-cost system. This simulator is limited to low mathematical complexity model that can be processed within the Digital Signal Processor (DSP).

Perhaps the most important issue concerning FC models and therefore previous FC simulators is their limited features. Effects like water flood, membrane drying, catalyst poisoning, and aging are difficult to predict. These topics, which are not accurately represented by models, are under study. Thus, the results might depart from reality (i.e. dynamic response, parts degradation, etc.). Particularly, a frequency response analysis could put into perspective the differences between an actual FC and a model.

In order to overcome this main drawback and expand the features of the existing designs a novel FC simulator system is proposed. This FC simulator introduces the concept of replacing the computer model of the FC with an actual small single FC. A single FC costs a small fraction of a FC stack and can reproduce the behavior of an expensive powerful FC stack using scale up rules. The dynamic behavior of the single FC is amplified using the power converter with fast dynamic response of chapter 4 to emulate the FC stack. This arrangement provides a real working environment at a low cost and allows a comprehensive design and study of FC systems and FC power electronics. The work described in this chapter was presented at the IEEE Power Electronics Specialist Conference (PESC 05') in 2005 [79].

6.1 The Proposed Fuel Cell Simulator

Figure 6.1 shows a block diagram of the proposed FC simulator, which uses a 150mW single DMFC as the system reference. The proposed fuel cell simulator emulates the electrical dynamic behavior of a FC stacks. This is achieved by controlling a fast dynamic power converter according to a reference signal that corresponds to the FC electrical output characteristics. The FC simulator system includes the following unique features:

- A small low cost single FC with electronic load is used to provide reference characteristics for the simulator to provide real accuracy to the system.
- A power converter with DSP control is specially designed to cope with the required dynamic characteristics as described in chapter 4.
- Control Area Network (CAN) bus interface.
- PC based system monitoring and analysis.

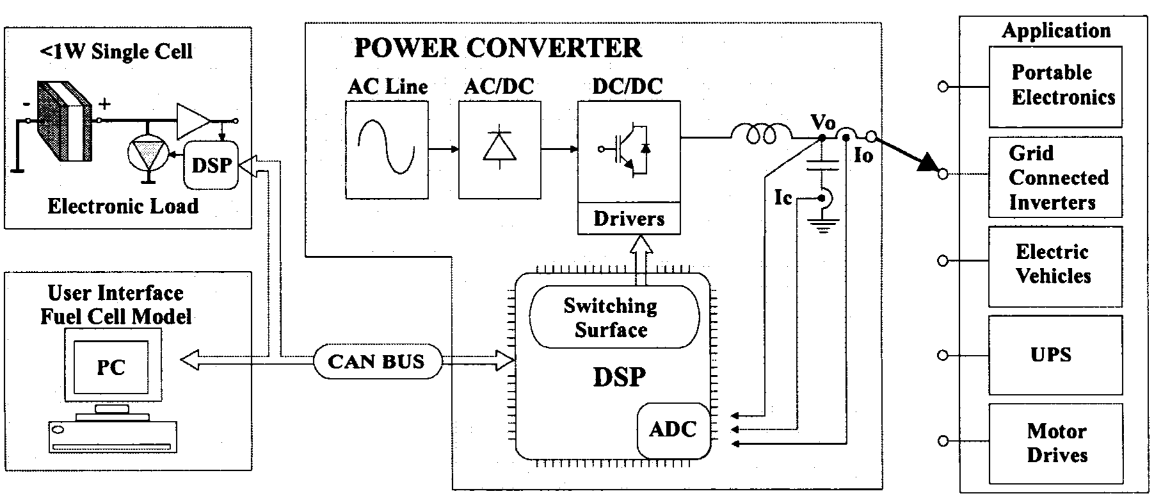

Fig. 6.1 Block diagram of the proposed FC simulator

6.2 System Description

As shown in Fig. 6.1, the system contains three main parts: A single FC connected to an electronic load, a power converter, and a computer. The DSP-controlled electronic load described in chapter 3 is connected to the single FC. The electronic load behaves like a current source that extracts power out of the single FC. This allows the dynamic operation of the single FC within its limits in order to generate the simulator reference signal. The power converter uses the reference signal to emulate the behavior of a FC stack in order to drive the actual application. The computer in the system may be used for monitoring, to run a computer-based model, or to perform dynamic tests on the single FC.

6.2.1 Reference Signal

The reference signal for the power converter can be generated using either a low cost single FC or a FC computer model. Each method for generating the reference signal has different features. The single FC only costs a small fraction of a fuel cell stack, and provides the actual dynamic behavior. The single cell dynamic behavior is amplified with the power converter using scale up rules and connected to the actual application (e.g. inverter, motor drives, UPS, etc). This allows a complete scale evaluation for the system and prevents possible results that depart from reality due to modeling inaccuracies. The evaluation may include fuel consumption, efficiency, dynamic response, and reliability tests. In addition, since most electrochemistry research in FC is conducted with single cells, the proposed FC simulator can use a state-of-the-art single cell to emulate the results of a FC stack driving real applications. This leads to cost and time savings for FC system development.

Computer-aided models are particularly useful because of their flexibility. They can be easily modified and updated according to new developments. Model variables are typically FC temperature, fuel concentration and flows rates, as well as mechanical parameters for the assembly [35]. From the electrical point of view, the FC output current is the main variable of the model and should be measured from the output of the power converter. Another advantage of the computer-aided model is that the variables involved in the electrochemical process can be controlled and monitored. However, there are still some doubts about the accuracy of the models and the lack of information about the parameters. For these reasons the use of a single cell in the FC simulator results in a more robust system. The system also includes an interrupt-based routine that allows the mode of operation to be switched between a computer-based model and the single cell module.

6.2.2 Electronic Load and User Interface

The electronic load connected to the single FC was constructed with a low cost DSP including CAN peripheral (TMS320C), fast serial DAC (TLV5636) and precision instrumentation amplifier (AD8554). The detailed hardware and software description of the electronic load is given in chapter 3, and a prototype of the system is shown in Fig 3.7. This special circuit provides effective parameter measurements and control of the single FC output current at a low cost with the additional advantage of the real-time processing capability of the DSP.

The user interface was entirely programmed with Builder C++ under windows operating system. The software drives a National Instruments CAN bus board (NI PCI-CAN Series 2). The voltage and current measurements of the reference single FC/Model and the power converter can be captured from the CAN bus transmissions and displayed on the PC screen. This information can also be stored for further analysis. In addition, the software allows the display and control of the parameters of the FC model and the single cell module through track bars and pop-up menus. Figure 6.2 shows the main screen of the user interface. Finally, the entire prototype of the system is shown in Fig. 6.3 where the power converter, the small single cell with electronic load, and the PC user interface are depicted.

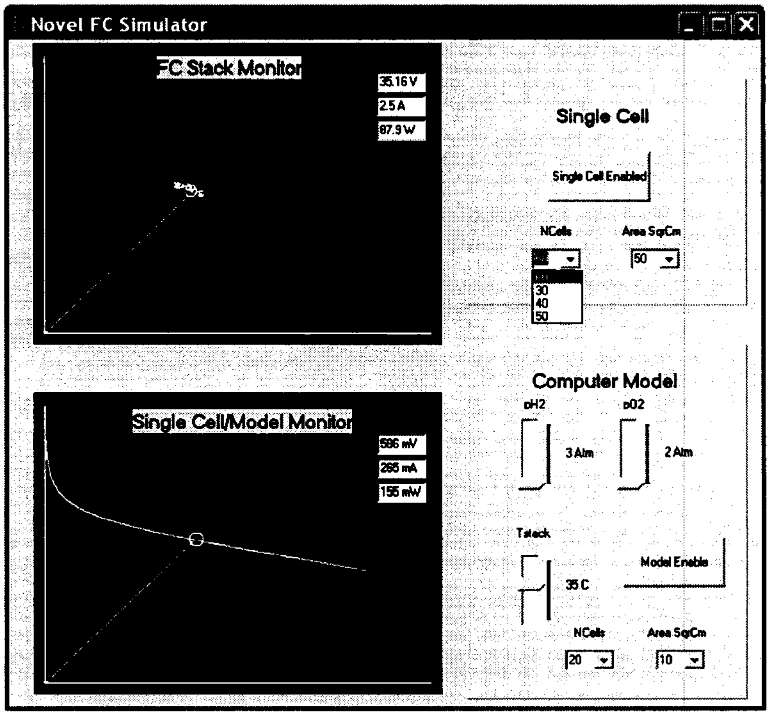

Fig. 6.2 User interface screen

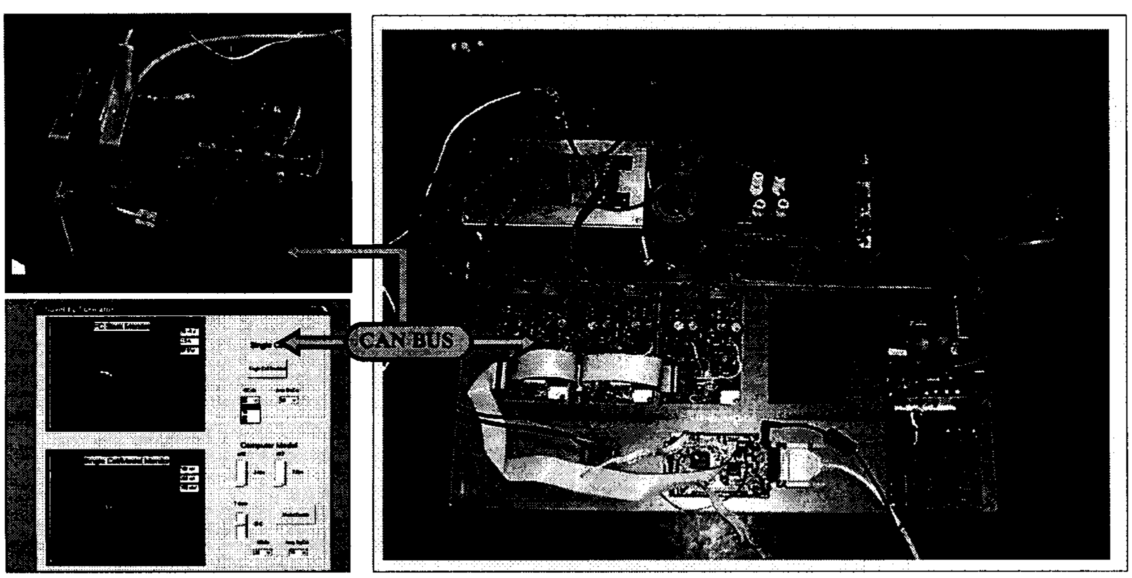

Fig. 6.3 Prototype of the proposed FC simulator system

6.3 Operating Principle of the Fuel Cell Simulator

Figure 6.4 shows the functional diagram, which illustrates the operating principle of the FC simulator. The diagram can be divided into two parts: The single FC connected to a current source on the left side of the dashed line, and a voltage source on the right side of the dashed line. The current source represents the electronic load connected to the single FC, while the voltage source corresponds to the power converter. The output current i_o is reflected on the single cell according to the scale rule function α emulating the effect of a bigger electrode effective area in the FC. At the same time, the voltage cell V_{cell} is amplified N times by the voltage source emulating N single FCs connected in series, thus emulating a FC stack.

The operating principle of the proposed simulator is as follows. The output current of the power converter is measured by the DSP and transmitted through the CAN bus. The DSP-controlled electronic load receives the information and proceeds to extract a proportional current from the single FC following the scale up rule function α. The single FC output voltage changes dynamically according to its output current. This voltage is measured by the DSP that controls the electronic load and transmitted through the CAN bus. The power converter receives this information and amplifies the single FC voltage with a gain of N, where N is the number of cells in series considered in the stack emulation. Under this mode of operation, the computer only monitors the exchange of parameters through the CAN bus. The system can operate without the computer, thus reducing the size and complexity of the system. The FC simulator can also be operated using a computer-based model. In this mode, the single FC module can be eliminated.

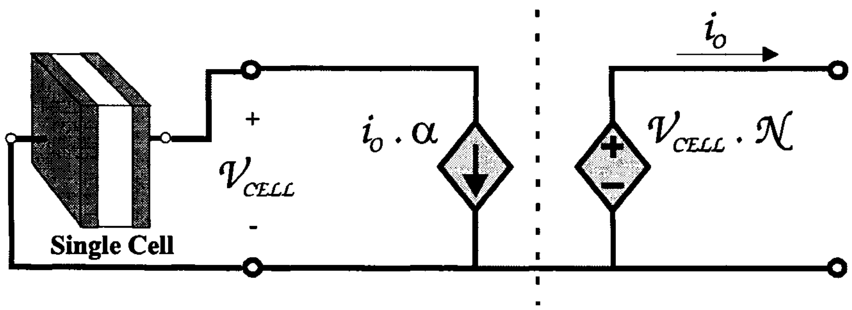

Fig. 6.4 Functional diagram of the FC simulator

6.4 Experimental Results

In the following example case, the proposed simulator is used to emulate a DMFC stack with $N = 60$ cells in series and an active cell area of 70.7cm^2. The current density (A/ cm^2) capability of the single FC is kept constant in this example resulting in

$$\alpha = \frac{\text{single cell active area}}{\text{stack active area}} = 0.075 \quad . \tag{6.1}$$

Two dynamic tests consisting of operation under 120Hz current ripple and operation under current steps were performed using the power module expansion described in section 3.5. Further details are provided below.

6.4.1 Single Fuel Cell Reference Setup

Preliminary preparation of the membrane and electrodes is described in section 2.1.2. The preparation of the Membrane Electrode Assembly (MEA) differs from the one described in section 2.1.2. For this chapter the membrane and electrodes (5.3cm^2) were placed into brass die and pressed for 3 min at 130°C with Carver Laboratory Press (model M), but the pressure was 43Kg cm^{-2} instead of 155Kg cm^{-2}. The effect of the reduced pressure improves the performance of the FC [80]. As a result the FC behavior is different from the results of chapter 2 and chapter 5. The MEA was evaluated in a commercial 5.3 cm^2 active area cell fed with 1 Mol aqueous MeOH at 0.15 *mL/min* and dry air at fixed flow rate of 75 *mL/min* Experiments were conducted at a cell temperature of 60+/-1 °C.

6.4.2 Fuel Cell Stack Emulation

Figures 6.5 and 6.6 show experimental results of the FC simulator under 120Hz current ripple operation. Figure 6.5 depicts the transient trajectory for both the single FC and the FC simulator response on a voltage versus current plot. The polarization curve shows an excellent match for the single FC and the FC simulator. The transient trajectory of the operating point shows a hysteretic behavior, which has a pivot on the polarization curve. This effect is produced by the double layer capacitor. The FC simulator successfully reproduced this effect. Figure 6.6 shows a time domain representation of the results under 120Hz current ripple operation where the traces represent: 1) power converter output voltage, 2) single FC output voltage, 3) single FC output current, and 4) power converter output current.

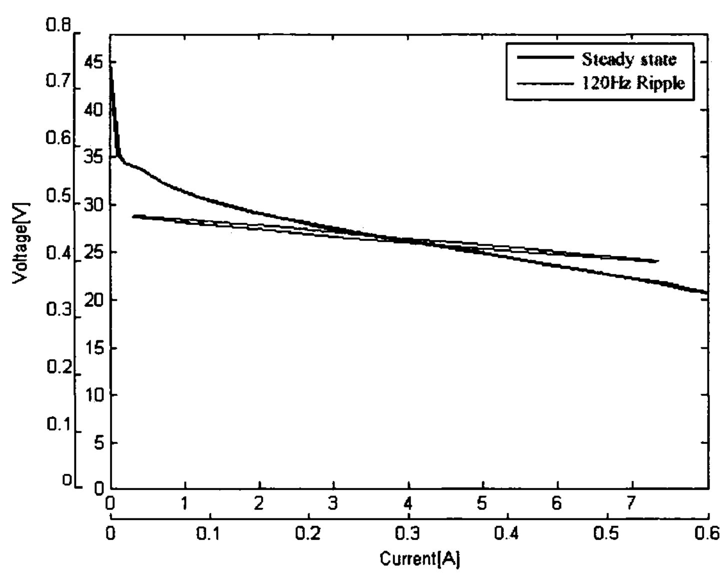

Fig. 6.5 Voltage versus current characteristics of the single FC and FC simulator under 120Hz current ripple test

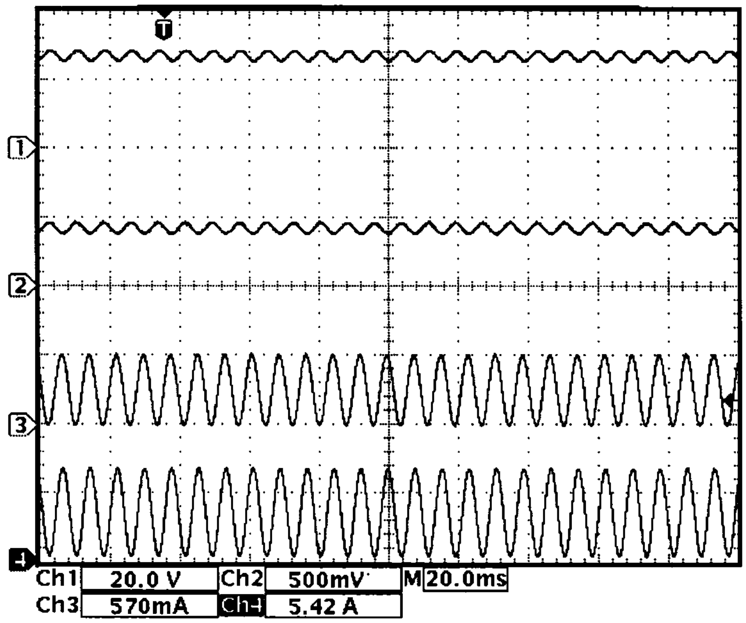

Fig. 6.6 120Hz current ripple operation: power converter output voltage (Ch1), single FC voltage (Ch2), single FC current (Ch3), and power converter output current (Ch4)

Figures 6.7 and 6.8 show experimental results of the FC simulator operating under current steps. Fig. 6.7 depicts the transient trajectory on a voltage-current plot. The current step responses reported an excellent match, including the high non-linear region of the polarization curve (low current). The transient trajectory of the operating point experienced a large deviation from the polarization curve during the transient interval. This is due to the effect of the double layer capacitor. The FC simulator also reproduced this effect successfully. The operating point finally lies on the polarization curve after the transient interval. Figure 6.8 shows the results on a time domain representation where the traces represent: 1) power converter output voltage, 2) single FC output voltage, 3) single FC output current, and 4) power converter output current.

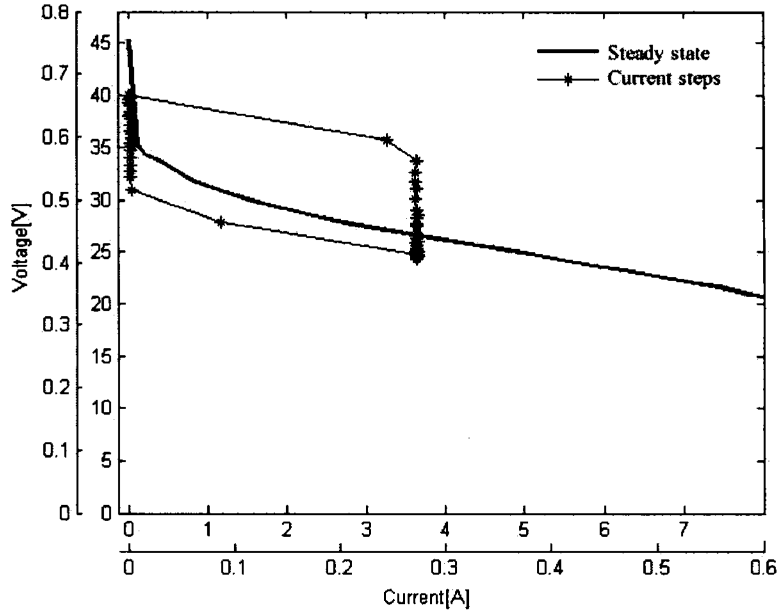

Fig. 6.7 FC simulator and single cell under current step tests: Voltage versus current characteristic of the single cell and FC simulator under current step test

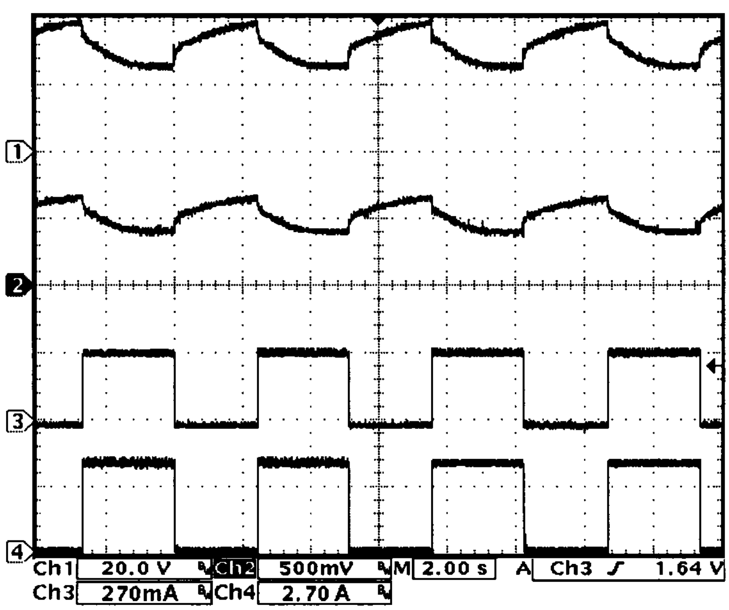

Fig. 6.8 Current step tests: power converter output voltage (Ch1), single FC voltage (Ch2), single FC current (Ch3), and power converter output current (Ch4)

6.5 Summary

A FC simulator based on a small single cell reference that emulates the electrical dynamic behavior of FC stacks was proposed and investigated experimentally. The concept of replacing the FC computer model with an actual low-cost single FC to prevent errors due to the modeling inaccuracies is presented. The electronic load of chapter 3 and the fast dynamic power converter of chapter 4 were used as part of the system. A 150mW single DMFC was used to illustrate the FC stack emulation. Experimental results show that the simulator accurately reproduces the behavior of an equivalent FC stack with 60 cells in series and an active cell area of $70.7 cm^2$, providing an excellent match of the scaled up characteristics.

Chapter 7

Conclusions

7.1 Concluding Summary

FC simulators are flexible affordable systems which may be employed to assist the development and testing of FC power electronics. Using a FC simulator leads to cost and space reductions, time saving, and improved safety. Moreover, power sizing flexibility and handling makes this system even more attractive than a bulky FC stack during R&D phase.

This thesis has presented the development of a novel FC simulator. In order to give insight into the FC technology, experimental results of the steady state and dynamic behavior of a single Direct Methanol FC were obtained and presented in chapter 2. The same procedure can be extended to other types of FCs. The experimental tests revealed how the operating point departs from the polarization curve during transients. This concept was investigated using voltage versus current plots to track the operating point trajectory. The structure of the FC generic model showed similarities with the actual FC behavior. The investigation confirmed the non-linear output characteristic of the FC and the identification of the dependence of the FC model parameter, R_a on the output current. In addition, the experimental tests on the single FC revealed the hysteresis behavior of the FC, which has been described in the literature as the "double layer capacitor" effect. The results of the experimental tests were used to build the empirical model for the stand-alone FC simulator which was presented in chapter 5. The double layer capacitor C was estimated by analyzing the results of the first order time constant of a current step response.

The development of a low cost Electronic Load for FCs based on a DSP was presented in chapter 3. The Electronic Load was used to test a DMFC in chapter 2, the power converter of chapter 4, and the entire FC simulator systems of chapter 5 and 6. It also plays an important role as part of the hardware in the loop concept of chapter 6. This special circuit, incorporating the real time processing capability of a DSP, provided effective parameter measurements and control of the FC output current at a low cost. The connection between the Electronic Load module and other equipment is performed through glue-less 2-wire CAN bus that ensures robust high-speed data transmission under noisy electrical environments.

A power converter for FC simulators with fast dynamic performance was developed and presented in chapter 4. The power converter was designed to have a dynamic response comparable to the FC response. The topology of the power converter was selected on the basis of reversible power flow capabilities, switch utilization, and possibility of using a switching surface control strategy. Since non-linear control strategies based on variable structure theory show better transient response than traditional small-signal based controllers, a control scheme based on a curved Switching Surface (SS) was used. A procedure for the selection of a curved SS based on normalized plots was presented. The normalized three-dimensional plots provide the required generality to evaluate transient performance for any given SS. As a result of the investigation, a switching surface referred to in this work as elliptic natural unloaded SS was selected. The proposed switching surface showed excellent transient behavior with no overshoot during start up. As well, a systematic approach for the selection and clarification of the characteristic features of SSs was developed. Finally, the control strategy was implemented in a DSP. Tests performed on the systems revealed low computational requirements with a maximum of 12 operations.

A simple approach to obtain an empirical model of the FC that matches with the structure of complex electrochemical models for fixed fuel concentration and temperature was presented in chapter 5. Unlike complex electrochemical models, this empirical model can be processed on a real time basis with a fixed-point DSP. Test results in the FC for steady state behavior, dynamic operation, and current step changes in the load showed good match between the experimental results and results of the empirical model.

A novel hardware in the loop FC simulator was proposed in chapter 6 to overcome modeling drawbacks and expand the features of the existing designs. This FC simulator introduces the concept of replacing the computer model of the FC with an actual small single FC. A single FC costs a small fraction of a FC stack and can reproduce the behavior of an expensive powerful FC stack using scale up rules. This arrangement provides a real working environment at a small cost and allows comprehensive design and study of FC systems and FC power electronics.

7.2 Conclusion

The following concluding remarks highlight the significance of the investigation undertaken in the thesis and represent the major contribution of the work.

The FC generic model presented in chapter 2 should not be expected to be accurate during current ripple operation. A frequency response analysis used for impedance spectroscopy, which is based on small signal perturbation, can put into perspective the differences between a model and the actual FC. In other words, the large signal generic model only matches reasonably with the actual FC response during step load changes (i.e. constant current steps). Models obtained using frequency response analysis, which are obtained on a DC operating point, are only valid for small signal on the point where the frequency response analysis is performed. The work by Choi, *et al.* [52] is a good example of the complexity of this approach. Unfortunately, large signal current ripple operation cannot be predicted accurately with frequency response analysis approach. Moreover, if the DC operating point changes, the small signal model is not valid anymore. Finally, effects like membrane water flood, membrane drying, catalyst poisoning, and aging are difficult to predict and are not accurately represented by models.

Discussion about FC models from the previous paragraph presents some of the limitations of FC modeling. For that reason, instead of using a model, the hardware in the loop FC simulator based on a small single FC results in a more robust system. Under this configuration, the emulation of a FC stack is obtained using electrode scale up rules. Thus, the accuracy of the FC stack emulation depends basically on the validity of the electrode scale up rules. Scale up of FC electrodes area is not a mature subject and this work does not attempt to validate scale up rules. A simple linear scale up rule that idealizes both steady state and dynamic behavior of a FC stack with bigger effective area of electrodes is selected to illustrate the hardware in the loop concept. It should be noted that non-linear scale up rules, that may contain dynamic terms, could be incorporated in the electrode area scaling function α. New scale up rules will be included in the FC simulator as soon as they become available in the literature. Finally, considering that the existing models with limited features also require scale up rules for the electrode area, the proposed hardware in the loop system is clearly superior.

With respect to the controls of the power converter, an attempt to demonstrate that a switching surface has good performance through one numerical example does not guarantee the validity for the entire range of possible parameters in the converter. This is perhaps the main disadvantage of previous work on switching surface control reported in the literature. Even though the equations presented are general, the graphical representation of the trajectories is only valid for the example analyzed. The drawback is that the trajectories as well as the performance of the converter dramatically change with a change of parameters. Thus, the entire geometry of the problem is modified every time the parameters change, resulting in a confusing design process and dubious performance analysis. The normalization process proposed in this work anchor the graphical representation of the switching surface leading to tremendous simplification. The behavior of any possible converter for a given switching surface can be evaluated under the proposed normalized graphical representation developed in the thesis. Moreover, the normalized plots provide additional insight into the operation of the control scheme:

- A switching surface that does not anchor in the plot when the parameters are changed simply results in a change of the performance.
- A simple approach that predicts the transient performance for any switching surface can be inferred from the normalized representation of the ideal switching surfaces. For any type of transient (i.e. start up or load change) a switching surface that lies above the corresponding ideal switching surface results in overshoot (the corresponding ideal switching surface only depends on the load resistance value R). On the other hand, a switching surface that lies below the corresponding ideal switching surface results in a poor transient response. The transient response improves as a given switching surface approaches the ideal switching surface. These observations have not been reported in literature.

The stand-alone FC simulator described in the thesis has unique design features that are expected to reduce the complexity and cost associated with the development of FC-based systems. For example, the system is based on a low cost DSP that processes a dynamic FC model and power converter controller in order to meet the dynamic requirements to emulate FCs. This results in a stand-alone system that is suitable for laboratory operation.

The hardware in the loop FC simulator proposed in the thesis provides an attractive approach to link electrochemistry investigation in single FC with research and development of FC power electronics applications, where an FC stack is required. The simulator enables a thorough evaluation of the FC system requirements before building an expensive FC stack. Since the simulator operates the actual single FC under real working conditions, it can provide valuable feedback in term of reliability. It can also help to develop control strategies for the entire combination of FC and application with the advantage of a low cost single FC. From the educational point of view the system provides a low cost real working environment for researchers to gain valuable insight into the behavior of FC stacks.

7.3 Future Work

The integration of the proposed FC simulator system in actual applications (for example, automotive, power generation, and distributed generation) could certainly help to identify new requirements and improvements in this state-of-the-art design. The potential of the FC simulator in R&D of integrated control strategies for an entire FC system plus final application is yet to be determined. In order to expand the power capabilities of the FC simulator for high power applications the development of a control strategy to connect converters in parallel is required.

From the point of view of the software user interface, the number of monitored variables can be upgraded to meet specific demands (for example, temperature and pressures). The analog to digital converter with multiple inputs available in the DSP-based electronic load provides the required hardware for this purpose.

The study and analysis of curved switching surface to control buck converters presented in the thesis can be extended to other power electronics converter topologies, including inverters. The fact that the ideal trajectories (time optimal) of any possible buck converter can be observed, enables the proposed normalized plot as a framework graphical tool for performance analysis of any control strategy. In other words, ideal trajectories can be compared against trajectories with a given control strategy.

Finally, the proposed electronic load is the starting point for the development of useful testing devices for FCs not commercially available. The built-in DSP provides a powerful platform for future measurement instruments, monitoring, and diagnosis systems. A flexible digital lock-in amplifier routine for impedance analysis is a good example of what can be achieved with this device. In addition, its low power consumption allows it to be mounted on site and be supplied by the FC system. This is an important requirement for monitoring and on-line diagnostic devices.

References

[1] J. E. Larminie and A. Dicks, *Fuel Cell Systems Explained.* Chichester, U.K.: Wiley, 2000.

[2] M.W. Ellis, M.R.Von Spakovsky, and D.J. Nelson, "Fuel cell systems: efficient, flexible energy conversion for the 21st century," Proceedings of the IEEE , Vol. 89 , pp. 1808-1818 , Dec. 2001.

[3] M. A. Laughton, "Fuel cells," Power Engineering Journal, Vol. 16, Issue 1, pp. 37-47, Feb. 2002.

[4] A. Emadi, S.S. Williamson, "Fuel cell vehicles: opportunities and challenges," IEEE Power Engineering Society General Meeting 2004, pp.1640-1645, June 2004.

[5] S. Romano, and J.T. Larkins, "Georgetown University Fuel Cell Transit Bus Program," Fuel Cells, Vol. 3, Issue 3, pp. 128-132, Nov 2003.

[6] S. Ishibashi, T. Aoki, S. Tsukioka, H. Yoshida, T. Inada, T. Kabeno, T. Maeda, K. Hirokawa, K. Yokoyama, T. Tani, R. Sasamoto, Y. Nasuno, "An ocean going autonomous underwater vehicle "URASHIMA" equipped with a fuel cell" International Symposium on Underwater Technology, UT '04, pp. 209-214, Taipei (Taiwan), April 20-23, 2004.

[7] H. Oman, "Fuel-cell powered airplane propulsion," IEEE Aerospace and Electronic Systems Magazine, Vol. 19, Issue 1, pp. 12-13, Jan 2004.

[8] N. Kato, T. Murao, K. Fujii, T. Aoiki, S. Muroyama, "1 kW portable fuel cell system based on PEFCs," The Third International Conference on

Telecommunications Energy Special, TELESCON 2000, pp. 209-213, Dresden (Germany), May 7-10, 2000.

[9] S. Gilbert "The nations largest fuel cell project, a 1 MW fuel cell power plant deployed as a distributed generation resource, Anchorage, Alaska project dedication August 9, 2000," Rural Electric Power Conference, pp. A4/1-A4/8, Little Rock (USA), April 29-May 1, 2001.

[10] D.H Archer, J.G. Wimer, M.C. Williams, "A phosphoric acid fuel cell cogeneration system retrofit to a large office building," Energy Conversion Engineering Conference, IECEC-97, pp.817–824, New York (USA), July 27-Aug 1, 1997.

[11] C.K. Dyer, "Fuel cells and portable electronics," 2004 Symposium on VLSI Circuits, pp. 124-127, Honolulu (USA), June 2004.

[12] C. Xie, J. Pavio, J. Hallmark, J. Bostaph, and A. Fisher, "Key requirements of micro fuel cell system for portable electronics," Energy Conversion Engineering Conference, IECEC '02, pp. 603-606, Washington D.C. (USA), July 2004.

[13] P. Enjeti, Book Chapter: Chapter #9: *Power Conditioning Systems for Fuel Cell Systems*, US Department of Energy Fuel Cell Handbook, Sixth Edition, 2002.

[14] J.M Correa, F. A. Farret, J. R. Gomes, and M. G. Simoes, "Simulation of fuel-cell stacks using a computer-controlled power rectifier with the purposes of actual high-power injection applications," IEEE Transactions on Industry Applications, Vol. 39 , Issue: 4, pp. 1136 - 1142, July-Aug., 2003

[15] P. Acharya, P. Enjeti, and I.J. Pitel, "An advanced fuel cell simulator," Applied Power Electronic Conference and Exposition, *APEC '04*, Vol. 3, pp. 1554 - 1558, Anaheim (USA), Feb. 22-26, 2004.

[16] T.-W. Lee, B.-K. Lee, S.-J. Jang, S.-H. Kim, and C.-Y. Won, "Development of A 3 kW fuel cell generation system with an active fuel cell simulator: topology, control, and design," Power Electronics Specialist Conference, IEEE PESC '04, Vol. 6, pp. 4743-4748, Aachen (Germany), June 20-25 2004.

[17] D.M. Bernardi, and M.W. Verbrugge, "Mathematical model of a gas diffusion electrode bonded to a polymer electrolyte," AIChE Journal, Vol. 37, Issue 8, pp 1151-1163, 1991.

[18] V. Gurau, H. Liu, and S. Kakaç, "Two-dimensional model for proton exchange membrane fuel cells," AIChE Journal, Vol. 44, Issue 11, pp 2410-2422, Nov. 1998.

[19] K. V. Zhukovsky, "Three dimensional model of oxygen transport in a porous diffuser of a PEM fuel cell," AIChE Journal, Vol. 49, Issue 12, pp. 3029-3036, Dec. 2003.

[20] Sukkee Um, C.-Y. Wang, and K. S. Chen, "Computational Fluid Dynamics Modeling of Proton Exchange Membrane Fuel Cells," J. Electrochem. Soc., Vol 147, Issue 12, p. 4485-4493, Dec. 2000.

[21] D. Natarajan and T. Van Nguyen, "A Two-Dimensional, Two-Phase, Multicomponent, Transient Model for the Cathode of a Proton Exchange Membrane Fuel Cell Using Conventional Gas Distributors," J. Electrochem. Soc., Vol. 148, Issue 12, pp. A1324-A1335, Dec. 2001.

[22] K. Sundmacher, T. Schultz, S. Zhou, K. Scott, M. Ginkel, and E. D. Gilles, "Dynamics of the direct methanol fuel cell (DMFC): experiments and model-based analysis," Chemical Engineering Science, Vol. 56, Issue 2, pp 333-341, Jan. 2001.

[23] H.P.L.H. van Bussel, F.G.H. Koene, and R.K.A.M. Mallant, "Dynamic model of solid polymer fuel cell water management," Journal of Power Sources, Vol. 71, Issues 1-2, pp. 218-222, March 1998.

[24] M. Eikerling, Yu. I. Kharkats, A. A. Kornyshev, and Yu. M. Volfkovich, "Phenomenological Theory of Electro-osmotic Effect and Water Management in Polymer Electrolyte Proton-Conducting Membranes," Journal Electrochemistry Society, Vol. 145, Issue 8, pp. 2684-2699, Aug. 1998.

[25] J. Kim, S. M. Lee, S. Srinivasan, and C. E. Chamberlin, "Modeling of Proton Exchange Membrane Fuel Cell Performance with an Empircal Equation," Journal Electrochemical Society, Vol. 142, Num. 8, pp. 2670-2674, Aug. 1995.

[26] J.H. Lee, T.R. Lalk, and A.J. Appleby, "Modeling electrochemical performance in large scale proton exchange membrane fuel cell stacks," Journal of Power Sources Volume 70, Issue 2 , pp. 258-268, February 1998.

[27] G. Squadrito, G. Maggio, E. Passalacqua, F. Lufrano, and A. Patti, "An empirical equation for polymer electrolyte fuel cell (PEFC) behaviour," Journal of Applied Electrochemistry, Vol. 29, Num. 12, pp. 1449-1455, Dec. 1999.

[28] L. Pisani, G. Murgia, M. Valentini, and B. D'Aguanno, "A new semi-empirical approach to performance curves of polymer electrolyte fuel cells," Journal of Power Sources, Vol. 108, Issues 1-2, pp. 192-203, June 2002.

[29] A. A. Kulikovsky, "The voltage–current curve of a direct methanol fuel cell: "exact" and fitting equations," Electrochemistry Communications, Vol. 4, Issue 12, pp.939-946, Dec. 2002.

[30] A. A. Kulikovsky, "The voltage–current curve of a polymer electrolyte fuel cell: "exact" and fitting equations," Electrochemistry Communications, Vol. 4, Issue 11, pp. 845-852, Nov. 2002.

[31] J. C. Amphlett, R. M. Baumert, R. F. Mann, B. A. Peppley, P. R. Roberge, and T. J. Harris, "Performance Modeling of the Ballard Mark IV Solid Polymer Electrolyte Fuel Cell. I. Mechanistic Model Development," Journal Electrochemical Society, Vol. 142, Num. 1, pp. 1-8 Jan. 1995.

[32] J. C. Amphlett, R. M. Baumert, R. F. Mann, B. A. Peppley, P. R. Roberge, T. J. Harris, "Performance Modeling of the Ballard Mark IV Solid Polymer Electrolyte Fuel Cell. II. Empirical Model Development," Journal Electrochemical Society, Vol. 142, Num. 1, pp. 9-15, Jan. 1995.

[33] J. C. Amphlett, R. M. Baumert, R. F. Mann, B. A. Peppley, P. R. Roberge and A. Rodrigues, "Parametric modelling of the performance of a 5-kW proton-exchange

membrane fuel cell stack," Journal of Power Sources, Vol. 49, Issues 1-3, pp. 349-356, April 1994.

[34] J. C. Amphlett, R. F. Mann, B. A. Peppley, P. R. Roberge, and A. Rodrigues, "A model predicting transient responses of proton exchange membrane fuel cells," Journal of Power Sources, Vol. 61, Issues 1-2, PP. 183-188, July-Aug. 1996.

[35] R. F. Mann, J. C. Amphlett, M. A. I. Hooper, H. M. Jensen, B. A. Peppley, and P. R. Roberge, "Development and application of a generalized steady-state electrochemical model for a PEM fuel cell," Journal of Power Sources, vol. 86, pp. 173–180, 2000.

[36] N. Mohan, T. M. Undeland, and W. P. Robbins, *Power Electronics: Converters, Applications, and Design*, Wiley; 3rd edition, 2002.

[37] R. W. Erickson, and D. Maksimovic, *Fundamentals of Power Electronics,* Springer, 2nd edition, 2001.

[38] J. Cardesin, J. Sebastian, P. Villegas, A. Hernando, and A. Fernandez, "Average small-signal model of buck converter used as power factor preregulator," Industry Applications Conference Annual Meeting, 37th IAS, Vol. 3, pp. 2147-2152, Pittsburgh (USA), Oct. 2002.

[39] K. Hirachi, and M. Nakaoka, "Improved control strategy on buck-type PFC converter," Electronics Letters, Vol. 34, Issue 12, pp. 1162-1163, June 1998.

[40] K. Matsui, I. Yamamoto, T. Kishi, M. Hasegawa, H. Mori, and F. Ueda, "A comparison of various buck-boost converters and their application to PFC," Annual Conference of the Industrial Electronics Society, IEEE IECON 02, Vol. 1, pp. 30-36, Roanoke (USA), Nov. 2002

[41] C. Qiao, and K.M. Smedley, "A topology survey of single-stage power factor corrector with a boost type input-current-shaper," IEEE Transactions on Power Electronics, Vol. 16, Issue 3, pp. 360-368, May 2001.

[42] Magna Power Electronic, "PQA Series power Supplies," Data Sheet.

[43] K. Ogata, *Modern control engineering*, Prentice Hall, 4th edition, 2002.

[44] B.C. Kuo, and F. Golnaraghi, *Automatic control systems*, J. Wiley, 7th edition, 1995.

[45] R. D. Middlebrook and S.Cuk, "A general unified approach to modeling switching converter power stages," Power Electronics Specialist Conference, IEEE PESC '76, pp. 18-34, 1976.

[46] G. Spiazzi, and P. Mattavelli, Book Chapter 8: *Sliding-Mode Control of Switched-Mode Power Supplies*, *The power electronics Handbook*, edited by T. Skvarenina, CRC Press, 2002.

[47] P. T. Krein, Book Section 8.2: Sliding Mode and Switching Surface Control, *Nonlinear Phenomena in Power Electronics: Attractors, Bifurcation, Chaos, and Nonlinear Control*, Piscataway, NJ: IEEE Press, 2001.

[48] V. I. Utkin, "Variable structure systems with sliding modes." IEEE Transactions on Automatic Control, Vol. AC-22, pp. 212-222, 1971.

[49] M. Ordonez, M. T. Iqbal, and J. E. Quaicoe, "Dynamic behavior of a Direct Methanol Fuel Cell," Newfoundland Electrical and Computer Engineering Conference, NECEC 2004, St. John's (Canada), Oct. 4, 2004.

[50] R. Gopinath; K. Sangsun, Jae-Hong Hahn; P.N. Enjeti, M.B.Yeary, J.W. Howze, "Development of a low cost fuel cell inverter system with DSP control," IEEE Transactions on Power Electronics, Vol. 19, Issue 5, pp.1256-1262, Sept. 2004.

[51] J. Wang, F.Z. Peng, J. Anderson, A. Joseph, R. Buffenbarger, "Low cost fuel cell converter system for residential power generation," IEEE Transactions on Power Electronics, Vol. 19, Issue 5, pp.1315-1322, Sept. 2004.

[52] W. Choi, P. N. Enjeti, and J. W. Howze, "Development of an equivalent circuit model of a fuel cell to evaluate the effects of inverter ripple current," Applied Power Electronics Conference and Exposition, IEEE APEC '04, Anaheim (USA), pp. 355-361 , Feb. 22-26, 2004.

[53] R. S. Gemmen, "Analysis for the Effect of the Ripple Current On Fuel Cell Operating condition," International Mechanical Engineering Congress and Exposition, ASME IMECE 2001, New York (USA), November 2001.

[54] R. Greef, R. Peat, L. M. Peter, D. Pletcher, J. Robinson, "*Instrumental Methods in Electrochemistry*," John Wiley & Sons, 1985.

[55] Ametek instruments for electrochemistry: http://www.princetonappliedresearch.com/products/Potentiostats.cfm

[56] Texas instruments, 2005, "TMS320LF2407A, LF2406A, LF2403A, LF2402A LC2406A, LC2404A, LC2403A, LC2402A DSP (Rev. K)," Data Sheet.

[57] Texas instruments, 2001, "TMS320LF/LC240xA DSP Controllers System and Peripherals Reference Guide (Rev. B)," Technical Manual.

[58] Texas instruments, 2000, "TMS320C2xx/TMS320C24x Code Composer," User's Guide.

[59] Texas instruments, 1999, "TMS320C2x/C2xx/C5x Optimizing C Compiler," User's Guide.

[60] Robert Bosch GmbH, 1991, "CAN Specification Version 2.0," Control Area Network Protocol Specification.

[61] Texas instruments, 2003, "Programming examples for the TMS320C24x/C240x CAN (Rev. A)," Technical Document.

[62] R. D. Middlebrook, "Small-signal modeling of pulse-width modulated switched-mode power converters," Proceedings of the IEEE, Vol. 76, Issue 4, pp. 343–354, April 1988.

[63] Li Rongyuan, A. Pottharst, N. Frohleke, and J. Bocker, "Analysis and design of improved isolated full-bridge bidirectional DC-DC converter," Power Electronics Specialist Conference, IEEE PESC '04, Aachen (Germany), pp. 521-526, June 20-25, 2004

[64] M. Jain, M. Daniele, and P. K. Jain, "A bidirectional DC-DC converter topology for low power application" IEEE Transactions on Power Electronics, Vol. 15, Issue 4, pp. 595-606, July 2000

[65] V. I. Utkin, Sliding Mode and Their Applications in Variable Structure Systems, Moscow: MIR, 1978.

[66] K.K.S. Leung, and H.S.H. Chung, "Derivation of a second-order switching surface in the boundary control of buck converters," IEEE Power Electronics Letters, Vol. 2, Issue 2, pp. 63–67, June, 2004.

[67] H. Sira-Ramirez, "Nonlinear P-I controller design for switchmode DC-to-DC power converters," IEEE Transactions on Circuits and Systems, Vol. 38, pp. 410–417, April 1991

[68] P. Mattavelli, L. Rossetto, G. Spiazzi, and P. Tenti, "General-purpose sliding-mode controller for dc/dc converter applications," Power Electronics Specialist Conference, IEEE PESC '93, pp. 609–615, Jun. 1993.

[69] H. Sira-Ramirez and M. Rios-Bolivar, "Sliding mode control of dc-to-dc power converters via extended linearization," IEEE Trans. Circuits Syst. I, vol. 41, no. 10, pp. 652–661, Oct 1994.

[70] V. S. C. Raviraj and P. C. Sen, "Comparative study of proportional-integral, sliding mode, and fuzzy logic controllers for power converters," IEEE Transaction on Industry Applications, vol. 33, no. 2, pp. 518–524, Mar./Apr. 1997.

[71] T. Siew-Chong, Y.M. Lai, M.K.H. Cheung, and C.K. Tse, "On the practical design of a sliding mode voltage controlled buck converter," IEEE Transactions on Power Electronics, Vol. 20, pp. 425-437, March 2005.

[72] H. Sira-Ramirez, "Sliding motions in bilinear switched networks," IEEE Transactions on Circuits and Systems, Vol. 34, Issue 8, pp. 919-933, Aug. 1987.

[73] B. Jammes, J.C. Marpinard, and L. Martinez, "Large-signal control of a buck converter based on time optimal control," European Conference on Circuits

Theory and Design, ECCTD ’93, Davos (Switzerland), pp. 1419-1423, Aug. 30-Sep. 3, 1993.

[74] Texas Instruments DSP’s: http://dspvillage.ti.com/

[75] M. Ordonez, M. T. Iqbal, and J. E. Quaicoe, “Development of a Fuel Cell Simulator Based on an Experimentally Derived Model,” Canadian Conference On Electrical And Computer Engineering, IEEE CCECE ’05, Saskatoon (Canada), May 1-4, 2005.

[76] G. Box, W.G. Hunter, and J.S. Hunter, *Statistics for experimenters*, Wiley, 1978.

[77] S. C. Chapra, R. P. Canale, *Numerical Methods for Engineers*, McGraw-Hill Science/Engineering/Math; 5 edition, 2005.

[78] W. H. Press, B. P. Flannery, S. A. Teukolsky, and W. T. Vetterling, *Numerical Recipes in C : The Art of Scientific Computing*, Cambridge University Press; 2 edition, 1992.

[79] M. Ordonez, M.T. Iqbal, and J. E. Quaicoe, “A Novel Fuel Cell Simulator,” Power Electronics Specialist Conference, IEEE PESC ’05, Recife (Brazil), June 12-16, 2005.

[80] C. Song and P.G. Pickup, "Effect of hot pressing on the performance of direct methanol fuel cells," Journal of Applied Electrochemistry, Vol. 34, pp. 1065–1070, 2004.